NASA CR-
141458

DYNAMICS OF MULTIRATE SAMPLED DATA CONTROL SYSTEMS

FINAL REPORT

Contract NAS9-13690

Prepared by

BOEING AEROSPACE COMPANY
Research & Engineering Division

Boeing Document No. D180-18438-1
October, 1974

(NASA-CR-141458) DYNAMICS OF MULTIRATE SAMPLED DATA CONTROL SYSTEMS Final Report, Oct. 1973 - Oct. 1974 (Boeing Aerospace Co., Seattle, Wash.) 146 p HC $5.75 CSCL 22B G3/18

N75-13915

Unclas
06506

Submitted to

NATIONAL AERONAUTICS & SPACE ADMINISTRATION
Lyndon B. Johnson Space Center
Houston, Texas

DYNAMICS OF MULTIRATE SAMPLED DATA CONTROL SYSTEMS

FINAL REPORT

Jay R. Naylor
Robert J. Hynes
Daniel O. Molnar

FOREWARD

This work was performed by the Research and Engineering Division, Boeing Aerospace Company, Seattle, Washington, 98124, under Contract NAS9-13690 with the Guidance and Control Systems Branch of the Avionics Systems Engineering Division, NASA-Johnson Space Flight Center, Houston, Texas. The NASA technical monitor on this contract was Bill Peters and he was assisted by Bernard Mercantel. This report covers work performed between October 1973 and October 1974.

ABSTRACT

The purpose of this contract was to determine the effect of the synthesis approach (single or multirate) on the machine requirements for a digital control system for the space shuttle boost vehicle. The study encompassed four major work areas: synthesis approach trades, machine requirements trades, design analysis requirements and multirate adaptive control techniques.

The primary results of this study are two multirate autopilot designs for the low Q and maximum Q flight conditions that exhibits equal or better performance than the analog and single rate system designs. Also, a preferred technique for analyzing and synthesizing multirate digital control systems is specified.

KEY WORDS

Adaptive Control

Computer Requirements

Digital Body Bending Compensation

Multirate Digital Control

TABLE OF CONTENTS

LIST OF FIGURES

LIST OF FIGURES (CONTINUED)

LIST OF FIGURES (CONTINUED)

LIST OF TABLES

1.0 INTRODUCTION

Single rate digital autopilot designs have been plagued by the divergent requirements of sampling at a high rate to prevent folding unwanted signals into the bandwidth of the control system while also trying to keep the sampling rate at a minimum to avoid finite accuracy arithmetic problems. The solution to this problem is to go to a multirate design where the sampling rates for the various computations can be specified in a more consistent manner. For example, cascade multirate filters can be defined with a fast update rate front end to circumvent the folding problem and to allow optimal performance of the high frequency filter requirements. The low frequency back end filter can be defined to alleviate arithmetic problems while meeting the low frequency filter requirements. Similarly, multiloop multirate designs can be used to meet different sampling rate requirements in different loops.

1.1 Study Approach

This study was performed to determine multirate analysis techniques and to study the effect of the system synthesis approach (single or multirate) on the machine requirements for a space shuttle type boost vehicle at low Q and maximum Q flight conditions. The applicability of adaptive control techniques to space shuttle was also investigated.

The study activities car, be grouped into the following major work areas:

Synthesis Approach Trades
Machine Requirement Trades
Design Analysis Requirements
Multirate Adaptive Control Techniques

This report is divided into sections covering these four tasks. A summary of the major study activities is given below.

The Synthesis Approach Trades task is involved with applying synchronous and multirate sampled data analysis and realization techniques to two fixed point in time linearized models of the plant and control system furnished by NASA-JSC. First, the models were verified on the Boeing analysis program MDELTA and then the analog control system was digitized using Tustin's bilinear transformation with frequency prewarping. Next, a digital control system was designed starting with a z-transformed model of the plant. Lastly, a multirate control system was designed. Comparisons were made between the gain and phase margin characteristics for the different designs. Hybrid simulations of the systems were implemented and the analysis results were verified using these simulations.

The objective of the Machine Requirements Trades task was to determine the effect of the synthesis approach on the machine requirements. The primary machine requirements and the effect of sampling rate on these requirements are reviewed. The machine requirements for a synchronous implementation versus a multirate implementation are discussed.

The Design Analysis task involved studying techniques for analyzing multirate sampled data systems. The primary existing techniques are reviewed and the state variable approach is discussed in detail. This latter approach was used to perform the analysis work in Task I.

A literature search and study of various parameter adaptive control schemes were conducted. Extensions to these techniques to make them applicable to a shuttle type application are outlined. The pseudo adaptive autopilot used on the SRAM missile is discussed. Two possible digital implementations for these adaptive control systems are discussed.

1.2 Study Results

The contract findings are summarized in the following paragraphs:

Synthesis Approach Trades - Single rate and multirate yaw plane autopilots were designed for the two fixed point in time plant models. For the low Q system the single rate and multirate designs gave near identical performance when judged in terms of frequency response characteristics although the multirate design exhibited slightly better phase stabilization of the first bending mode. From a frequency response standpoint, the max Q multirate design gave much better gain stabilization of the body bending modes than the single rate system. The hybrid simulation results verified the analysis predictions in all cases considered. A multirate design methodolngy was developed and is outlined below:

1. Continuous root locus
2. Z-plane root locus and frequency response at sampling rates of interest
3. Determination of high update rate and low update rate filter requirements
4. Multirate frequency response and root locus
5. Fine tuning multirate design based upon (4).

Machine Requirements Trades - The effect of the single rate and multirate designs resulting from Task 1 on 'ie machine requirements was negligible from a computer wordlength standpoint. This is primarily due to the fact that the allowable range in variation of the sampling period was restricted to a positive interger times T = .04 sec. which is the basic frame time for the Space Shuttle G&C computer. It was determined from both folding and stability standpoints that the lowest acceptable sampling rate had a period of T = .08 seconds. The frame time of .04 sec. was slow enough to begin with to preclude any finite accuracy arithmetic problems for the filters considered for this system. The multirate design did free up computer time over the T = .04 single rate designs as not all the computations needed to be performed every cycle. Also, the max Q multirate design .'as a simpler design to implement because it was possible to replace a first order filter by a sample and hold element. The hybrid computer wordlength studies verified 'he aforementioned conclusions as they showed that all filters could be implemented on a 16 bit computer.

Design Analysis Requirements - The two primary techniques that were studied for an.lyzing multirate systems were the switch decomposition method of Kranc [11] and the state transition approach of Kalman and Bertram [3]. The switch decomposition technique is shown to present severe computer implementation problems in the area of separating the branch variables from the loop equations. The state variable approach is demonstrated to be straightforward to apply to a wide class of sampled data systems and to be easily implemented on a digital computer. The state transition method is therefore recommended for analyzing multirate systems and a preferred method of defining the state transition matrices is specified.

Multirate Adaptive Control Techniques - T'ie parameter adaptive control algorithm of Lion [22] is shown to offer the best chance for doing online adaptive control based upon identifying the vehicle characteristics. Pseudo-adaptive control techniques as used on the Boeing SRAM are also outlined and look as if they would offer le:s technical risk than a full adaptive system.

2.0 . .NTHESIS APPROACH TRADES

The purpose of this section is to outline a methodology for designing multirate compensation for sample data control systems. To meet this goal, the section is broken into seven subsections. Subsection 2.1 presents two analog plant models which are used as examples in developing the design methodology. Subsection 2.2 addresses how different sampling rates c.. affect the control system performance. In Subsection 2.3 synchronous compensation is formed by applying Tustin's method with frequency scale pre-warping to the analog compensation in the two plant models. Subsection 2.4 presents a single rate digital design for one of the plant models where the analog compensation has been removed and replaced with a sampler and zero-order hold. Subsection 2.5 presents a multirate design for both plant models. In Subsection 2.6 the results of a simulation which verify the multirate designs are presented. Subsection 2.7 summarizes Section 2.0 with a general outline on the methodology to use in designing multirate systems.

2.1 Continuous Plant Gain and Phase Margins

The block diagrams of the two plant models used in developing the digital filters are shown in Figures 2.1.1 and 2.1.2. Both systems model the yaw dynamic of the space shuttle. The first system is for the lift off or low Q flight conditions. The second system is for the max Q flight conditions. In each case the design criterion is the same. The digital compensation is to replace the analog compensation while meeting the following constraints:

1) The rigid mode gain and phase margins are to duplicate those of the continuous system.
2) The first body bending mode is to be phase stabilized.
3) The higher body bending modes are to be gain stabilized.

The Nichol's chart for each of these systems where the loop has been opened at K is shown in Figures 2.1.3 and 2.1.4.

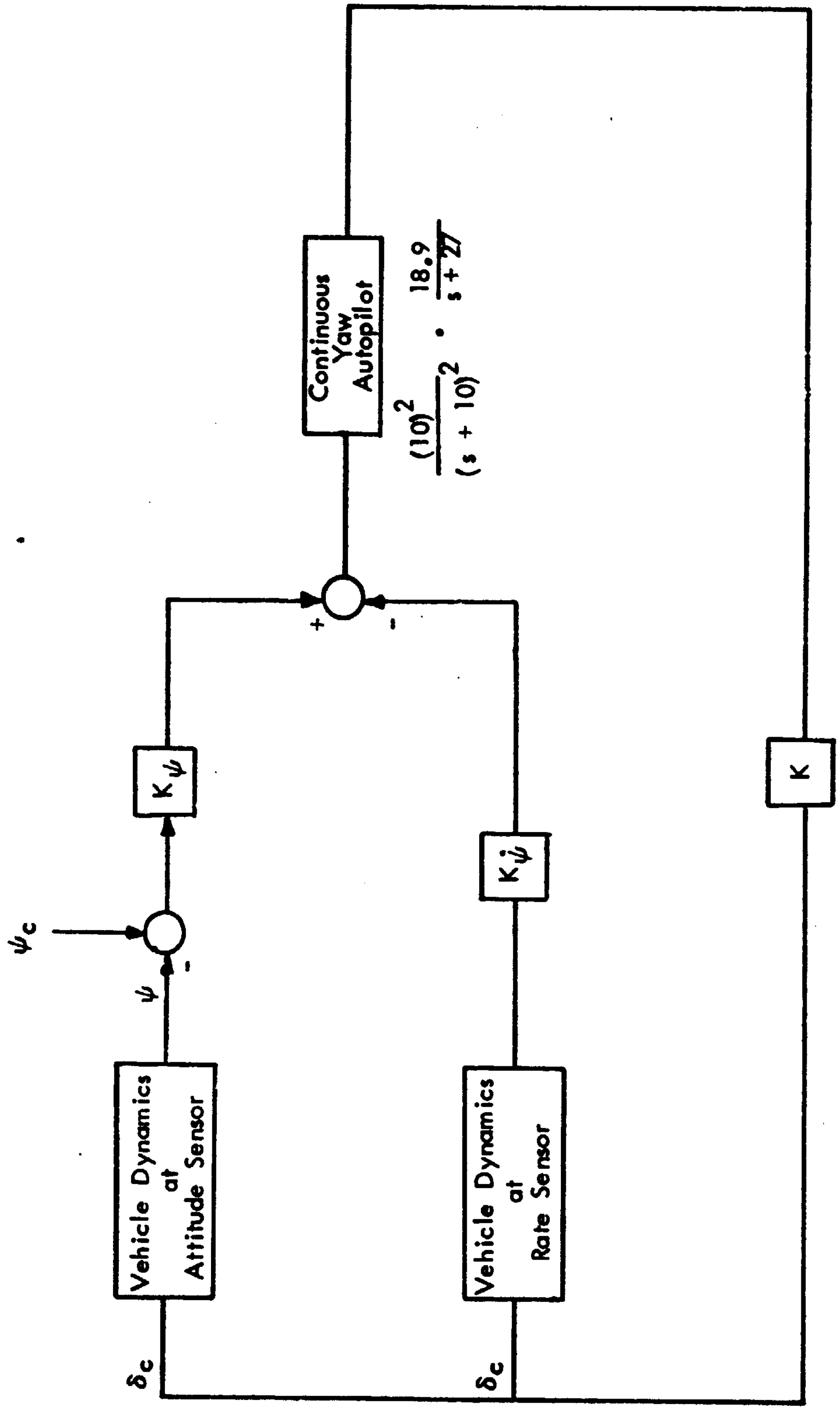
ψ_c
ψ
-
K_ψ
Vehicle Dynamics at Attitude Sensor
δ_c
Vehicle Dynamics at Rate Sensor
δ_c
$K_{\dot{\psi}}$
+
-
Continuous Yaw Autopilot
$\frac{(10)^2}{(s+10)^2} \cdot \frac{18.9}{s+27}$
K

FIGURE 2.1.1: BLOCK DIAGRAM OF CONTINUOUS LOW Q SYSTEM

FIGURE 2.1.2: BLOCK DIAGRAM of CONTINUOUS MAX Q SYSTEM

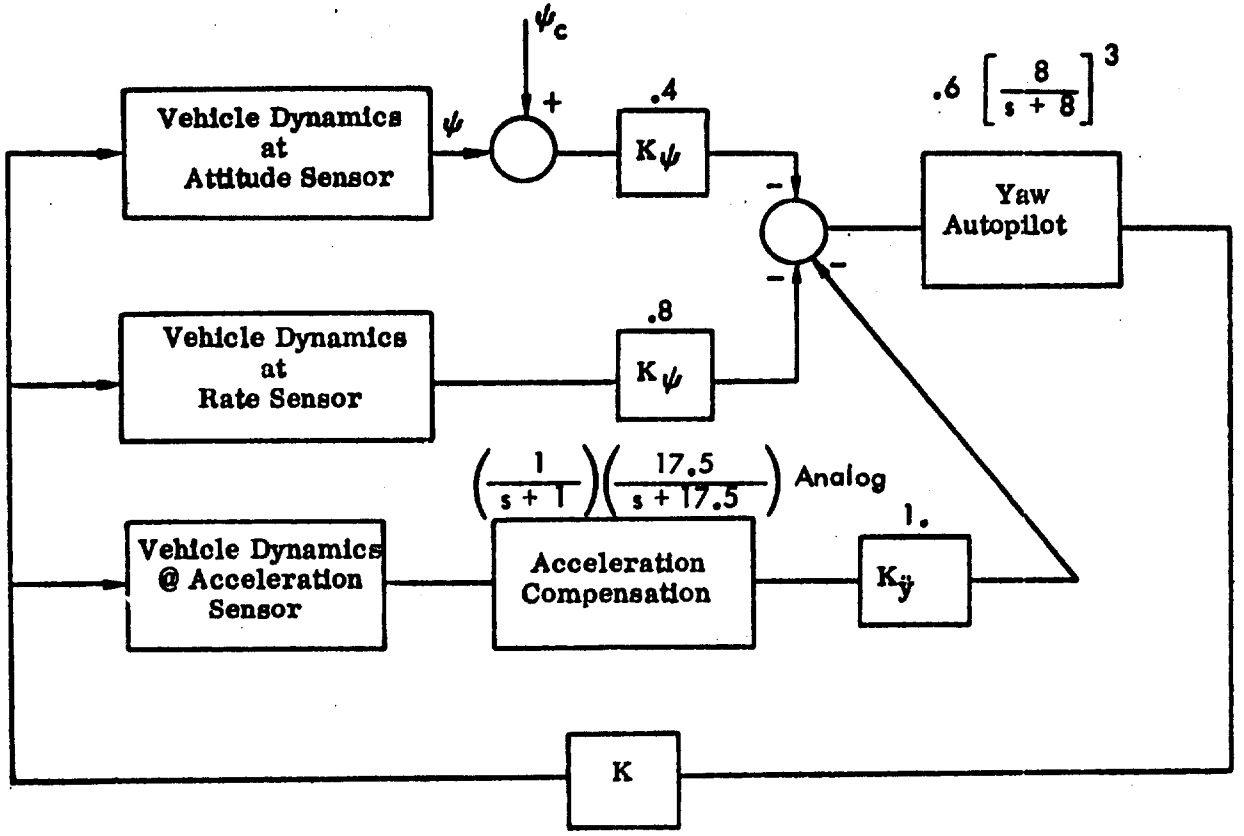
ψ_c
+
Vehicle Dynamics at Attitude Sensor
ψ
.4
K_ψ
−
−
−
$.6 \left[\frac{8}{s+8}\right]^3$
Yaw Autopilot
Vehicle Dynamics at Rate Sensor
.8
K_ψ
$\left(\frac{1}{s+1}\right)\left(\frac{17.5}{s+17.5}\right)$ Analog
Vehicle Dynamics @ Acceleration Sensor
Acceleration Compensation
1.
$K_{\ddot{y}}$
K

REPRODUCIBILITY OF THE
ORIGINAL PAGE IS POOR

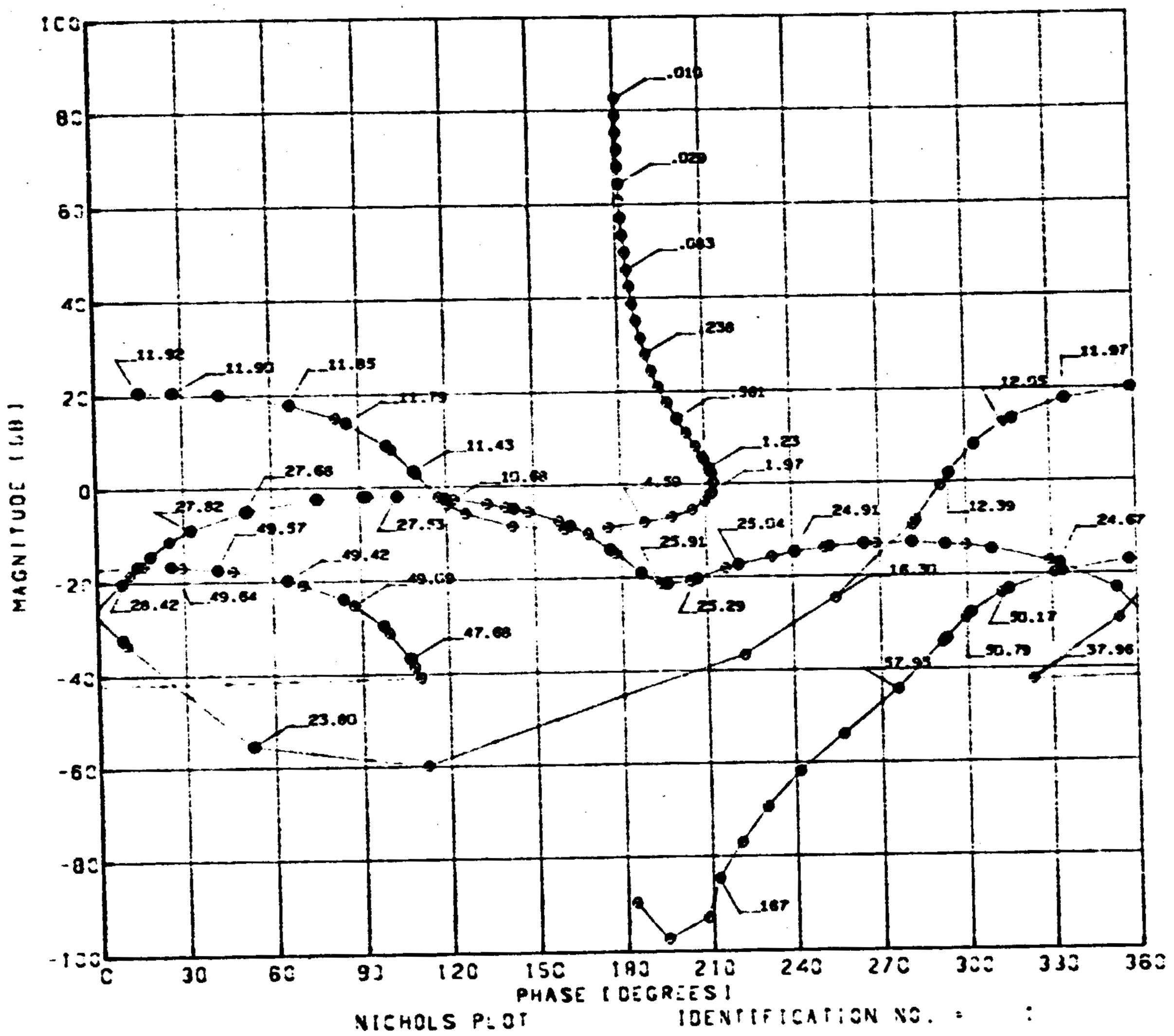

22 JAN 74

Figure 2.1.3: Continuous System Nichols Chart for Lift Off Flight Condition

Gain Margin = 8.82 db @ 5.29 rad/sec
Phase Margin = 32°

1st Body Bending Mode at 11.91 rad/sec
2nd Body Bending Mode at 23.74 rad/sec
3rd Body Bending Mode at 24.79 rad/sec
4th Body Bending Mode at 49.67 rad/sec

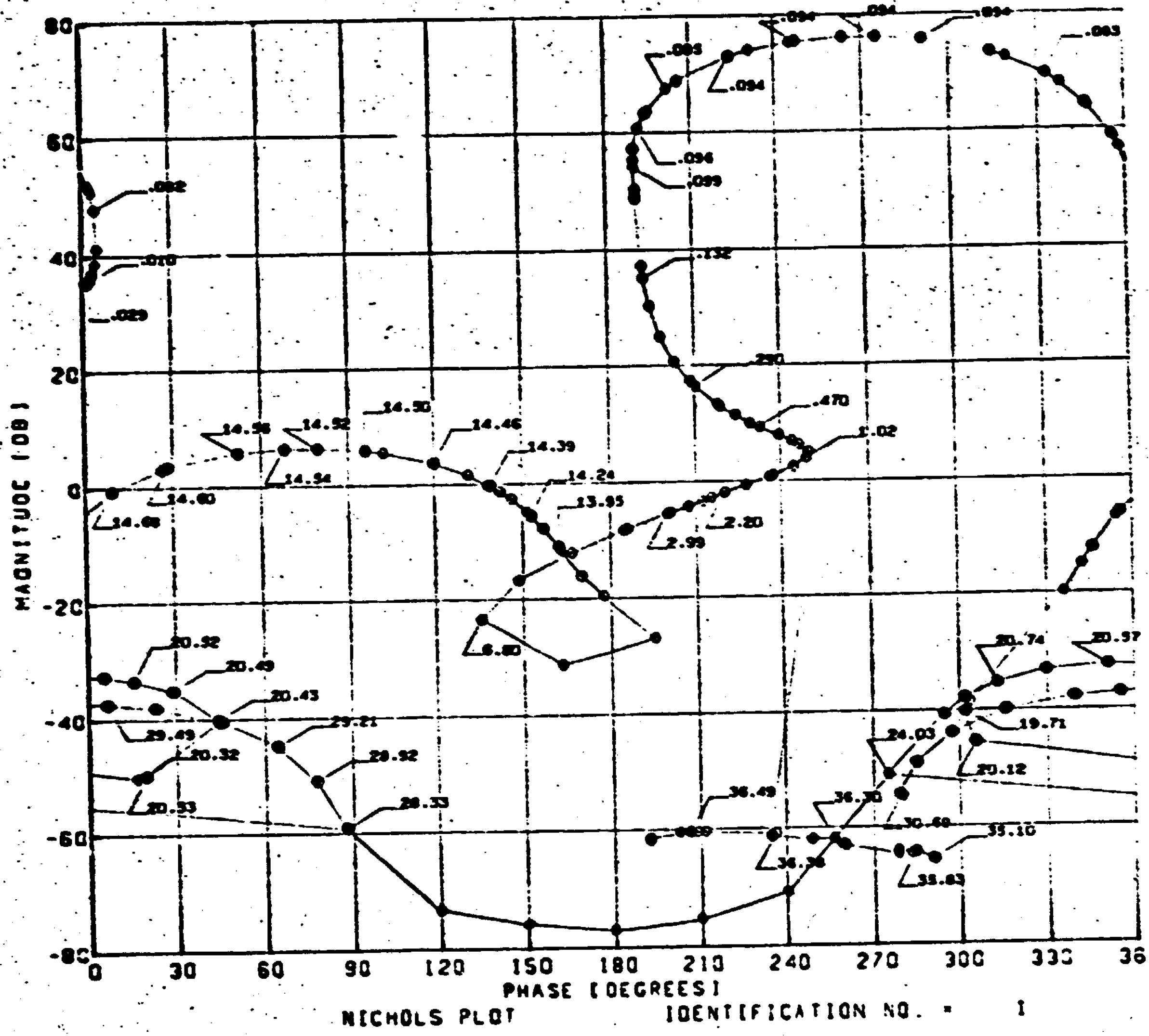

06 APR 74

Figure 2.1.4: Nichol's Chart for the Continuous System at Maximum Q
Gain Margin = 9.14 db @ 3.84 rad/sec
Phase Margin = 51.16°

REPRODUCIBILITY OF THE
ORIGINAL PAGE IS POOR

2.2 Sampling Rate Requirements

The choice of the sampling frequency is of prime importance when converting an analog system to a sampled data system. If analog break frequencies in the continuous system are greater than half the sampling frequency, $\frac{\omega_s}{2}$, the poles corresponding to these frequencies will fold into the primary strip. If a pair of poles fold near the $\omega = 0$ region it can adversely affect the rigid mode dynamics. Choosing a larger sampling rate alleviates this problem, but too large a rate can cause the system to be driven by truncation errors. A happy median needs to be selected in order to avoid these problems. In Section 2.0 the sampling rates of $T = 0.04$ seconds and $T = 0.08$ seconds are used for the synchronous and multirate designs. In Section 3.0 the problem of choosing a proper sampling rate is treated in greater detail.

2.3 Digitized Continuous Autopilot

Low Q System

The continuous autopilot $G_c(s) = \frac{(10)^2}{(S+10)^2}$ can readily be digitized using Tustin's method with frequency scale pre-warping. This involves replacing S with $\frac{2}{T} \quad \frac{Z-1}{Z+1}$ and the analog break frequency with $\frac{2}{T}\tan\left(\frac{\omega_A T}{2}\right)$.

In order to reduce coefficient sensitivity problems $G_c(s)$ is implemented as two cascaded first order filters. The general result for one of the cascaded first order filters is as follows:

$$D.(Z) = \frac{\dfrac{\tan\left(\frac{\omega_A T}{2}\right)}{1+\tan\left(\frac{\omega_A T}{2}\right)} + \dfrac{\tan\left(\frac{\omega_A T}{2}\right)}{1+\tan\left(\frac{\omega_A T}{2}\right)}\,z^{-1}}{1 + \dfrac{\tan\left(\frac{\omega_A T}{2}\right)-1}{\tan\left(\frac{\omega_A T}{2}\right)+1}\,z^{-1}}$$

where ω_A = analog filter break frequency

T = sampling rate

$z = e^{ST}$.

With sampling periods of T = .04 and .08 seconds and an analog break frequency of ω_A = 10 rad/sec. this equation becomes

T = .04

$$D_1(z) = \frac{.168537\ (1 + z^{-1})}{1 - .6629251z^{-1}}$$

T = .08

$$D_1(z) = \frac{.2971743\ (1 + z^{-1})}{1 - .40565128z^{-1}}$$

The corresponding digital representations for $G_s(s) = \frac{18.9}{s + 27}$ also follow by applying Tustin's method.

They are

T = .04

$$D_2(z) = 0.2625 \frac{(1 + z^{-1})}{1 - 0.2504z^{-1}}$$

and

T = .08

$$D_2(z) = 0.4562 \frac{(1 + z^{-1})}{1 + 0.3056z^{-1}}$$

In order to complete the digital design a digital filter is added to compensate for the phase and gain introduced by the zero order hold. The compensation used in this design is the simple lead-lag filter given below. Placing the pole and zero on the

$$G_c(z) = 1.3846 \frac{1 + 0.3\ z^{-1}}{1 + 0.8\ z^{-1}}$$

negative real axis inside the unit circle allows good zero-order hold compensation for small frequencies ($\omega < \frac{\omega_S}{4}$) and gain attenuation from the zero-order hold for large frequencies ($\frac{\omega_S}{4} \leq \omega \leq \frac{\omega_S}{2}$). The corresponding Nichols charts for the low Q system with T = 0.08 and 0.04 seconds are shown in Figures 2.3.1 and 2.3.2.

Max Q System

In this section the effects of digitizing the analog compensation for the max Q model are discussed. For sampling intervals of T = 0.04 and T = 0.08 seconds the digital filters for the continuous autopilot $G_c(S) = 0.6\left[\frac{8}{S+8}\right]^3$ and the compensation in the acceleration feedback loop $G_a(S) = \left[\frac{1}{S+1}\right]\left[\frac{17.5}{S+17.5}\right]$ are as follows:

T = 0.04

$$Z_{\substack{\text{Tustin's}\\ \text{Frequency}\\ \text{Pre-Warping}}}\left[G_c(s)\right] = 0.6\left[\frac{0.161379(z+1)}{1.161379z - 0.838621}\right]^3$$

$$Z_{\substack{\text{Tustin's}\\ \text{Frequency}\\ \text{Pre-Warping}}}\left[\frac{1}{s+1}\right] = \left[\frac{0.020003(z+1)}{1.020003z - 0.979997}\right]$$

$$Z_{\substack{\text{Tustin's}\\ \text{Frequency}\\ \text{Pre-Warping}}}\left[\frac{17.5}{s+17.5}\right] = \left[\frac{0.365028(z+1)}{1.365028z - 0.634972}\right]$$

T = 0.08

$$Z_{\substack{\text{Tustin's}\\ \text{Frequency}\\ \text{Pre-Warping}}}\left[G_c(s)\right] = 0.6\left[\frac{0.331389(z+1)}{1.331389z - 0.668611}\right]^3$$

$$Z_{\substack{\text{Tustin's}\\ \text{Frequency}\\ \text{Pre-Warping}}}\left[\frac{1}{s+1}\right] = \left[\frac{0.040021(z+1)}{1.040021z - 0.959979}\right]$$

$$Z_{\substack{\text{Tustin's}\\ \text{Frequency}\\ \text{Pre-Warping}}}\left[\frac{17.5}{s+17.5}\right] = \frac{0.842288(z+1)}{1.842288z - 0.157712}.$$

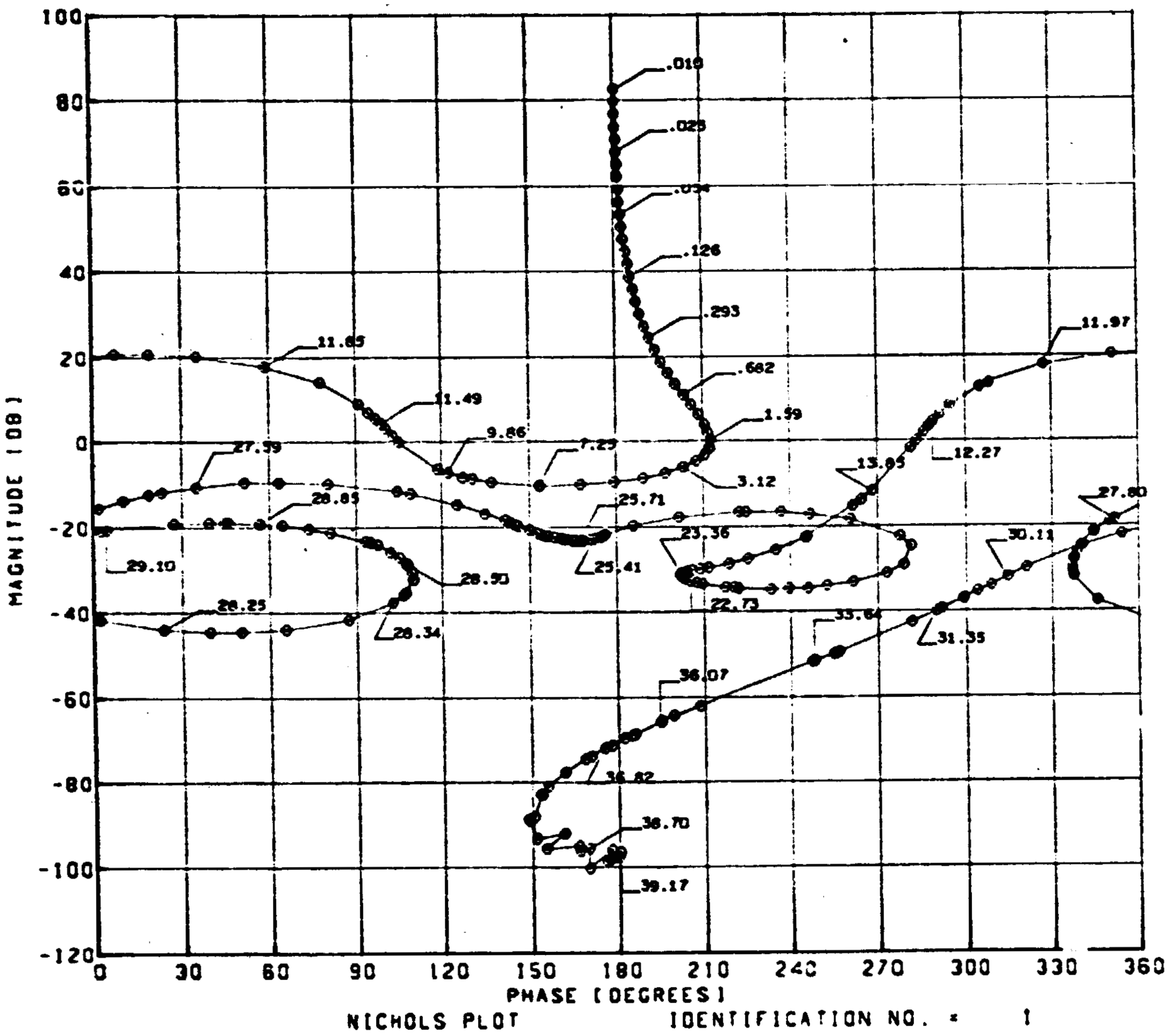

05 FEB 74

Figure 2.3.1: Digitized Continuous System Nichols Chart for Lift Off Conditions.

T = 0.08 Seconds

Gain Margin = 9.34 db @ 5.10 rad/sec
Phase Margin = 32.5°

$1.3846 \dfrac{z + 0.3}{z + 0.08}$ used to compensate ZOH effects at frequencies below $\omega_s/4$

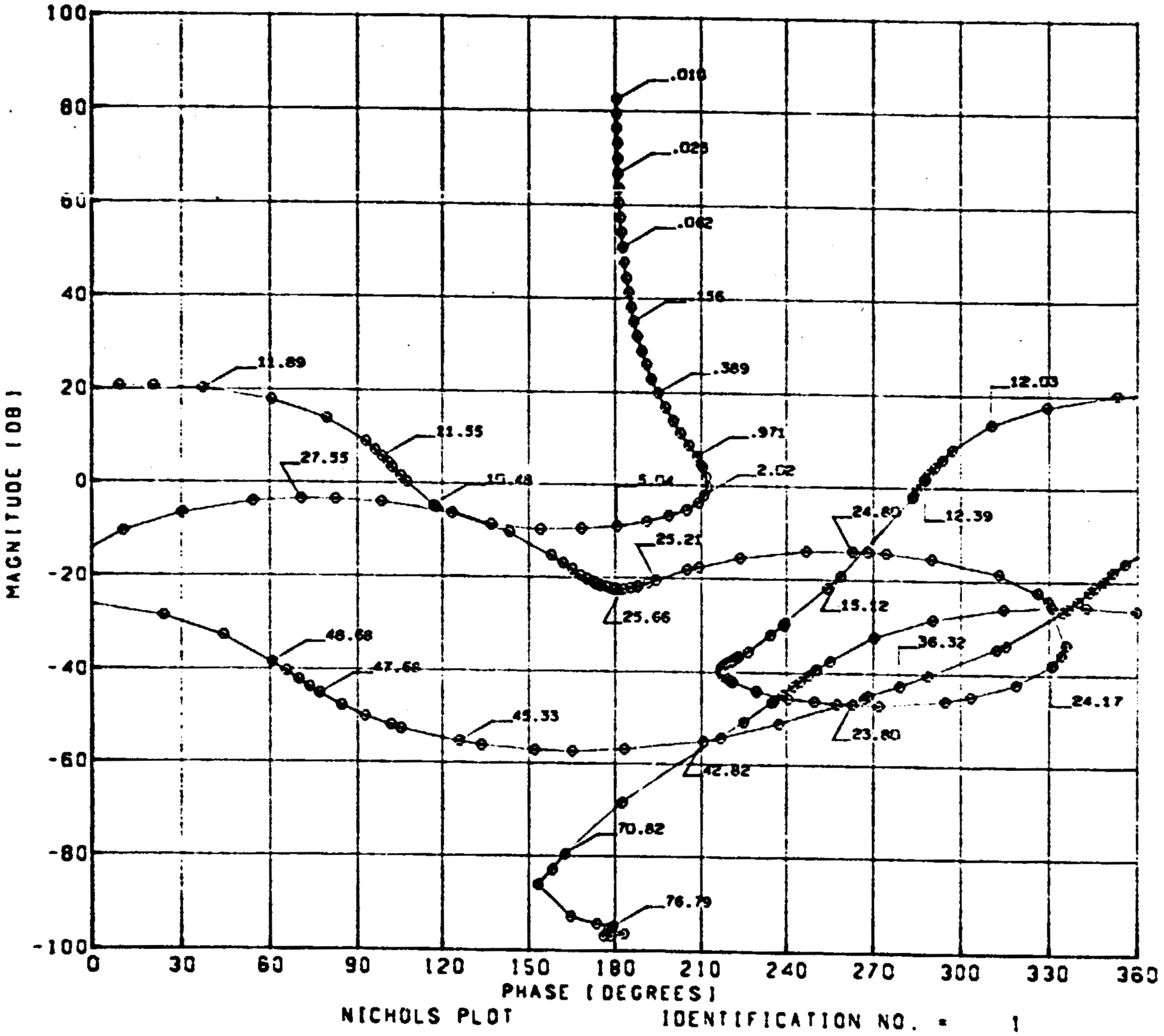

05 FEB 74

Figure 2.3.2 Digitized Continuous System Nichols Chart for Lift Off Conditions. T = 0.04 Seconds

The Nichol's charts for the max Q system with just the analog autopilots digitized are shown in Figures 2.3.3 and 2.3.4. Both frequency responses closely resemble the frequency response of the continuous system shown in Figure 2.1.4.

The effects of including the digital compensation in the accelerometer feedback loop are shown in Figures 2.3.5 through 2.3.10. Figures 2.3.5 and 2.3.6 show the frequency response of the max Q system with one of the lag filters of $G_a(s)$ digitized. The Nichol's chart of the system with Tustin's Frequency Pre-Warping $\left[\frac{1}{s+1}\right]$ is shown in Figure 2.3.5 and the frequency response with Tustin's Frequency Pre-Warping $\left[\frac{17.5}{s+17.5}\right]$ is shown in Figure 2.3.6.

In Figures 2.3.7 and 2.3.8 both lag filters in the acceleration compensation are digitized. The compensation for the zero-order hold is given below and is the same lead-lag filter used with the lift-off flight model.

$$G_{ZOH} = 1.3846 \frac{z + 0.3}{z + 0.8}$$

Digitizing the compensation in the acceleration feedback loop illustrates an important point which should be kept in mind when using Tustin's method to synthesize digital first order lag filters. If the object is to design compensation for a sample data system, using Tustin's method with frequency pre-warping is the same as designing in the w-plane. If Tustin's method with frequency pre-warping is used to digitize analog compensation, however, the resulting digital filter is used to approximate the analog filter's frequency response. Usually this is a good approximation. As shown in Figures 2.3.3 through 2.3.6 the rigid mode gain and phase margin for the partially digitized max Q system differs slightly from the phase and gain margins of the continuous system. When all of the analog compensation is digitized, however, the approximation begins to break down. For T = 0.04 seconds the gain margin drops from 9.14 db to 6.12 db and the phase margin from 51.16° to 42.69°. In addition, the loop at 8 radians/sec. present in Figures 2.3.3 through 2.3.6 is missing in Figures 2.3.7 and 2.3.8. This results from a pair of complex zeros located inside the unit circle near 8 radians/sec. moving outside the unit circle when all of the analog compensation

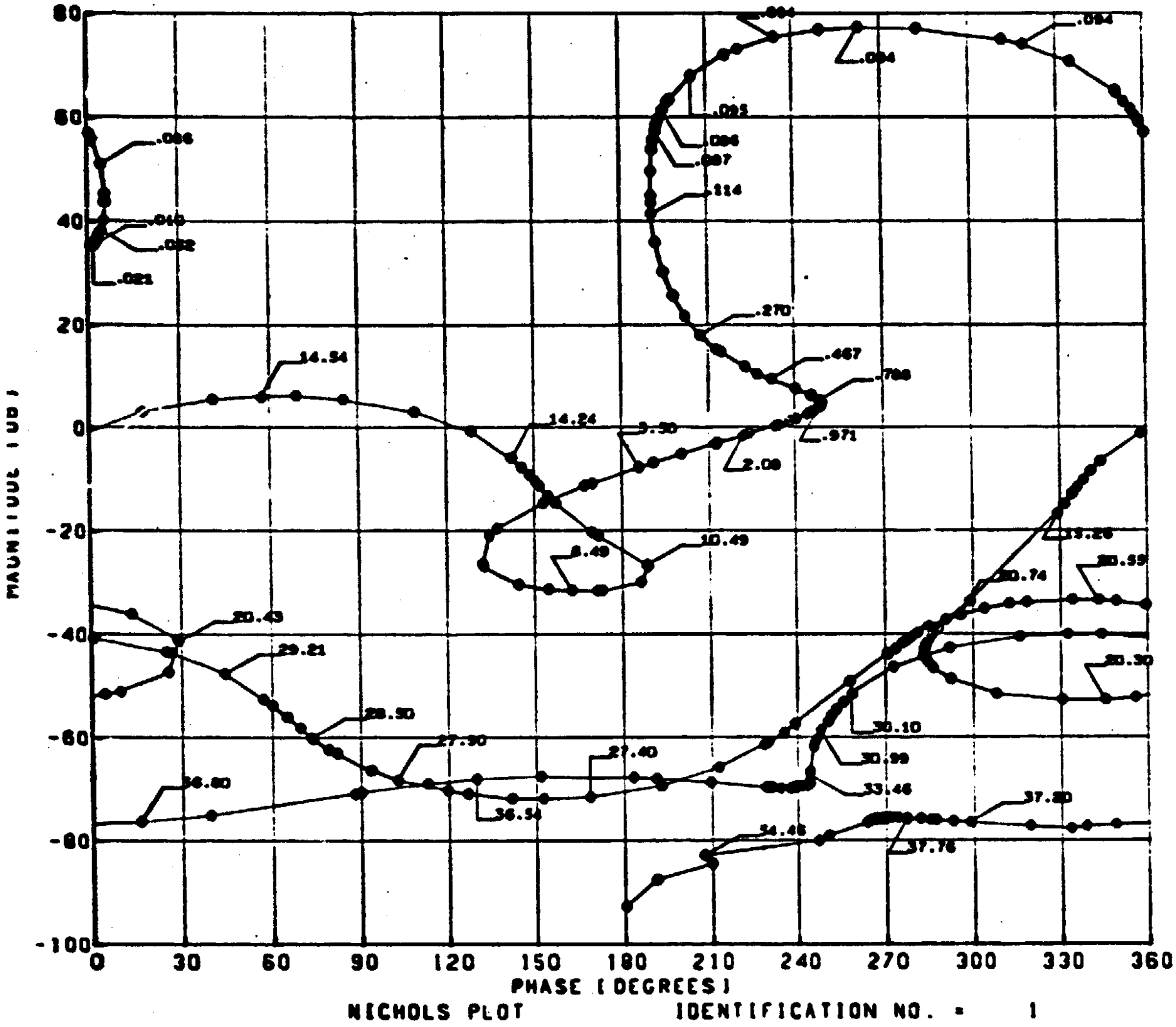

Figure 2.3.3: 17 MAY 74

Nichols Chart for Max Q System with Continuous Autopilot Digitized using Tustin's Frequency Pre-Warping Method, T = 0.04

Gain Margin = 8.73 db @ 3.74 rad/sec

Phase Margin = 50.24°

$1.3846 \ \frac{z+0.3}{z+0.8}$ used for ZOH Compensation

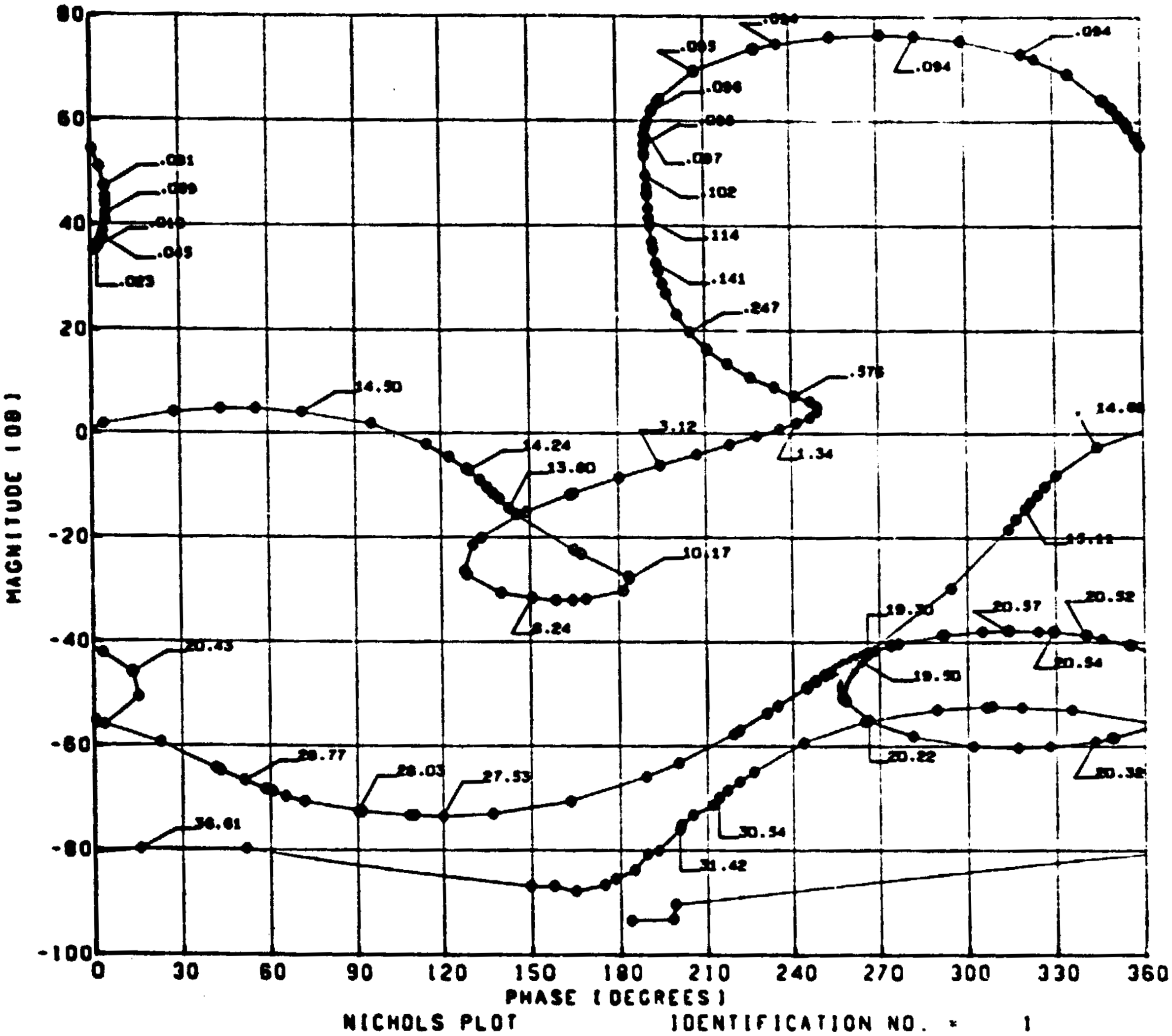

17 MAY 74

Figure 2.3.4: Nichol's Chart for Max Q System with Continuous Autopilot Digitized using Tustin's Frequency Pre-Warping Method, T = 0.08

Gain Margin = 8.45 db @ 3.69 rad/sec
Phase Margin = 50°

$$1.3846 \; \frac{z + 0.3}{z + 0.8}$$ used for ZOH Compensation

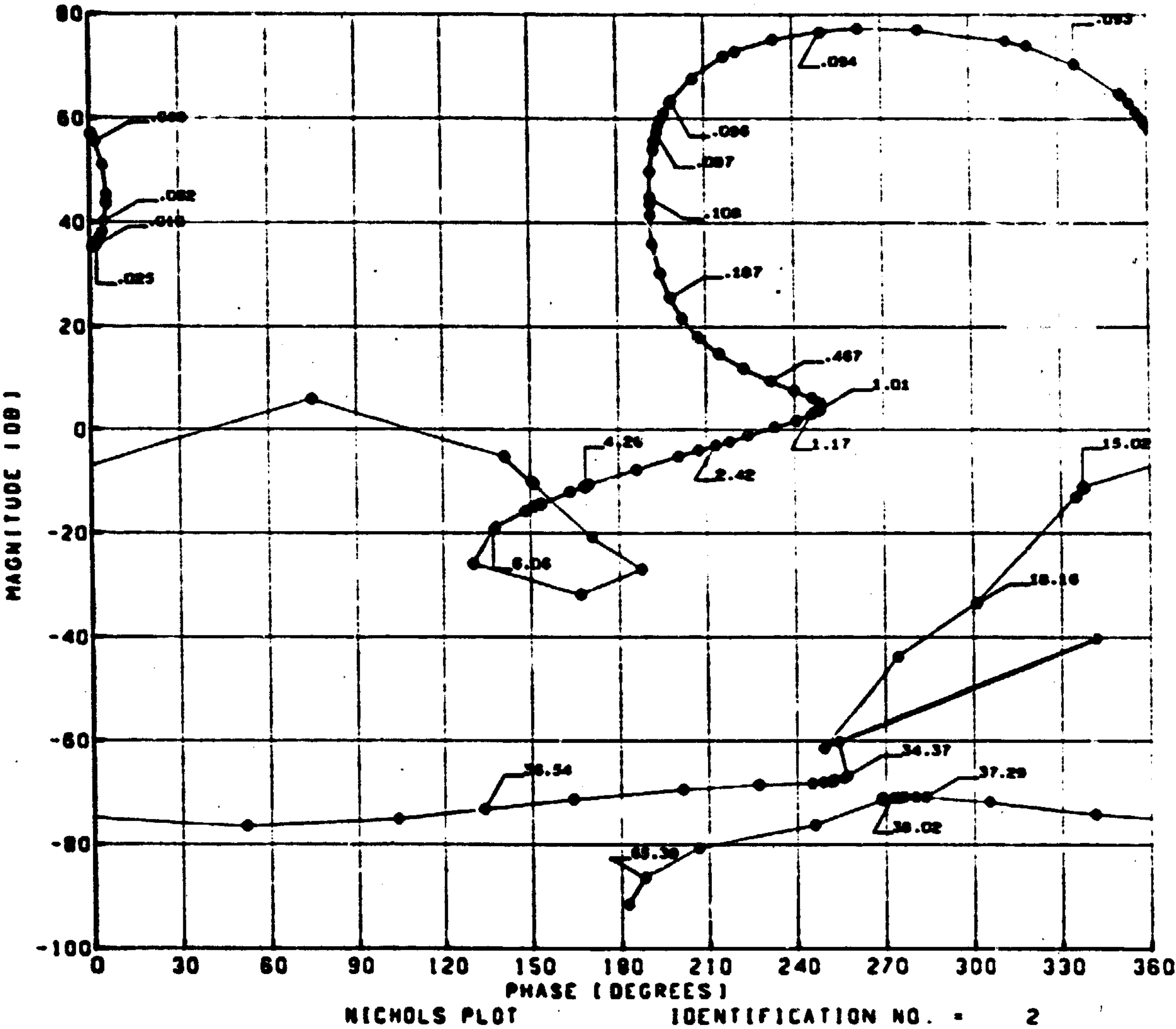

28 MAY 74

Figure 2.3.5: Nichol's Chart for Max Q System with Continuous Autopilot and $\left[\frac{1}{s+1}\right]$ Digitized using Tustin's Frequency Pre-Warping Method, T = 0.04

Gain Margin = 8.679 db @ 3.75 rad/sec
Phase Margin = 50.26°

$1.3846 \frac{z + 0.3}{z + 0.8}$ used for ZOH Compensation

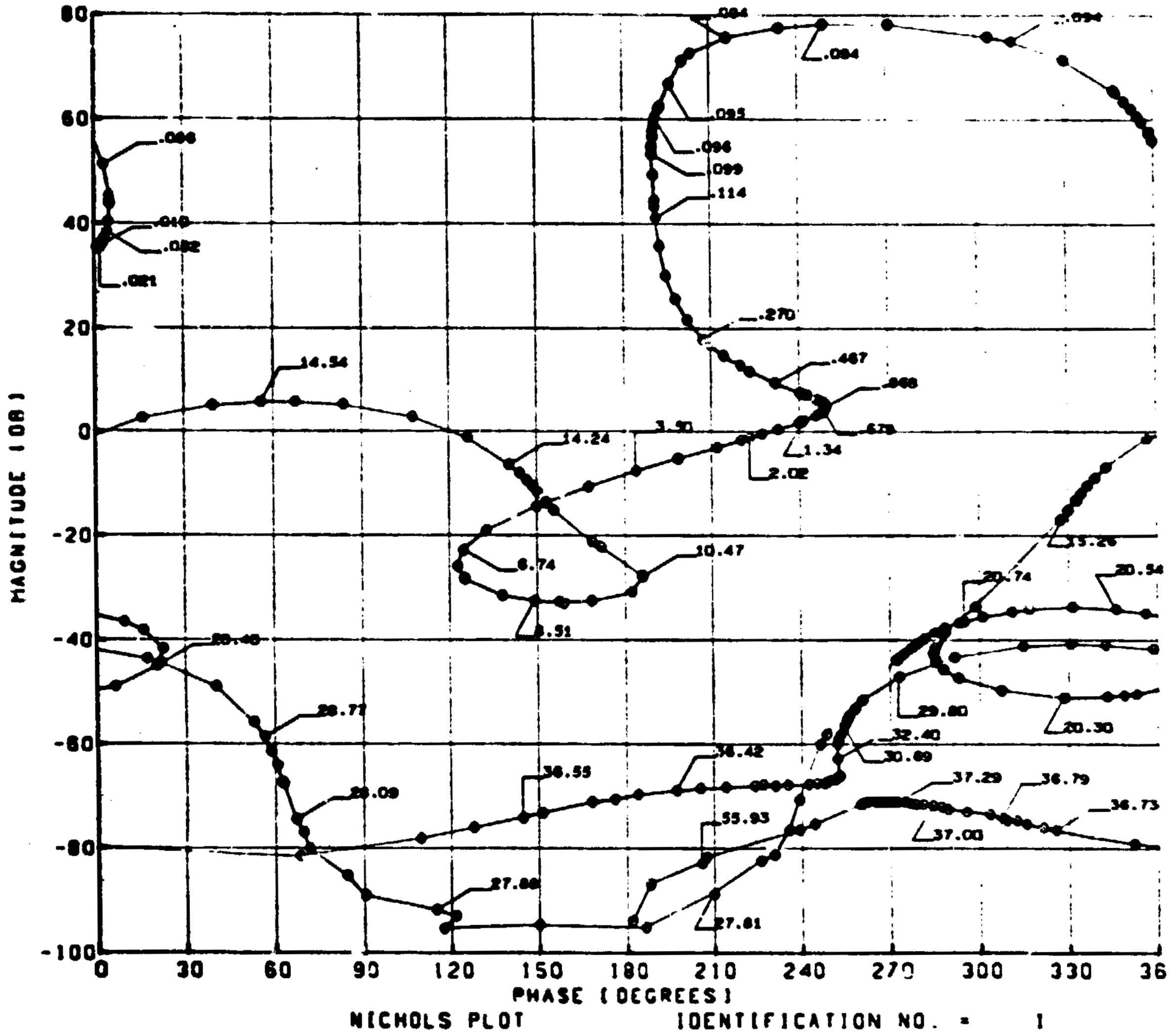

28 MAY 74

Figure 2.3.6: Nichol's Chart for Max Q System with Cor tinuous Autopilot and $\left[\frac{17.5}{s + 17.5}\right]$ Digitized using Tustin's frequency Pre-Warping Method, T = 0.04

Gain Margin = 8.221 db @ 3.66 rad/sec
Phase Margin = 49.11°

$1.3846 \frac{z + 0.3}{z + 0.8}$ used for ZOH Compensation

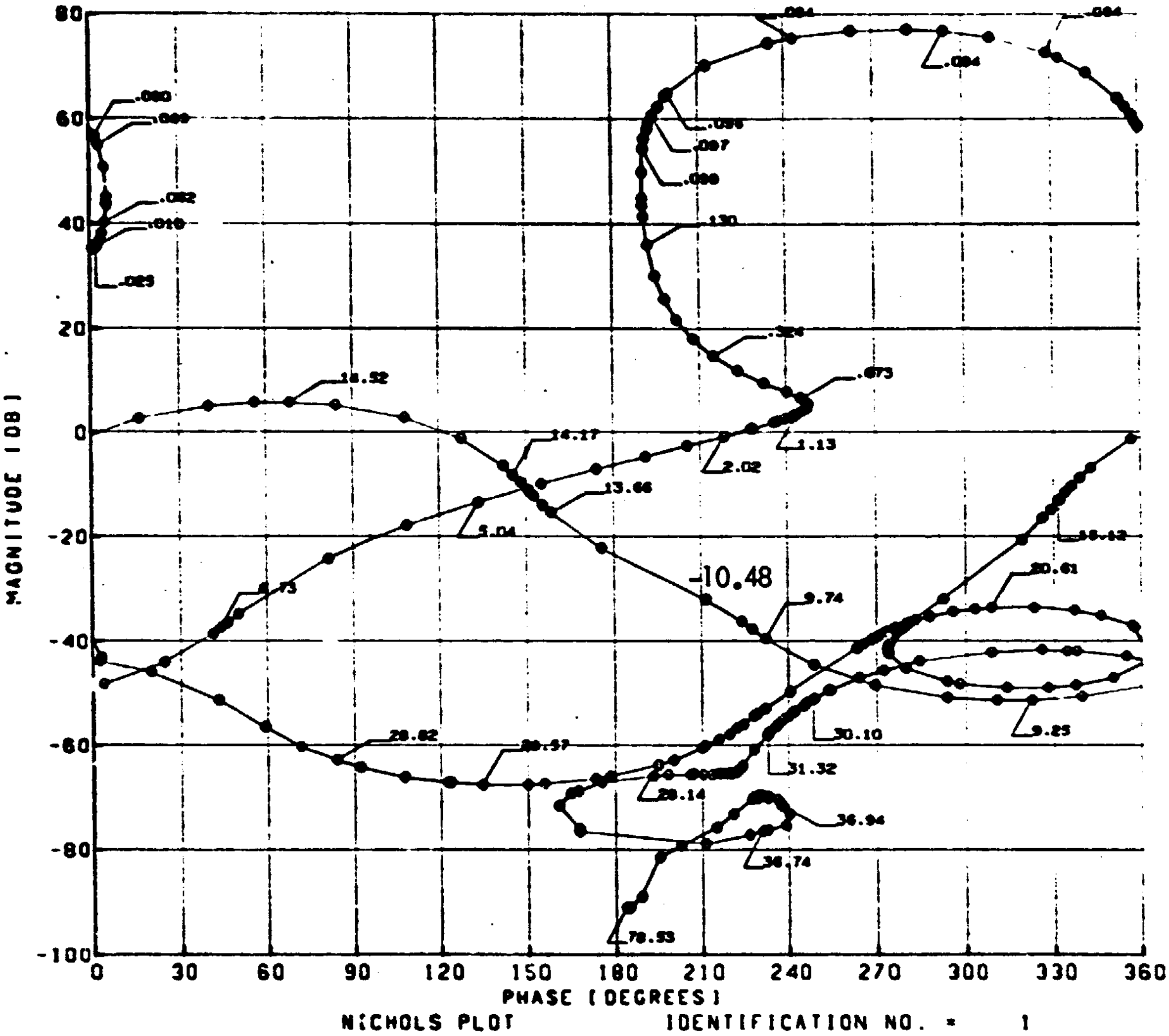

Figure 2.3.7:

19 MAY 74

Nichols Chart for Max Q System with Continuous Autopilot and Acceleration Compensation Digitized using Tustin's Frequency Pre-Warping Method, T = 0.04

Gain Margin = 6.123 db @ 3.29 rad/sec
Phase Margin = 42.69°

$1.3846 \dfrac{z + 0.3}{z + 0.8}$ used for ZOH Compensation

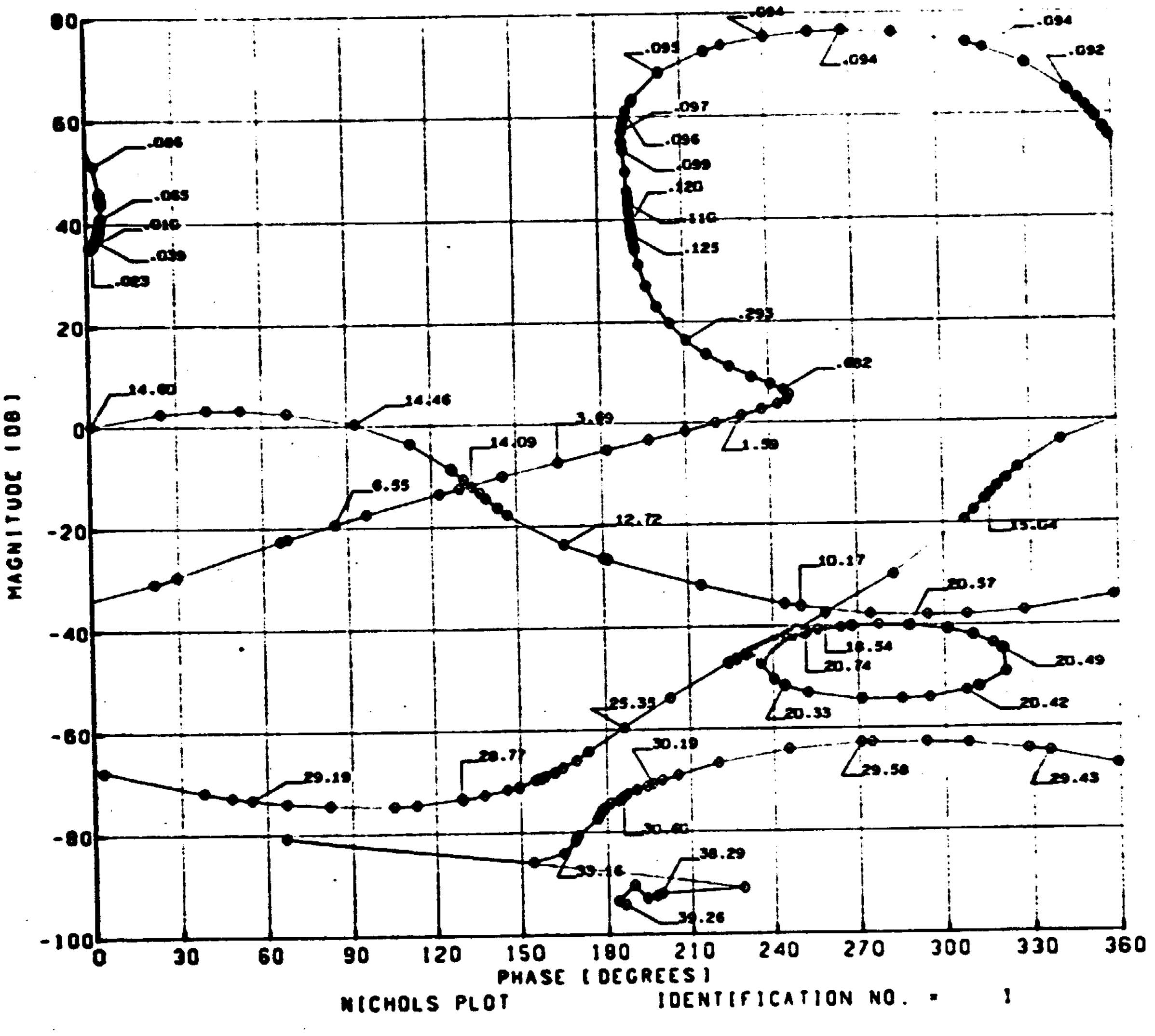

Figure 2.3.8: Nichol's Chart for Max Q System with Continuous Autopilot and Acceleration Compensation Digitized using Tustin's Frequency Pre-Warping Method, T = 0.08

21 MAY 74

Gain Margin = 5.392 db @ 3.17 db

Phase Margin = 40°

$1.3846 \dfrac{z + 0.3}{z + 0.8}$ used for ZOH Compensation

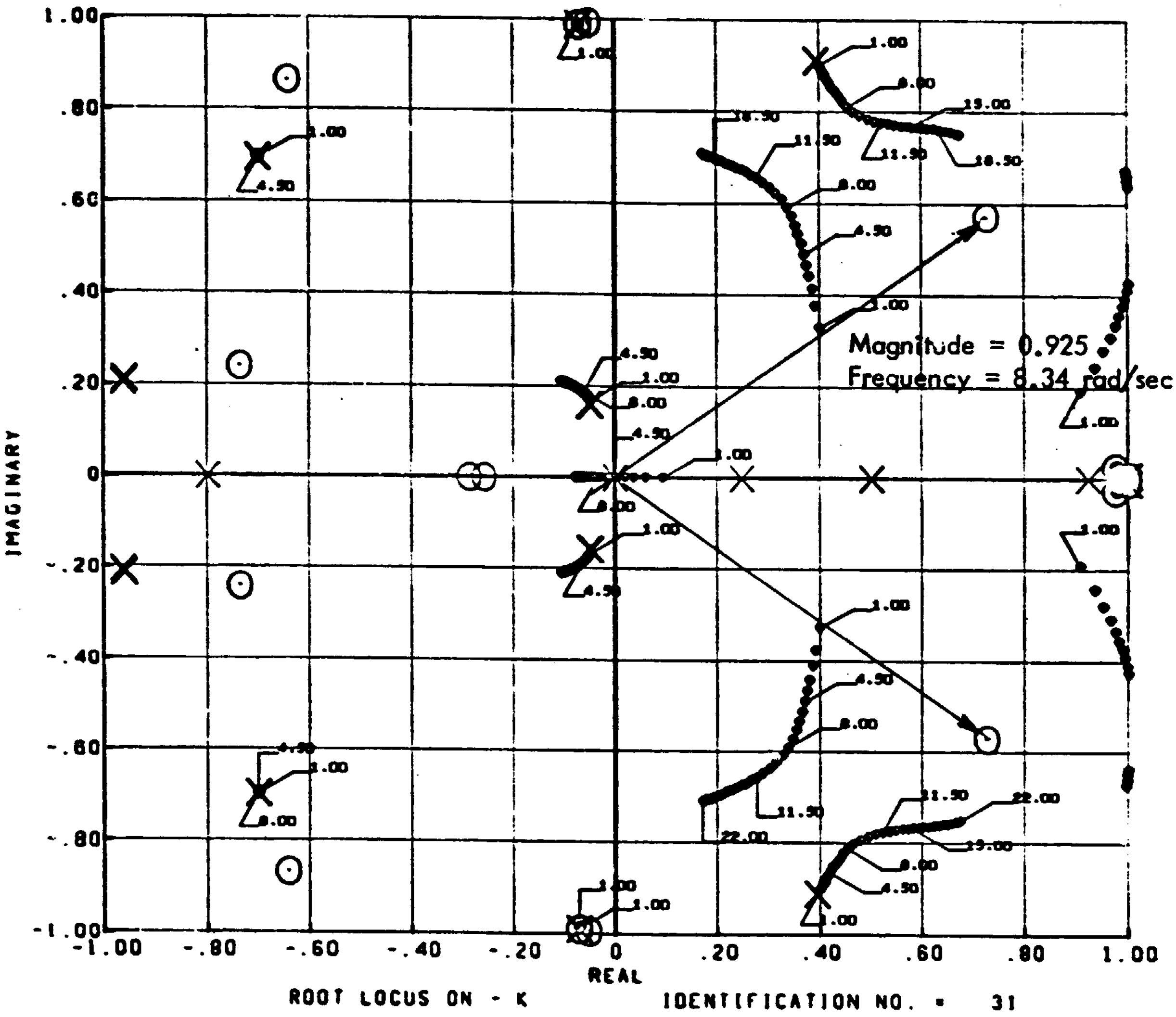

17 MAY 74

Figure 2.3.9: Root Locus for Max Q System with Continuous Autopilot Digitized using Tustin's Frequency Pre-Warping Method, T = 0.08

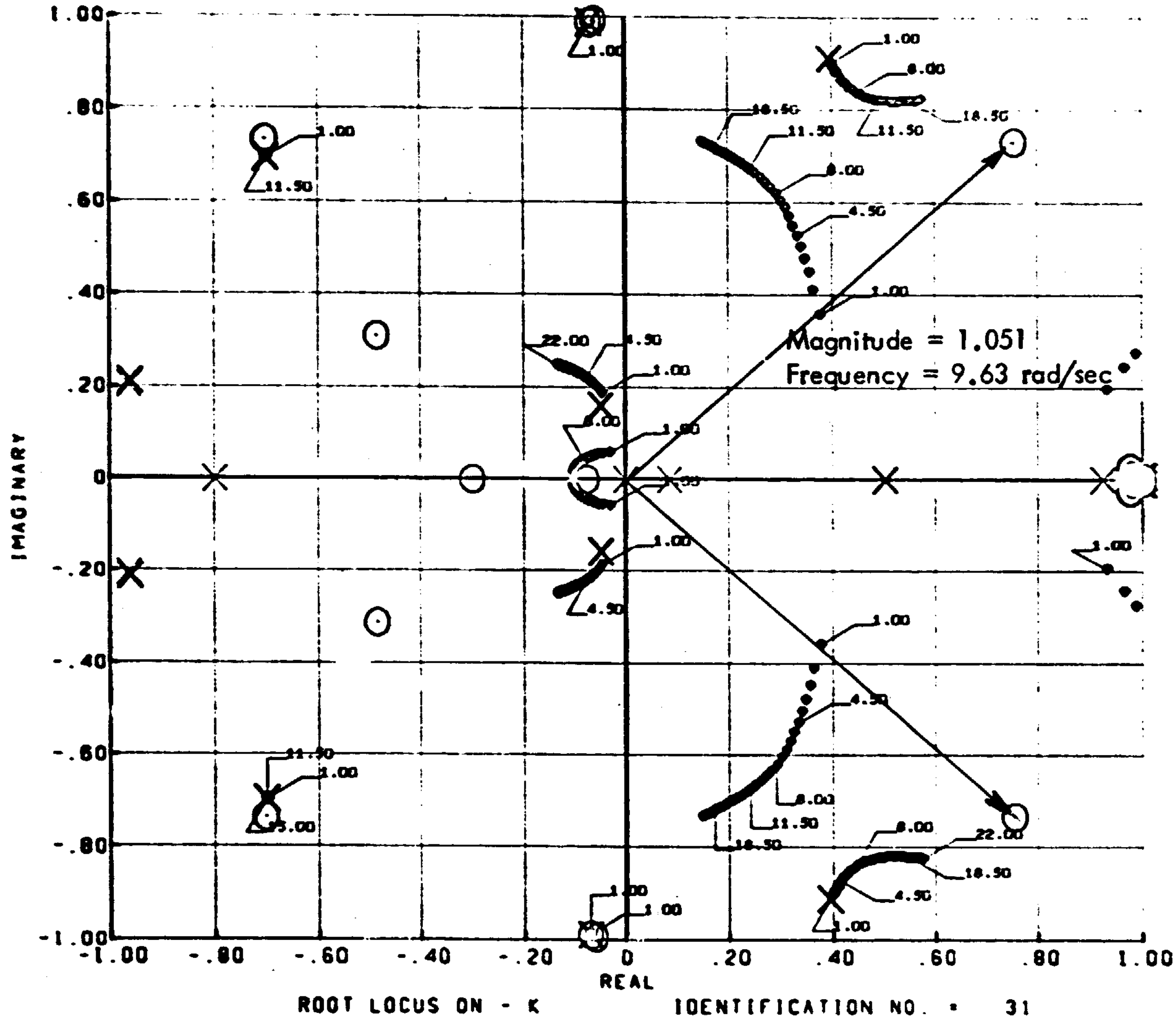

21 MAY 74

Figure 2.3.10: Root Locus for Max Q System with Continuous Autopilot and Acceleration Compensation Digitized using Tustin's Frequency Pre-Warping Method, T = 0.08

is digitized. The root locus of the max Q system with just the continuous autopilot digitized and the root locus with all of the compensation digitized illustrate this point. They are respectively shown in Figures 2.3.9 and 2.3.10 for T = 0.08.

2.4 Digital Autopilot Design for the Low Q Model

As a starting point in the design of a digital autopilot, frequency response plots are run for the low Q model with the analog compensation replaced with a sampler and zero-order hold. The block diagram of the system is shown in Figure 2.4.1. The uncompensated frequency response plots are shown in Figures 2.4.2 and 2.4.3 where the loop has been opened at K. From these plots it is seen that compensation which would phase and gain stabilize the rigid mode and first body bending mode and in addition reduce the system gain at frequencies above 11.50 radians/second is required.

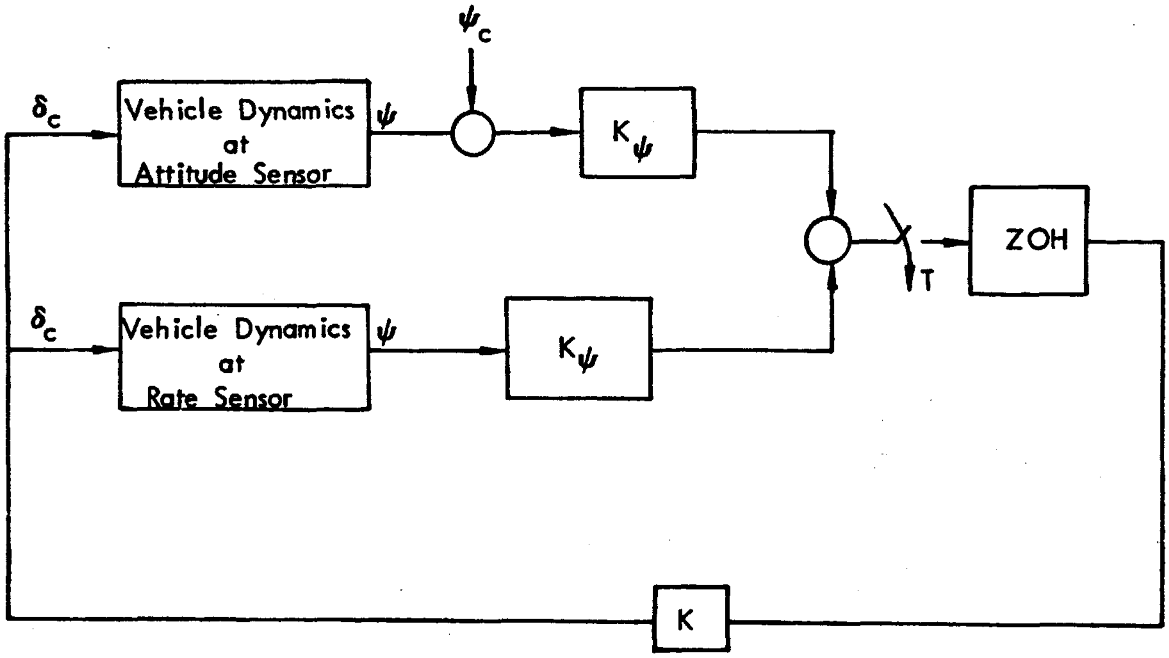
ψ_c
δ_c
Vehicle Dynamics at Attitude Sensor
ψ
K_ψ
ZOH
T
δ_c
Vehicle Dynamics at Rate Sensor
ψ
K_ψ
K

Figure 2.4.1: Block Diagram of Uncompensated Low Q System

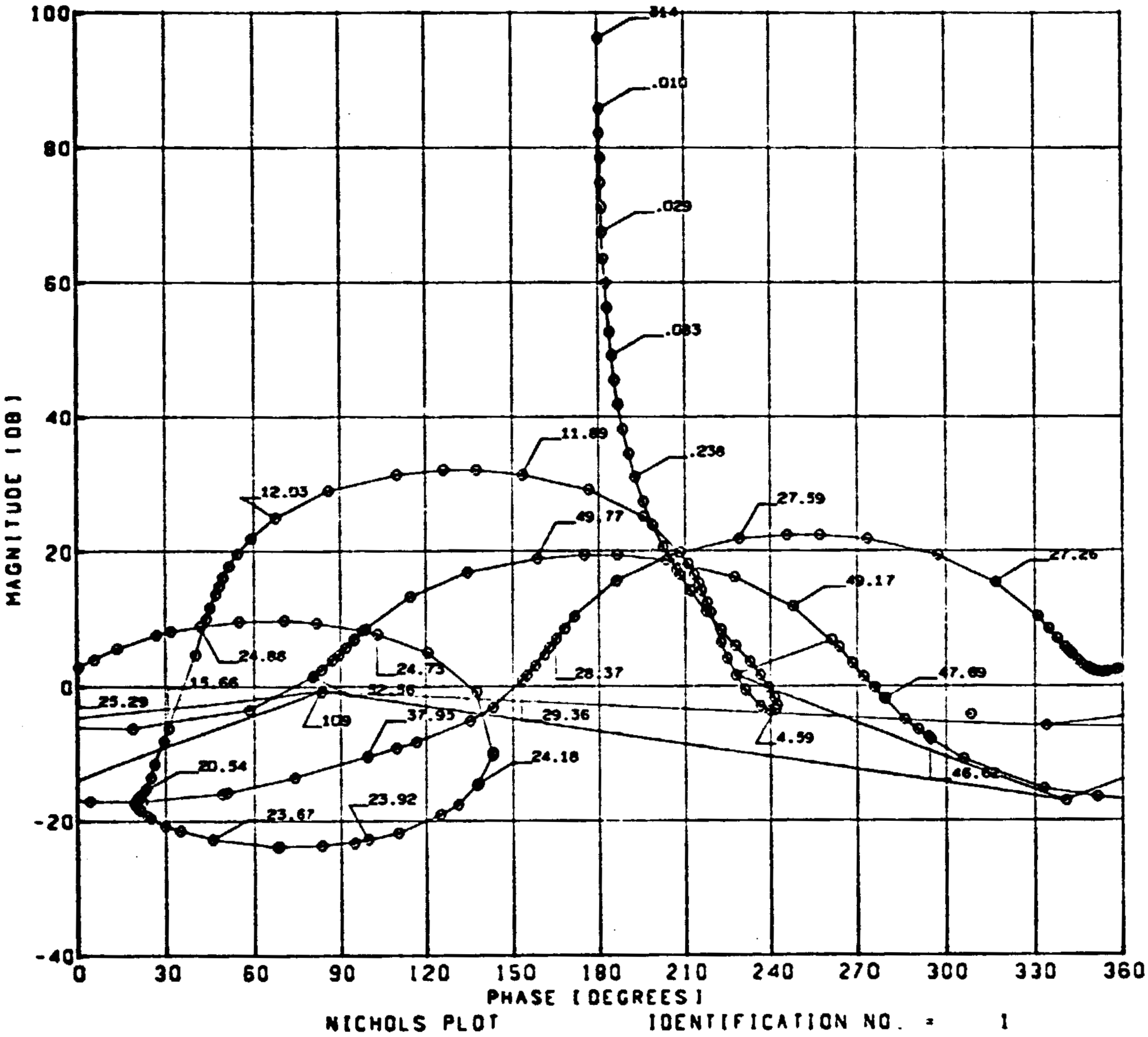

04 FEB 74

Figure 2.4.2 Nichols Chart for Uncompensated System T = .04 Seconds

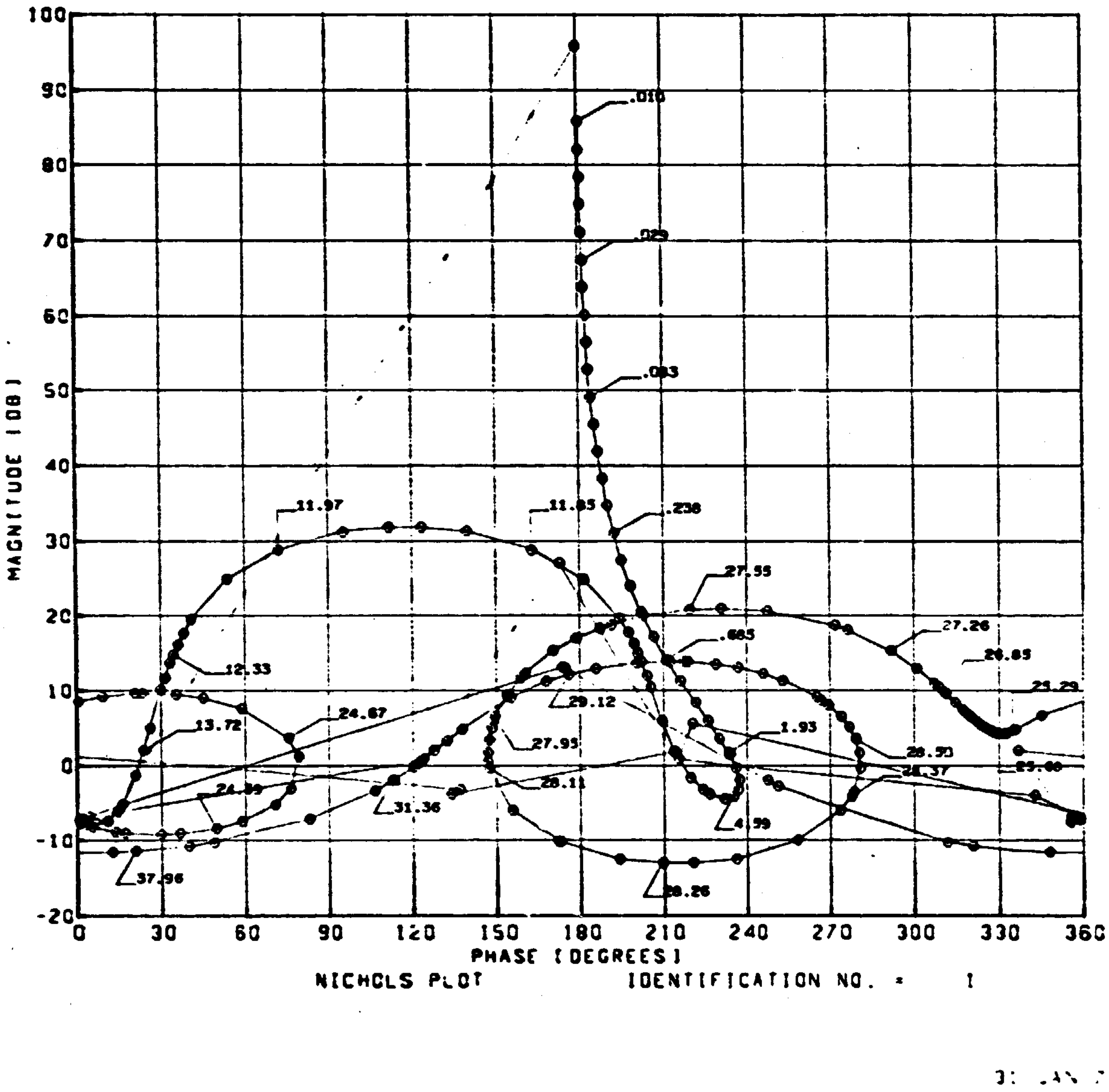

Figure 2.4.3 Nichols Chart for Uncompensated System T = .08 Seconds

Digital System Design for T = 0.08 Seconds

Based upon studying the frequency response in Figure 2.4.3 the rigid mode is phase and gain stabilized with the digital equivalent of the following s-plane filter.

$$G(s) = 0.6764 \left(\frac{8}{S + 8}\right) \left(\frac{12}{S + 12}\right)$$

The digitized version of this filter using Tustin's method with frequency scale prewarping is as follows:

$$G(z) = 0.6764 \left(\frac{0.2489\ Z + 0.2489}{Z - 0.50219}\right) \left(\frac{0.34237\ Z + 0.34237}{Z - 0.3153}\right)$$

The Nichol's chart is shown in Figure 2.4.4.

It was noted in Section 2.2 that a small sampling frequency will cause analog break frequencies to fold into the primary strip. This is the case for T = 0.08 seconds. The body bending poles at ±49.67 rad/sec. in the continuous system fold into the primary strip at ±28.87 rad/sec. for the digital system, near the vicinity of the second and third body bending poles. This presents an advantage in designing the body bending mode compensation. By introducing a notch filter at 27.5 rad/sec., additional gain margin is given to each of the three higher body bending modes as well as introducing phase lag to the first body bending mode. The phase lag from the notch filter is used to help center the first body bending mode about the -1 point on the Nichol's chart. Figures 2.4.5 and 2.4.6 show the exploded root locus of the rigid mode compensated system and the rigid mode compensated system with a digital notch filter included. The zeros located at $z = -0.580 \pm j\ 0.750$ pull the body bending poles at ±27.54 rad/sec away from the unit circle at right angles for small values of the open loop gain K. This makes the gain margin of the third body bending mode very sensitive to K. The location of the complex poles to complete the digital notch filter are placed along the constant frequency lines at $z = -0.4738 \pm j\ 0.6446$. The digital notch filter then becomes

$$D_3\ (z) = \frac{0.8459z^2 + 0.98127z + 0.76040}{z^2 + 0.94758z + 0.64}$$

The corresponding Nichol's chart is shown in Figure 2.4.7.

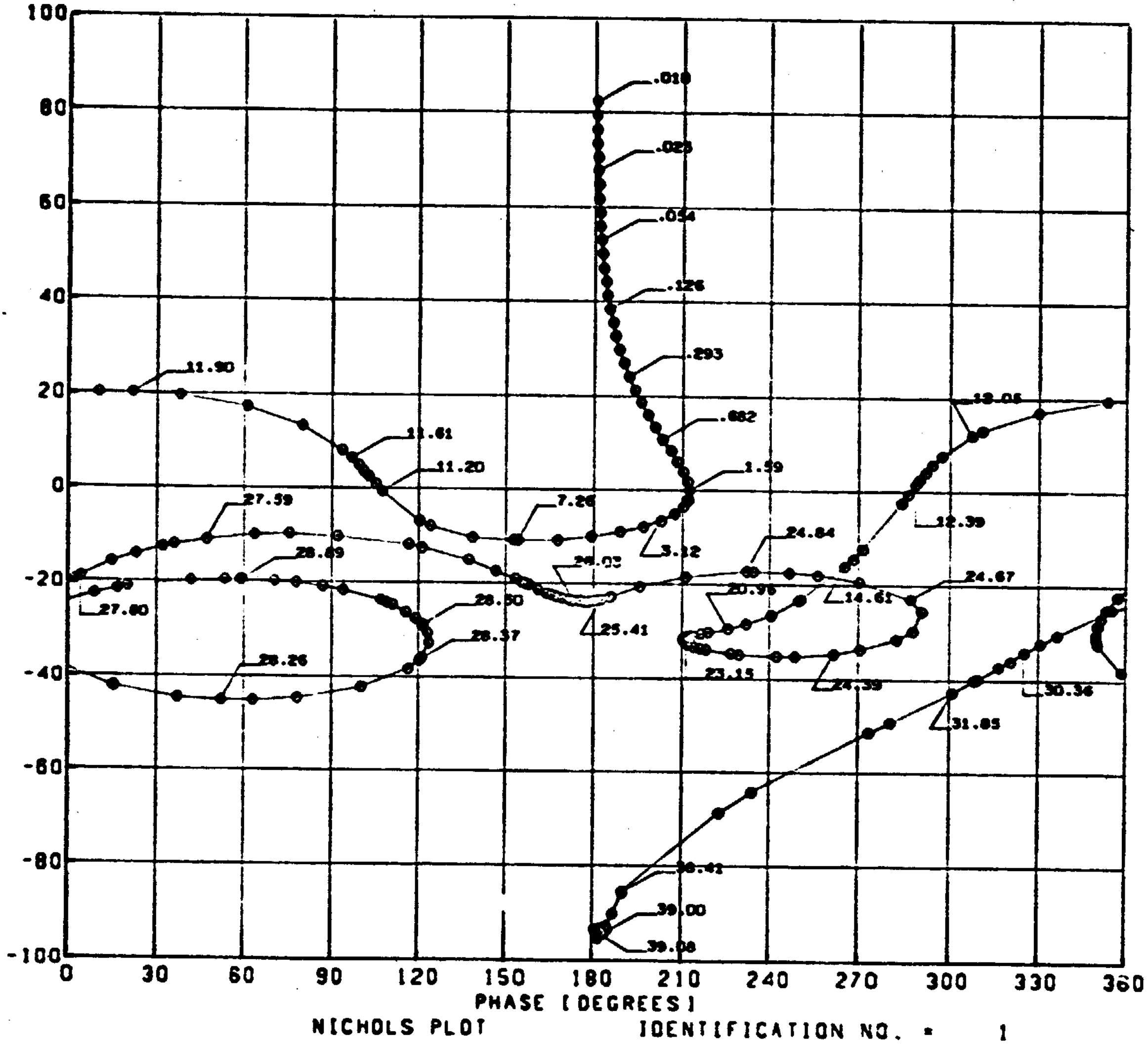

FIGURE 2.4.4:

27 FEB 74

NICHOL'S CHART OF DIGITIZED AUTOPILOT USED FOR RIGID MODE COMPENSATION,

T = 0.08

Gain Margin = 8.92 db @ 5.08 rad/sec

Phase Margin = 32.2°

$$\text{Autopilot} = \mathcal{Z}_{\substack{\text{Tustin's}\\ \text{Freq.}\\ \text{Pre-warp}}} \left[\frac{12}{S+12} \cdot \frac{8}{S+8} \right]$$

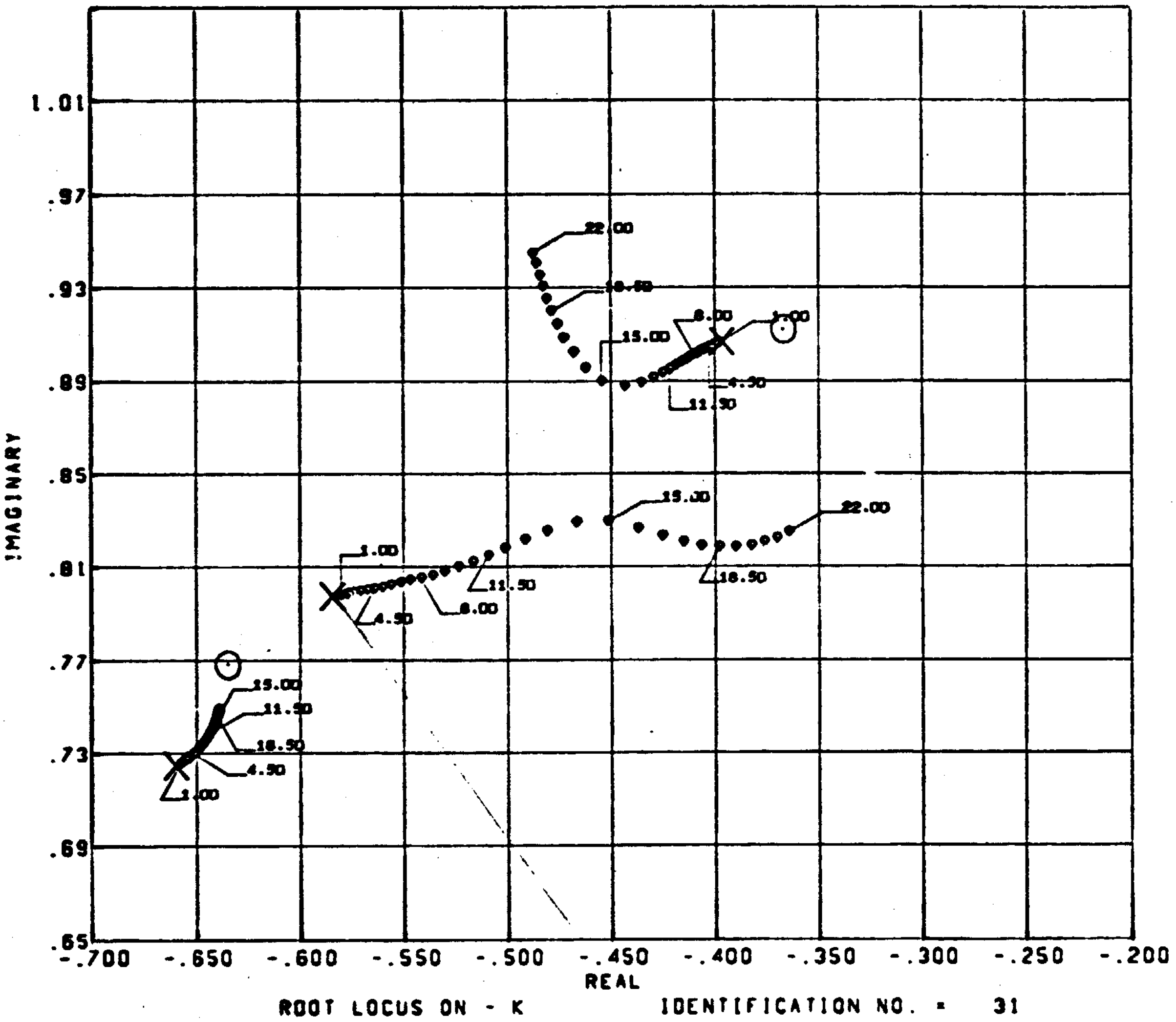

FIGURE 2.4.5:

27 FEB 74

EXPLODED ROOT LOCUS OF DIGITIZED AUTOPILOT USED FOR RIGID MODE COMPENSATION , T = 0.08

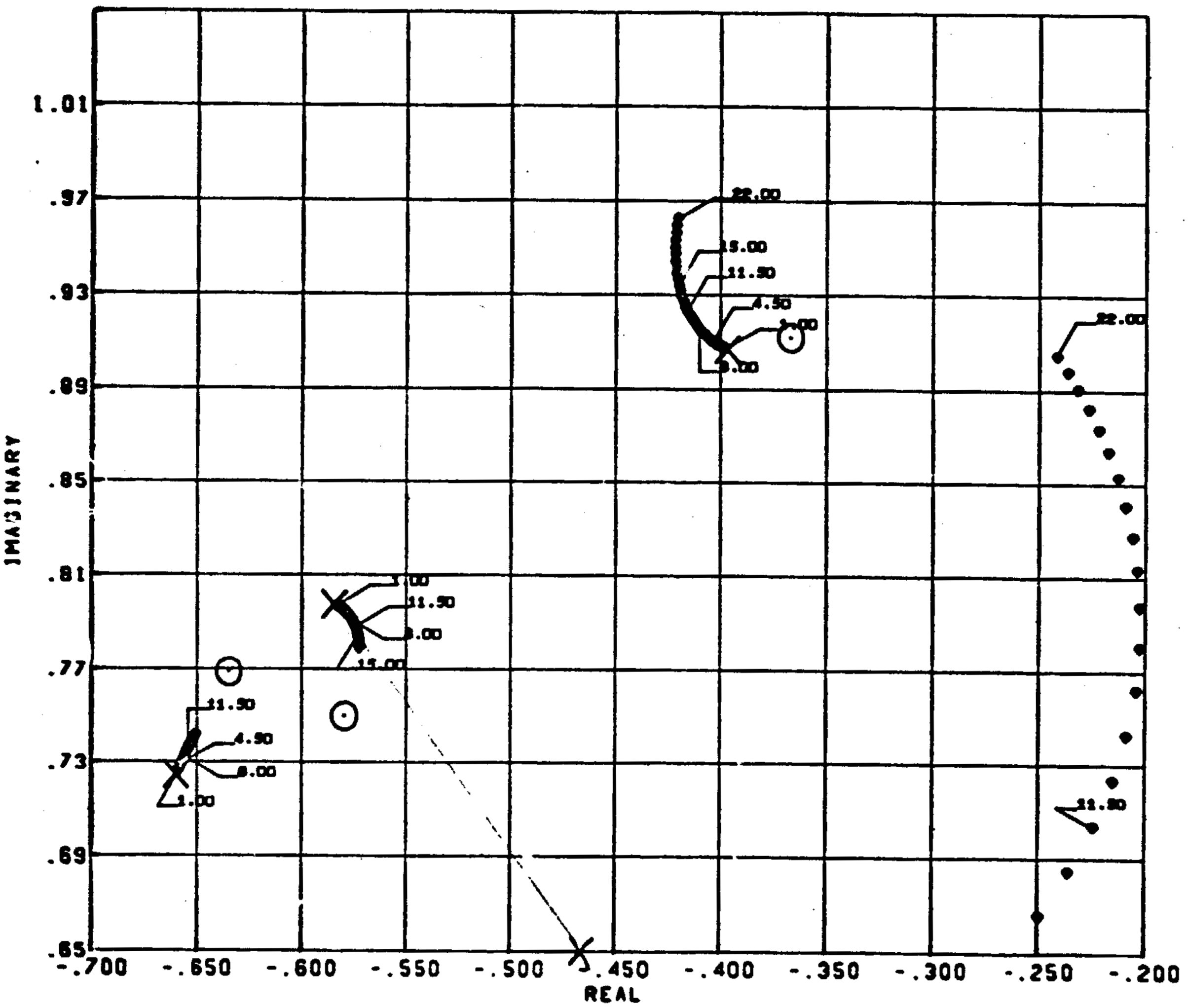

ROOT LOCUS ON - K IDENTIFICATION NO. = 31

25 FEB 74

FIGURE 2.4.6

EXPLODED ROOT LOCUS OF DIGITIZED AUTOPILOT FOR RIGID AND BODY BENDING MODE COMPENSATION, T = 0.08

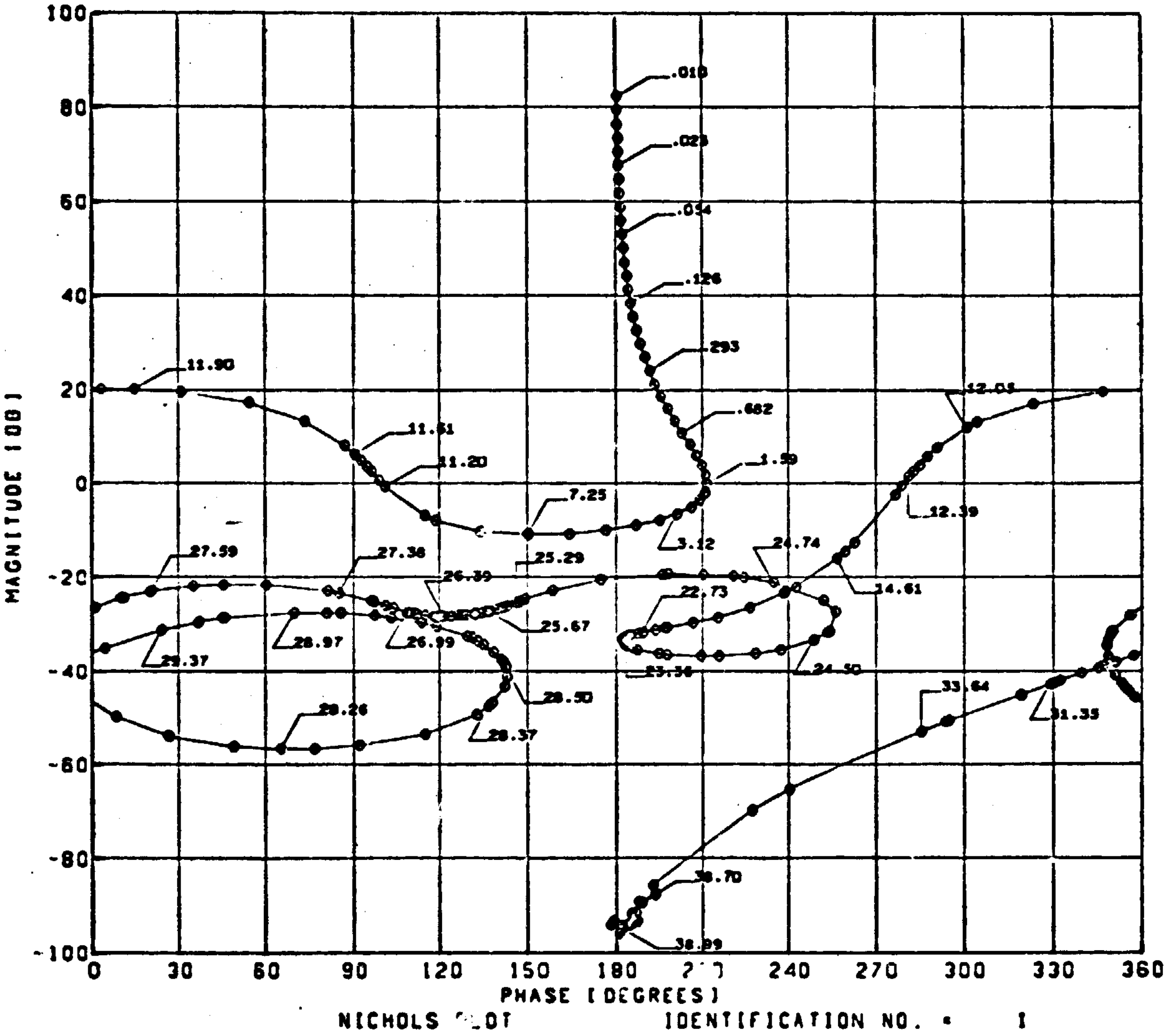

27 FEB 74

Figure 2.4.7: Rigid and Body Bending Mode Compensated Lift Off System, T = 0.08

Gain Margin = 9.58 db @ 4.88 rad/sec
Phase Margin = 31.4°

First Body Bending Mode Phase Margins = +100°, -80°

Gain Margins

+19.25 db @ 24.83 rad/sec
+21.42 db @ 27.53 rad/sec

Digital System Design for T = 0.04 Seconds

This section provides a digital autopilot design for the low Q model at T = 0.04 seconds. In Section 2.5 the design is combined with the autopilot design at T = 0.08 seconds to provide a multirate digital autopilot for the low Q model.

As a starting point in designing a digital autopilot the phase and gain margins are set for the systems rigid mode. This is accomplished by the digital equivalent of the following s-plant filter

$$G(s) = 0.8279 \left(\frac{8}{s+8}\right) \cdot \left(\frac{12}{s+12}\right)$$

The digitized version of this filter using Tustin's method with frequency scale pre-warping is as follows.

$$G(z) = 0.8279 \left(\frac{0.13895z + 0.13895}{z - 0.722090}\right) \left(\frac{0.19660z + 0.19660}{z - 0.606791}\right)$$

The corresponding Nichol's chart is shown in Figure 2.4.8.

To increase the gain margin of the three higher body bending modes a digital notch filter is used. Figures 2.4.9 and 2.4.10 respectively show the root locus of the rigid mode compensated system and the rigid and body bending mode compensated system.

For the rigid mode compensated system the body bending poles at ±27.54 rad/sec migrate outside the unit circle for a small value of K. This is evident from both the root locus in Figure 2.4.9 and the Nichol's chart in Figure 2.4.8. In Figure 2.4.10 the body bending poles at ±27.54 rad/sec are pulled into the compensation zeros located at $z = +0.4000 \pm j\,0.8500$. This keeps the third body bending poles inside the unit circle. The location of the complex poles to complete the digital notch filter are placed at $z = +0.3500 \pm j\,0.4873$. The complete digital notch filter is given by D(z).

$$D(z) = \left(\frac{z^2 - 0.800z + 0.8825}{z^2 - 0.700z + 0.3600}\right)$$

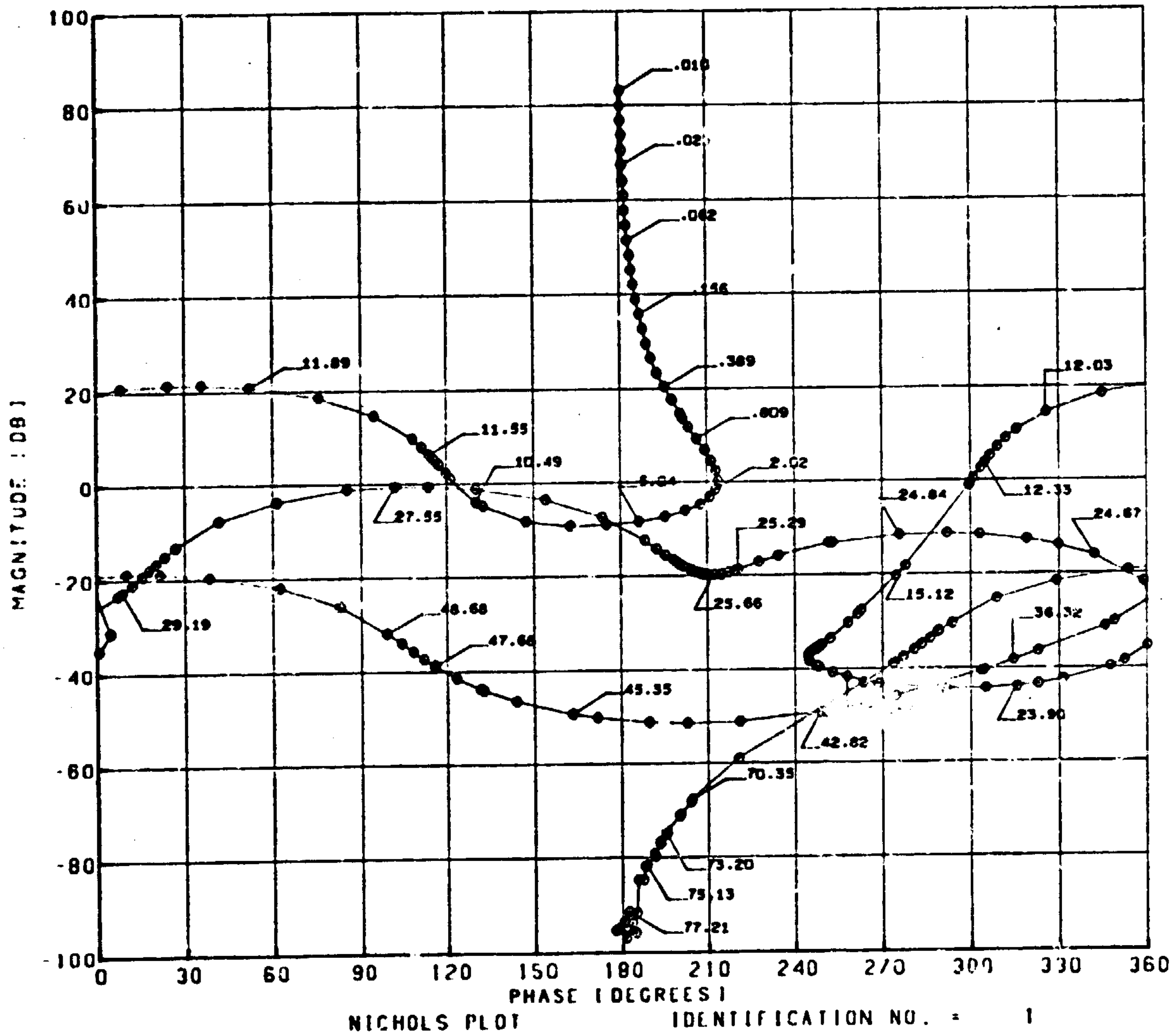

20 JUN 74

Figure 2.4.8: Nichol's Chart of Rigid Mode Compensated Lift Off System, T = 0.04 Seconds

Gain Margins = 8.69 db @ 5.61 rad/sec
Phase Margins = 33.6°

First Body Bending Mode Phase Margins = -57° and +120°

Third Body Bending Mode Gain Margin = +0.52 db

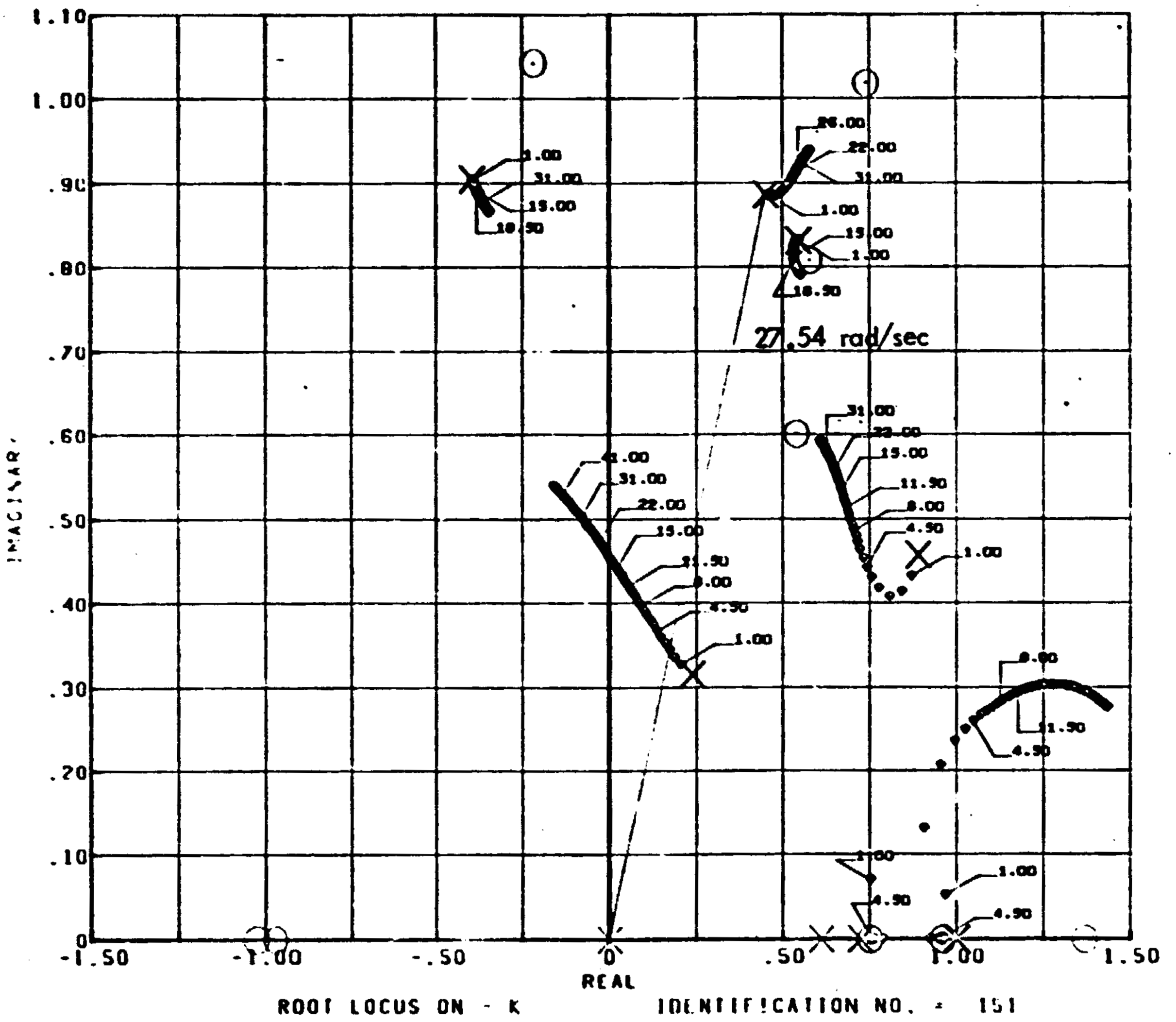

ROOT LOCUS ON - K IDENTIFICATION NO. = 151

20 JUN 74

Figure 2.4.9: Root Locus of Rigid Mode Compensated Lift Off System T = 0.04 Seconds

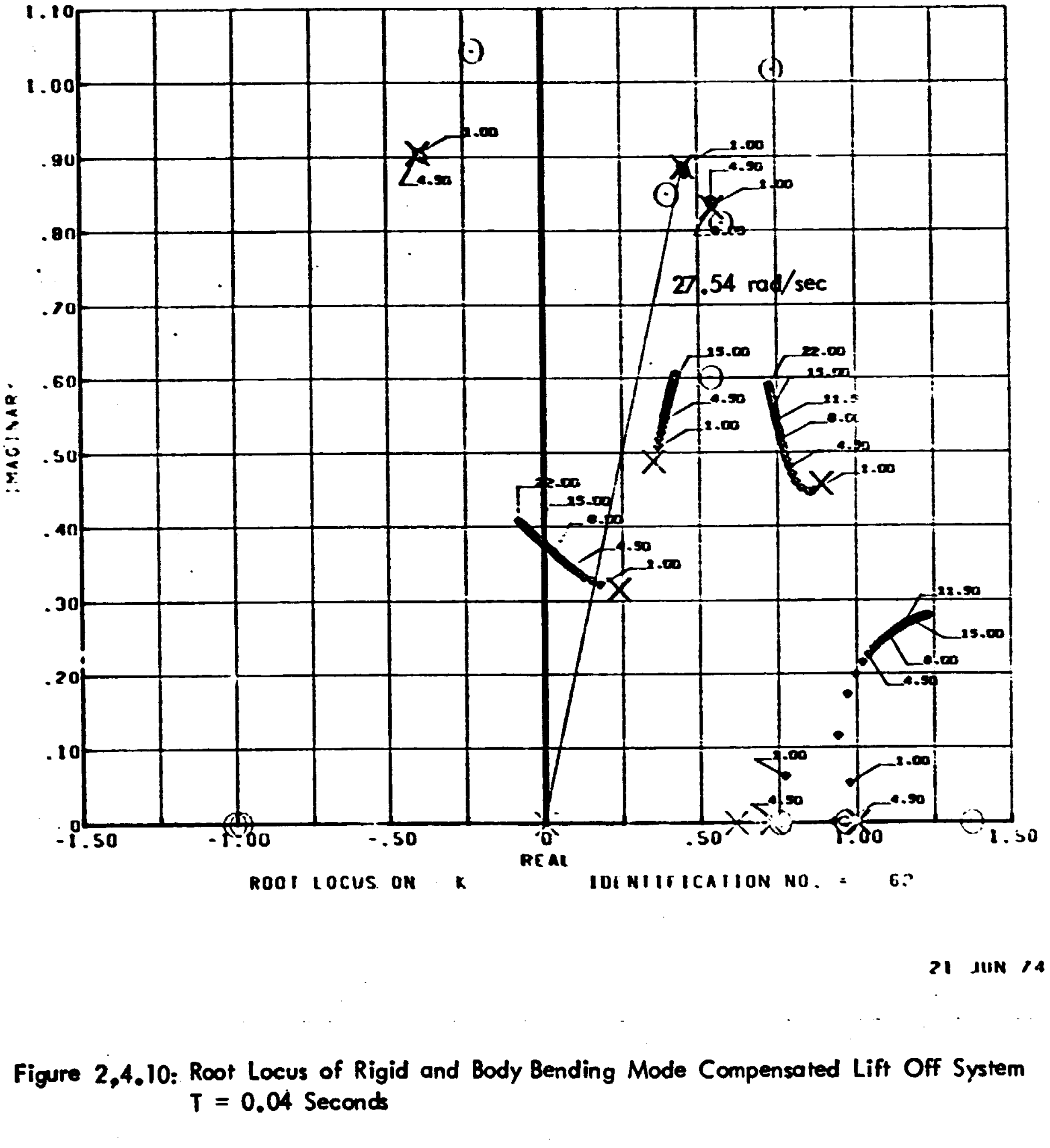

Figure 2.4.10: Root Locus of Rigid and Body Bending Mode Compensated Lift Off System T = 0.04 Seconds

The Nichol's chart for the rigid and body bending mode compensated system is shown in Figure 2.4.11. It can be compared w the rigid and body bending mode compensated system at T = 0.08 seconds which is shown in Figure 2.4.7.

At this point digital autopilots have been designed which meet or exceed the design requirements imposed on the system by the continuous autopilot. In Section 2.5 the multirate autopilots for the low Q and max Q systems are presented.

2.5 Multirate Autopilot

Two multirate digital autopilot designs are discussed in this section. First the low Q digital autopilots at T = 0.04 and T = 0.08 seconds are used to form a low Q multirate autopilot. This design will be used to outline a multirate design methodology in Subsection 2.7. Next the max Q multirate digital autopilot design, using a zero order hold as digital compensation in the acceleration feedback loop, is discussed.

Low Q Multirate Autopilot

A block diagram of the low Q multirate system is shown in Figure 2.5.1. The rigid mode is compensated at the slow sampling rate to keep the system design out of the z = +1 region in the z-plane. This helps reduce coefficient accuracy requirements and keeps the system from being driven by round-off noise. The body bending filter is used for compensating the higher frequencies and is therefore sampled at the higher rate. This yields a higher $\omega_s/2$ which minimizes the amount of noise folding into the primary strip.

Having previously designed rigid and body bending mode filters for the single autopilot the same filters are used for the multirate system. In Section 2.4 the rigid mode was compensated at T = 0.08 seconds with the digital equivalent of the following s-plane filter

$$G(s) = K \left(\frac{8}{s+8}\right) \left(\frac{12}{s+12}\right) \quad \text{where } K = 0.6764.$$

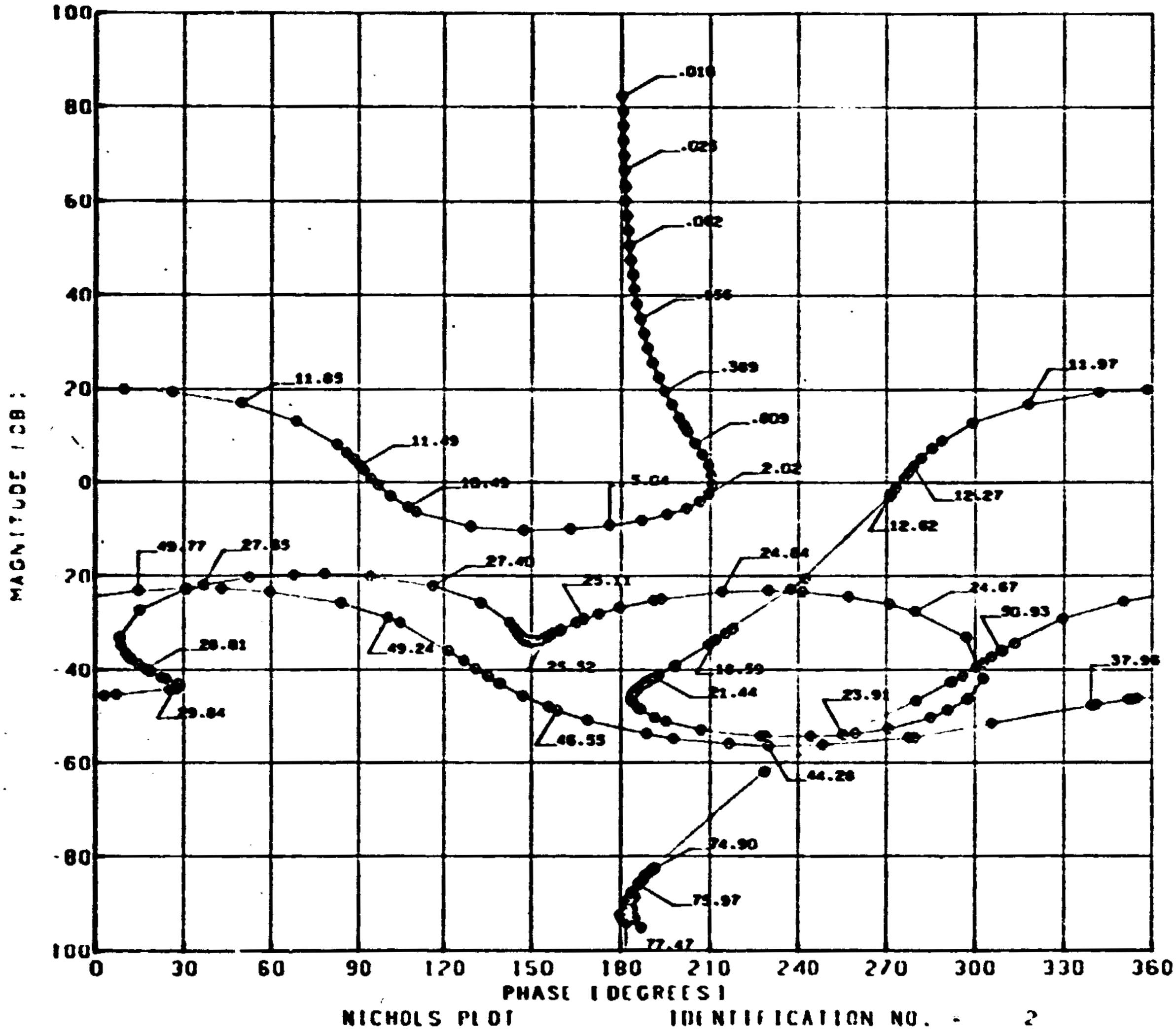

21 JUN 74

Figure 2.4.11: Nichol's Chart of Rigid and Body Bending Mode Compensated Lift Off System.
T = 0.04 Seconds

Gain Margin = 8.82 db @ 4.727 rad/sec
Phase Margin = 30.4°
First Body Bending Mode Phase Margins = -84.165, + 94.902°

Gain Margins

23.114 db @ 24.80 rad/sec
19.447 db @ 27.53 rad/sec
22.592 db @ 49.69 rad/sec

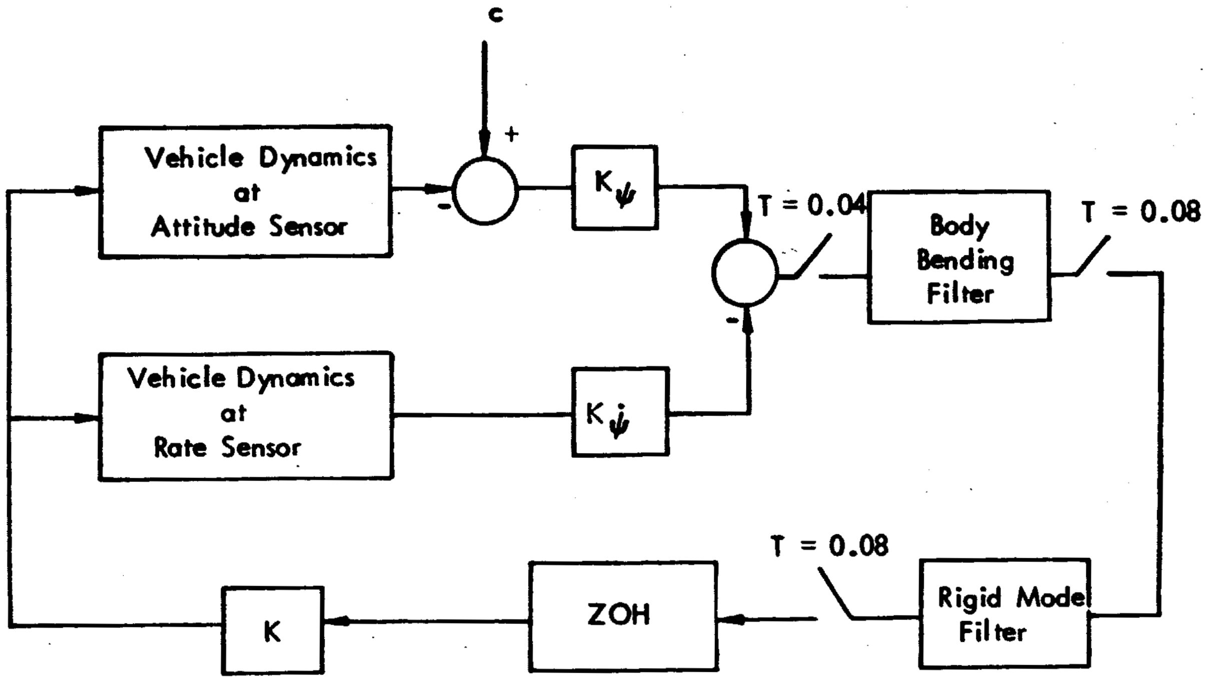

Figure 2.5.1: Block Diagram of Multirate Lift Off System

The digitized version of this filter using Tustin's method with frequency scale prewarping is as follows:

$$G(z) = K \left(\frac{0.2489z + 0.2489}{z - 0.50219}\right) \left(\frac{0.34237z + 0.34237}{z - 0.3153}\right)$$

In Section 2.4 the body bending mode fiiter at T = 0.04 seconds was the following D (z).

$$D(z) = \frac{z^2 - 0.800z + .8825}{z^2 - 0.700z + .3600}$$

Combining D(z) and G(z) and using a K of 0.6839 a multirate design is constructed. The frequency response and root locus plot for this system are shown respectively in Figures 2.5.2 and 2.5.3. To get slightly better phase stability on the first body bending mode the compensation poles in Figure 2.5.3 are moved to $z = -0.18 \pm j\,0.3177$. This corresponds to $z = 0.3 \pm j\,0.519$ for T = 0.04. The Nichol's chart for this system with K = 0.81283 is shown in Figure 2.5.4.

Examining Figures 2.4.11, 2.4.7, 2.1.3 and 2.5.4 reveals the multirate autopilot design for the low Q model has no distinct advantage over the single rate design. The four frequency responses all meet the same phase and gain margin requirements. In addition the rigid mode compensation for both sampling rates is well removed from the z = +1 point. Therefore a multirate system yields no computational advantage over a single rate system.

Maximum Q Multirate Autopilot

The continuous maximum Q autopilot design as shown in Figure 2.1.4 is used as a starting point for the maximum Q multirate design. The continuous system has two lag filters in the accelerometer loop -- one breaking at 1 rad/sec and the other breaking at 17.5 rad/sec. The 1 rad/sec lag filter is being used to reduce the bandwidth of this loop while the 17.5 rad/sec filter is used to attenuate body bending effects.

The max Q multirate design is very similar to the analog design. The 1 rad/sec analog filter is left in the loop to reduce the bandwidth of the sampled acceleration signal and a sample and hold operating at a sampling rate of T = .08 sec is used instead of the lag filter at 17.5 rad/sec. The sampler and hold contributes a phase lag

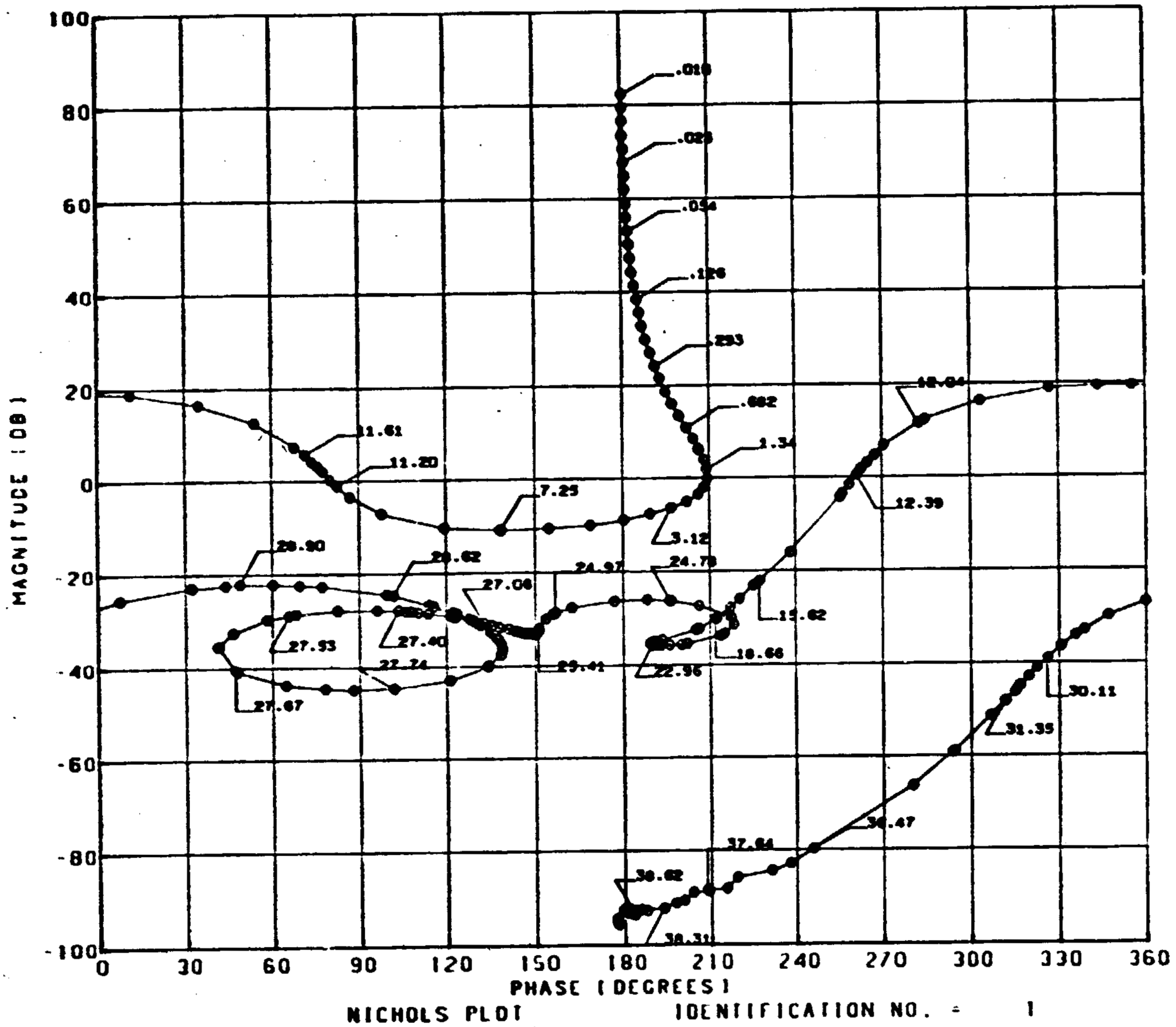

28 JUN 74

Figure 2.5.2: Nichol's Chart of the Multirate Low Q System

Gain Margin = 8.86 db @ 4.36 rad/sec
Phase Margin = 29°

First Body Bending Mode Phase Margins = -100°, +80°

Gain Margins

25.96 db @ 24.80 rad/sec
27.66 db @ 27.44 rad/sec
22.00 db @ 28.85 rad/sec

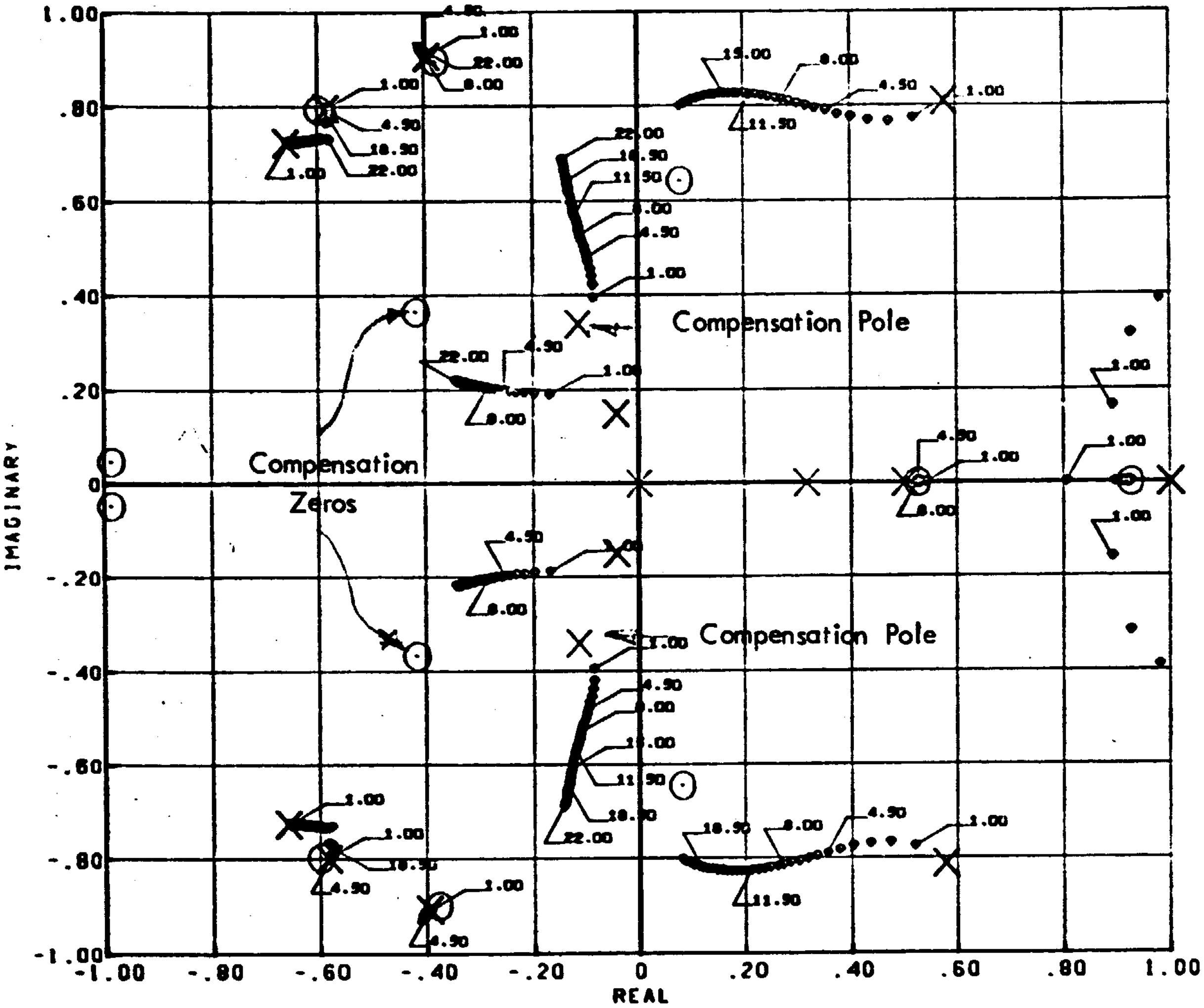

ROOT LOCUS ON - K IDENTIFICATION NO. = 62

24 JUN 74

Figure 2.5.3: Root Locus of Multirate Low Q System

Additional Zeros Located at -615.5, -1.21, 2.29

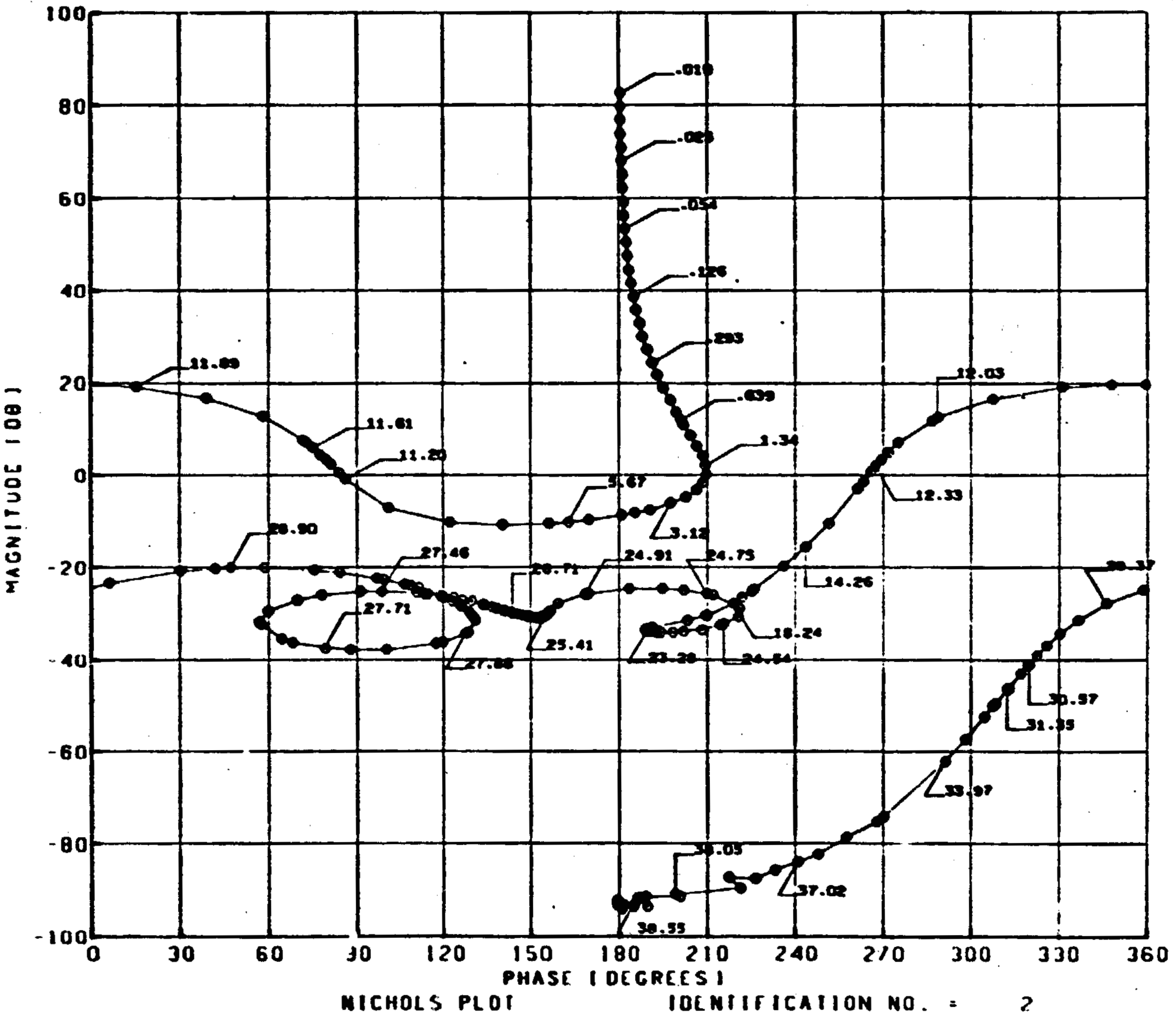

28 JUN 74

Figure 2.5.4: Nichol's Chart of the Fine-Tuned Multirate Low Q System

Gain Margin = 8.79 @ 4.44 rad/sec
Phase Margin = 29.5°

First Body Bending Mode Phase Margins = -95°, +84°

Gain Margins
24.58 db @ 24.80 rad/sec
25.16 db @ 27.46 rad/sec
19.85 db @ 28.85 rad/sec

of 40.1° and a gain attenuation of .74 db at 17.5 rad/sec and the characteristics are very similar to a lag filter at higher frequencies. This design simplifies the requirements for the acceleration loop compensation while not degrading system performance. For the multirate design the forward loop analog compensation is replaced with a digital autopilot given by

$$T = 0.04$$

$$K \left\{ \begin{matrix} \text{Tustin's} \\ \text{Frequency} \\ \text{Prewarping} \end{matrix} \left[\frac{4}{s+4} \right] \right\}^3 = K \left\{ \frac{.0742207\,(z+1)}{z = .851559} \right\}^3$$

where K = .33113.

Figure 2.5.5 gives the Nichol's Chart for this multiloop multirate autopilot. The phase and gain margins of the rigid mode duplicate those of the continuous system and the gain and phase margins of the body bending modes have been increased. A definite improvement has been made with the multirate design.

2.6 Performance Results

The performance results involve verifying the analysis results via a hybrid computer simulation. Open loop frequency response from the hybrid simulation is compared with the open loop frequency response generated by the analysis. The hybrid computer is used to generate a frequency response for the closed loop system

$$w(s) = \frac{G(s)\ H(s)}{1 + G(s)\ H(s)} \ .$$

The open loop frequency response, G(s) H(s), is derived from the measured closed loop response by the following relationships.

Open Loop Gain

$$K_o = \frac{K_c}{\sqrt{K_c^2 - 2K_c \cos\theta_c + 1}}$$

Open Loop Phase

$$\sin\theta_o = \frac{K_o}{K_c} \sin\theta_c$$

where K_c = closed loop gain

θ_c = closed loop phase

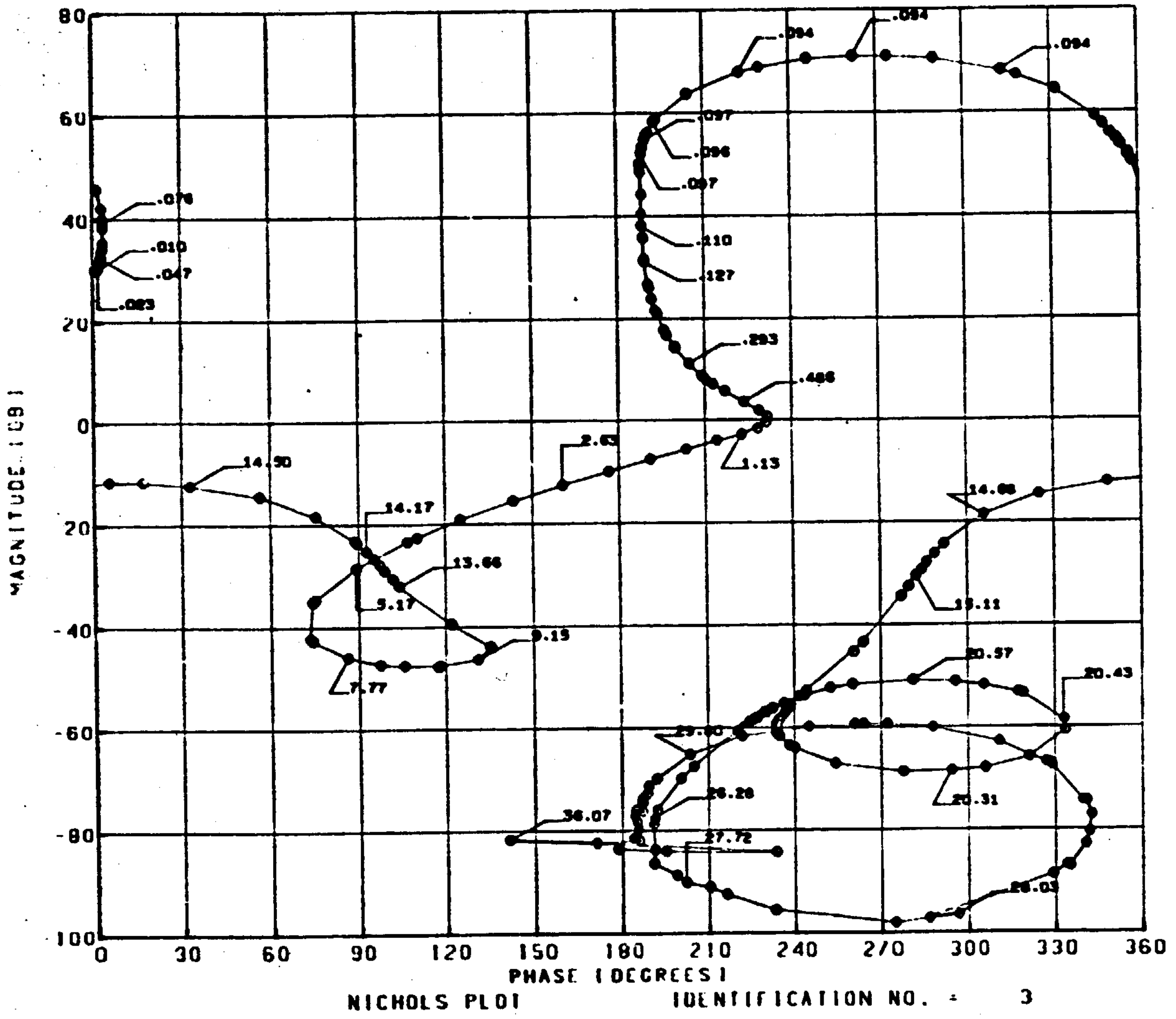

28 JUN 74

Figure 2.5.5: Nichol's Chart of Max Q Multirate System

Gain Margin = 9.14 db @ 2.13 rad/sec

Phase Margin = 51.4°

This assures that all the poles in the simulation are not in the right half plane or on the $j\omega$ axis for the continuous systems and not on or outside the unit circle for the digital systems. The systems that were verified are discussed below.

Continuous Frequency Response for Low Q and Max Q Systems

The continuous systems were verified by running thc frequency response for the original analog control system/vehicle combinations. The simulation results are plotted in Figure 2.6.1 and 2.6.2. Thcse figures show the analysis results and simulation results agree for the continuous system for all frequency values considered.

Digital Filter Programming Form

Since all the digital filters programmed were either lag filters or body bending filters i.e. they involve attenuation, the direct canonic state variable programming form was used to realize these filters. A general second order representation for this programming form is shown in Figure 2.6.3. The relationship between the filter coefficients and the scaled coefficients is as follows:

$$S = \frac{SFZ_o}{SFE_i} \times \frac{1}{G_1{}'} \qquad D' = D \times \frac{1}{G_1{}'}$$

$$A' = \frac{SFE_o}{SFZ_o} A \times \frac{1}{G_2{}'} \qquad E' = E \times \frac{1}{G_1{}'}$$

$$B' = \frac{SFE_o}{SFZ_o} B \times \frac{1}{G_2{}'}$$

$G_1{}'$ = Input 1st Summing Point (Summing Gain)

$$C' = \frac{SFE_o}{SFZ_o} C \times \frac{1}{G_2{}'}$$

$G_2{}'$ = Input 2nd Summing Point (Summing Gain)

A scaled flow diagram is illustrated in Figure 2.6.4. In the results which follow on the digital simulations the real axis pole-zero filters are realized as first order filters and complex pole-zero filters as second order filters.

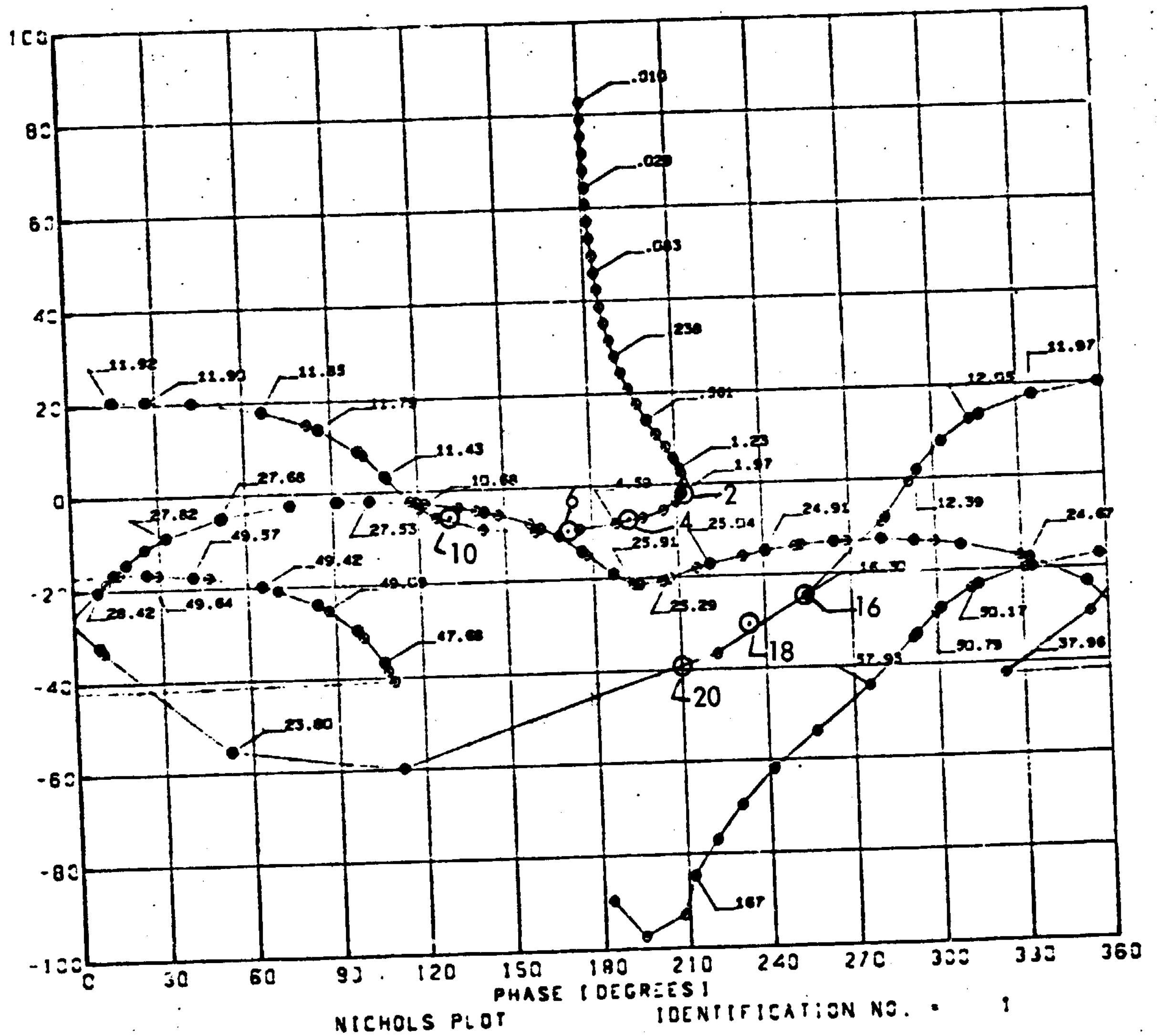

22 JAN 74

Figure 2.6.1: Analog System Nichols Chart for Lift Off Flight Condition

⊙ Simulation Derived Open Loop Frequency Response Points

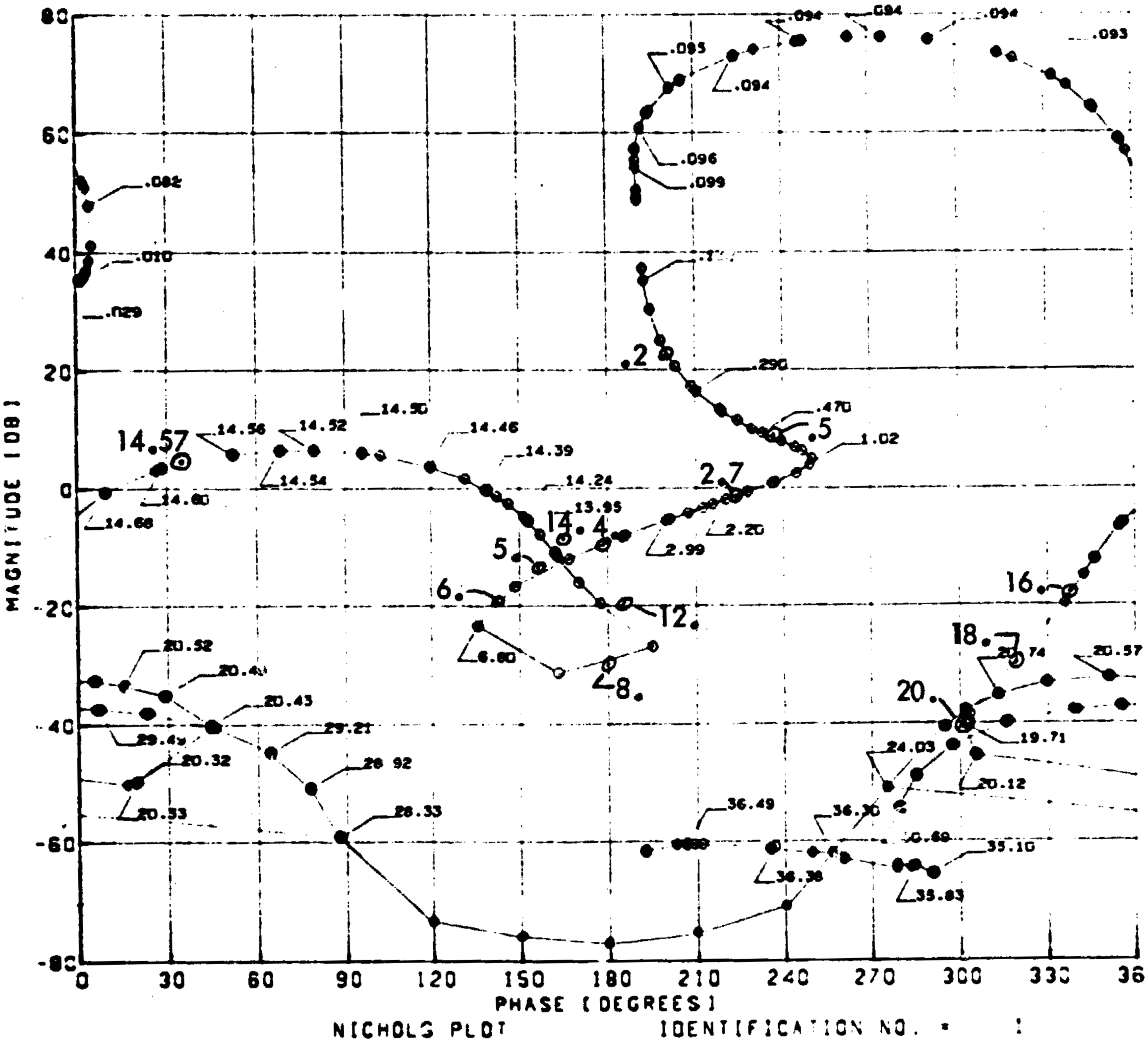

06 APR 74

Figure 2.6.2: Nichol's Chart for the Continuous System at Maximum Q

⊙ Simulation Derived Open Loop Frequency Response Points

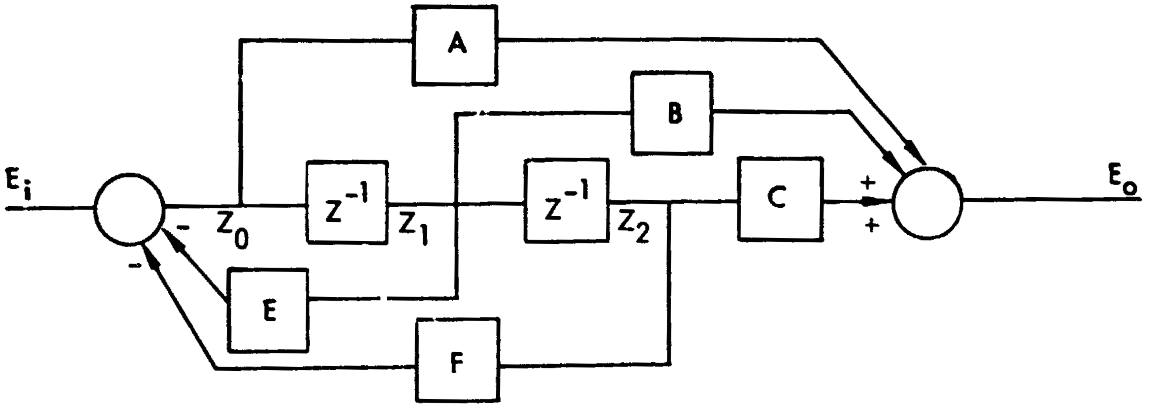

Figure 2.6.3: Second Order Direct Canonic State Variable Diagram

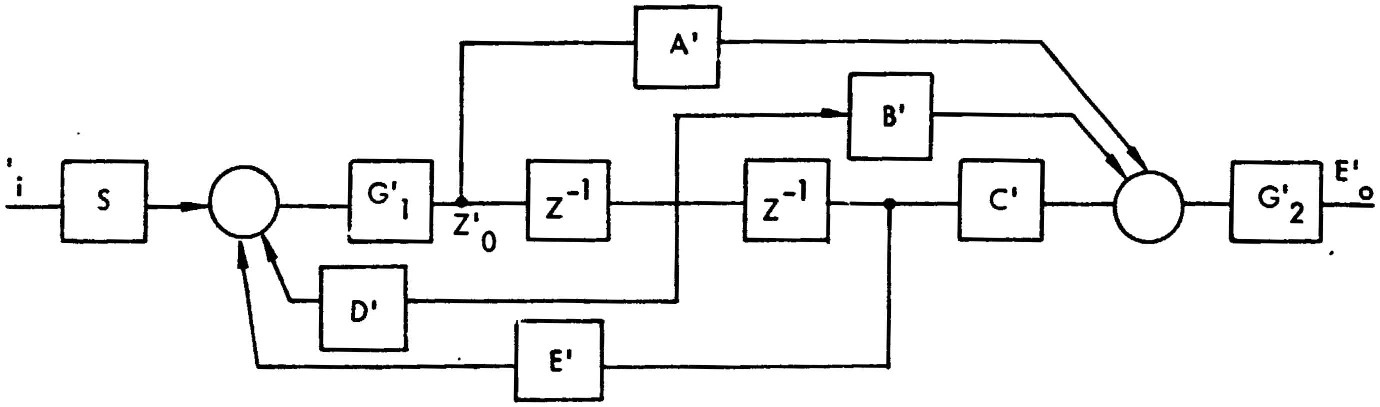

Figure 2.6.4: Scaled State Variable Flow Chart

Digitized Analog System for the Low Q Model, T = 0.08

The next system considered was the digitized analog autopilot for the low Q system. The analog autopilot was digitized using Tustin's method with frequency scale pre-warping at T = 0.08 seconds. The comparison between the analysis generated and simulation generated open loop frequency response data is shown in Figure 2.6.5. Again the simulation results agree with the analysis results for all frequencies considered.

Digital Design for the Low Q Model, T = 0.08

This design was for the low Q model with the analog autopilot replaced with a sampler and zero-order hold. The digital autopilot design appeared in Subsection 2.4. The comparison between the analysis and simulation frequency response data is shown in Figure 2.6.6. The results agree for all frequencies considered.

Multirate Design for the Low Q System

The comparison between the analysis results and the simulation results is shown in Figure 2.6.7. This plot shows that the analysis and simulation results agree perfectly at low frequencies and begin to diverge at higher frequencies. This high frequency effect was not noticed for the other digital filters because the frequency response data was not taken at the higher frequencies. This divergence between the simulation and the analysis results was expected because of the time delay due to A/D setup time, computation time and D/A setup time in the simulation. The time delay equaled approximately .006 seconds for the XDS 9300 used in the simulation. The effect of a time delay is to add phase lag to the frequency response that is given as follows:

$$\theta = -57.3\ \omega\tau_D$$

The triangle points represent the corrected simulator results when the pure time delay effects are subtracted out. Therefore, any discrepancies between the results are physically explainable.

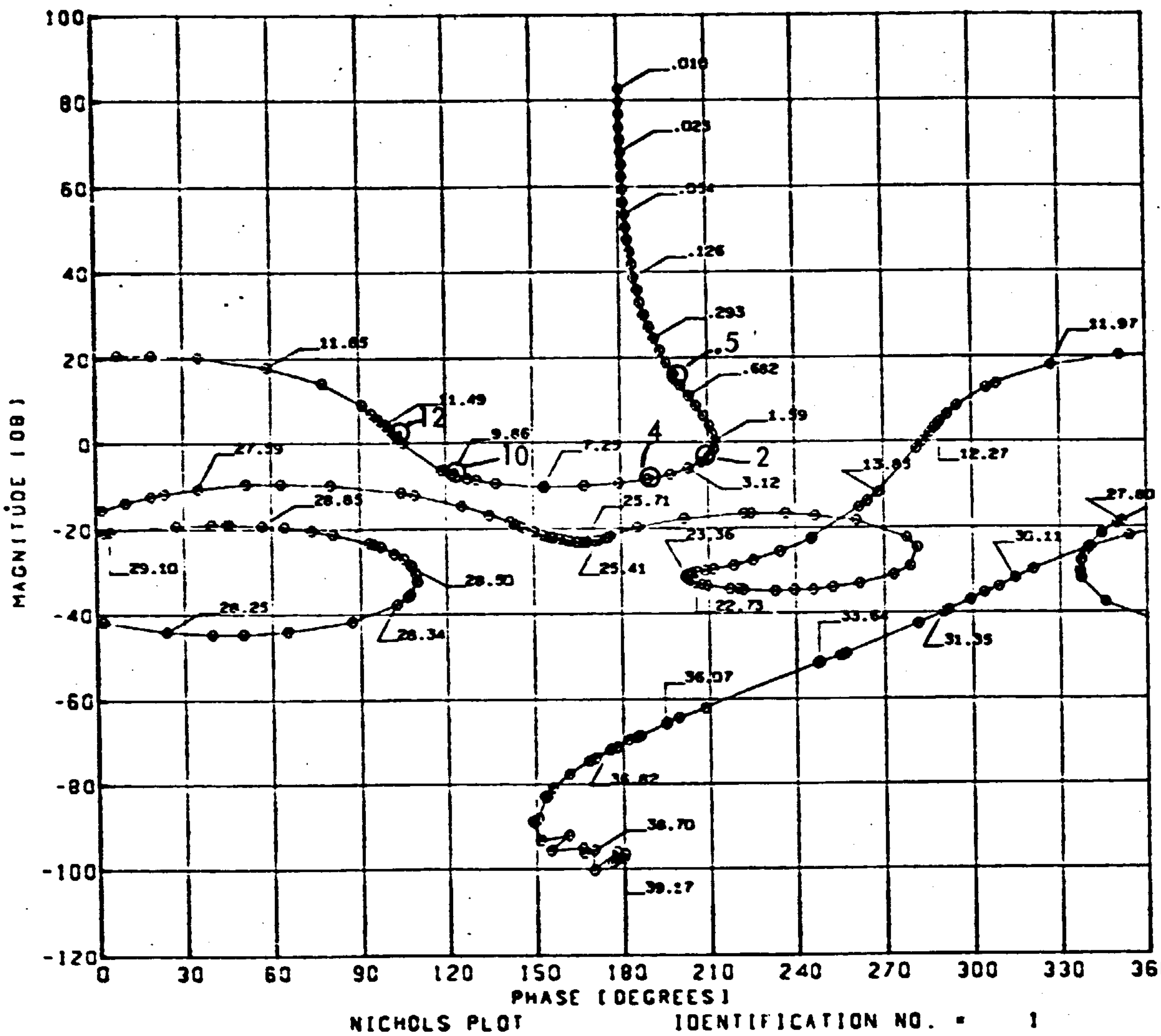

05 FEB 74

Figure 2.6.5: Digitized Continuous System Nichols Chart for Lift Off Conditions.

T = 0.08 Seconds

⊙ Simulation Derived Open Loop Frequency Response Points

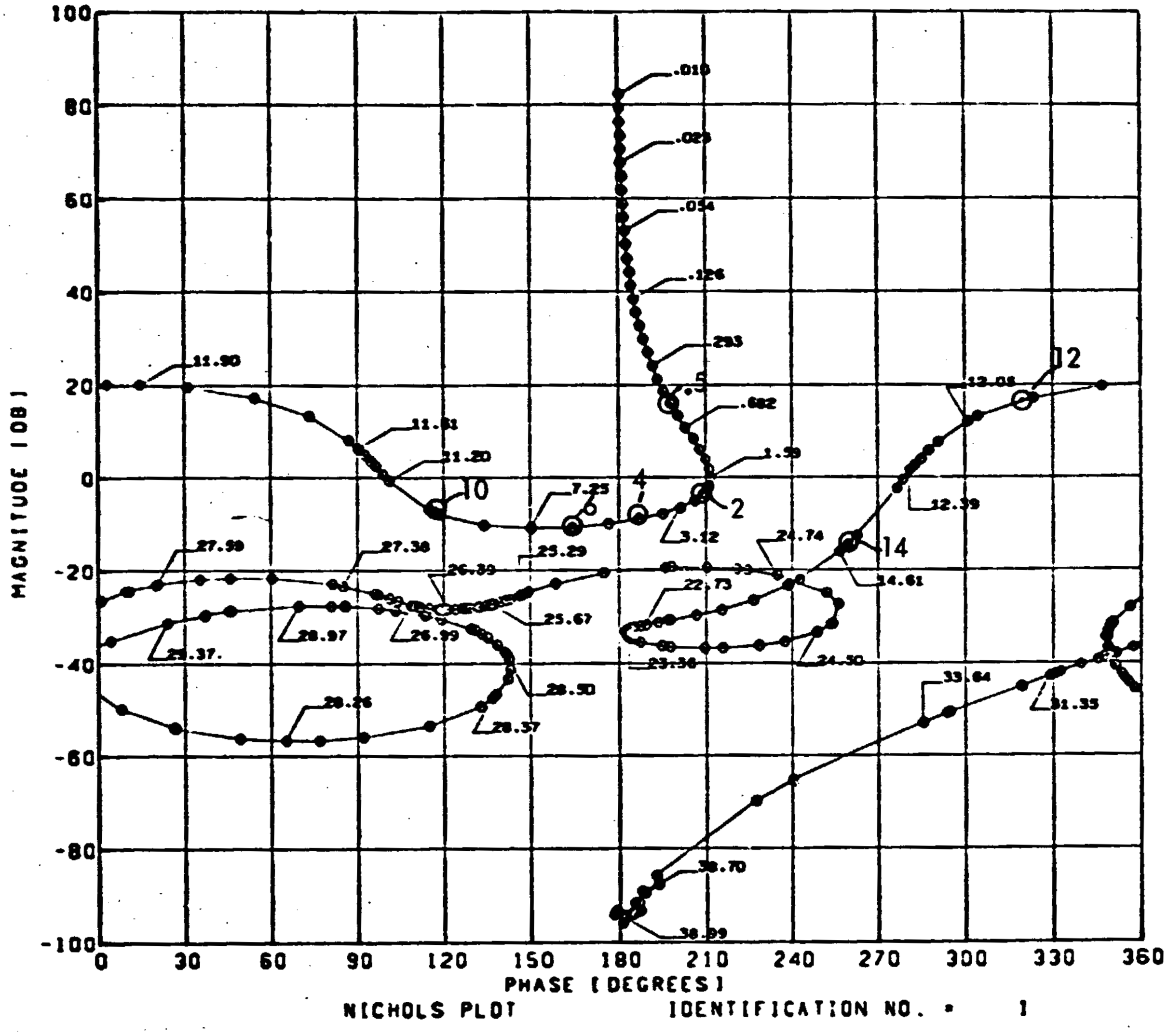

FIGURE 2.6.6:

27 FEB 74

NICHOL'S CHART OF DIGITAL AUTOPILOT FOR RIGID AND BODY BENDING MODE COMPENSATION

Gain Margin = 9.58 db @ 4.88 rad/sec

Phase Margin = 31.4°

⊙ - Simulation Derived Open Loop Frequency Response

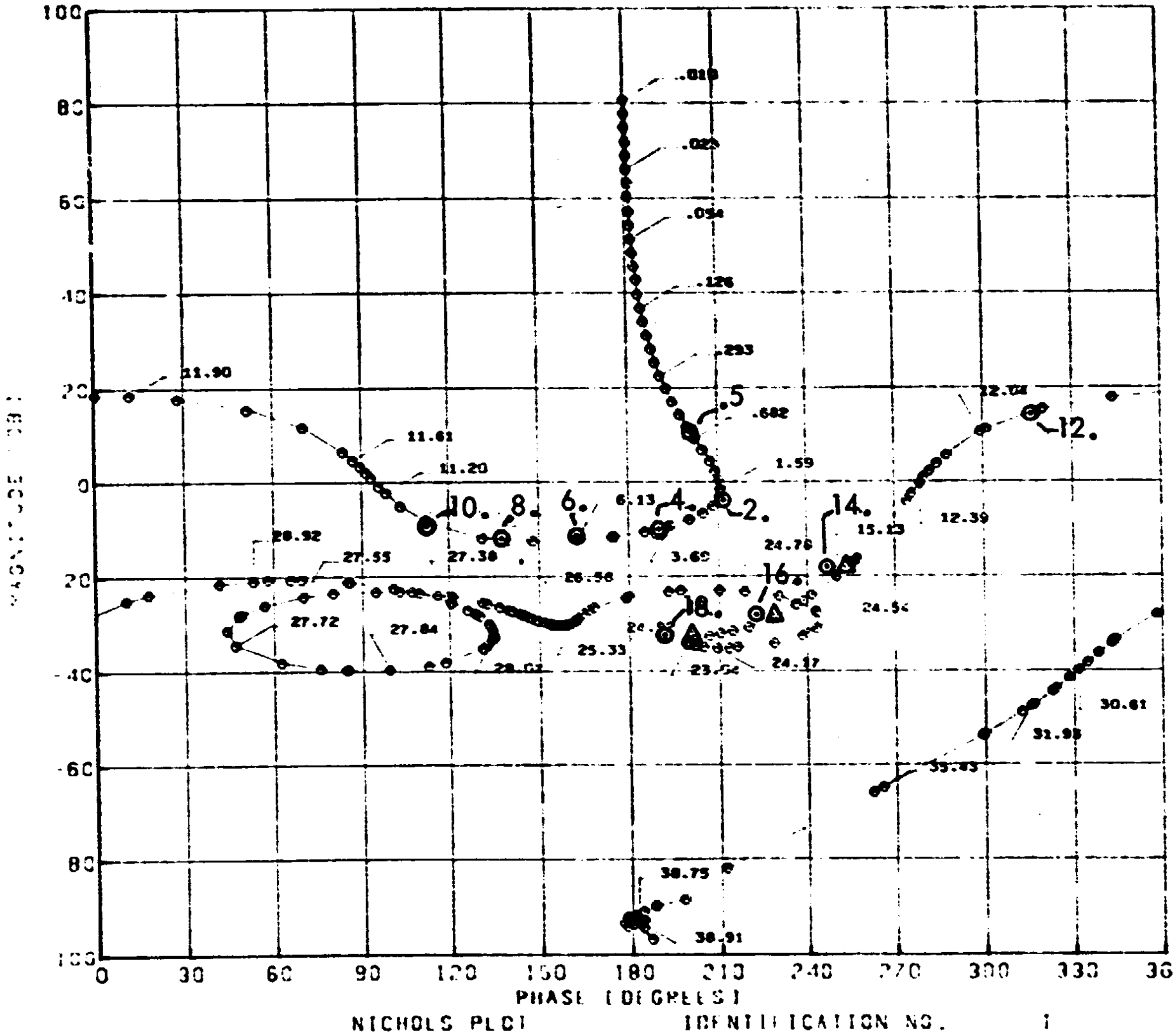

19 JUL 74

Figure 2.6.7: Nichol's Chart for Multirate System with Rigid and Body Bending Mode Compensation

⊚ - Simulation Derived Open Loop Frequency Response

Δ - Adjusted to Remove Computational Delay

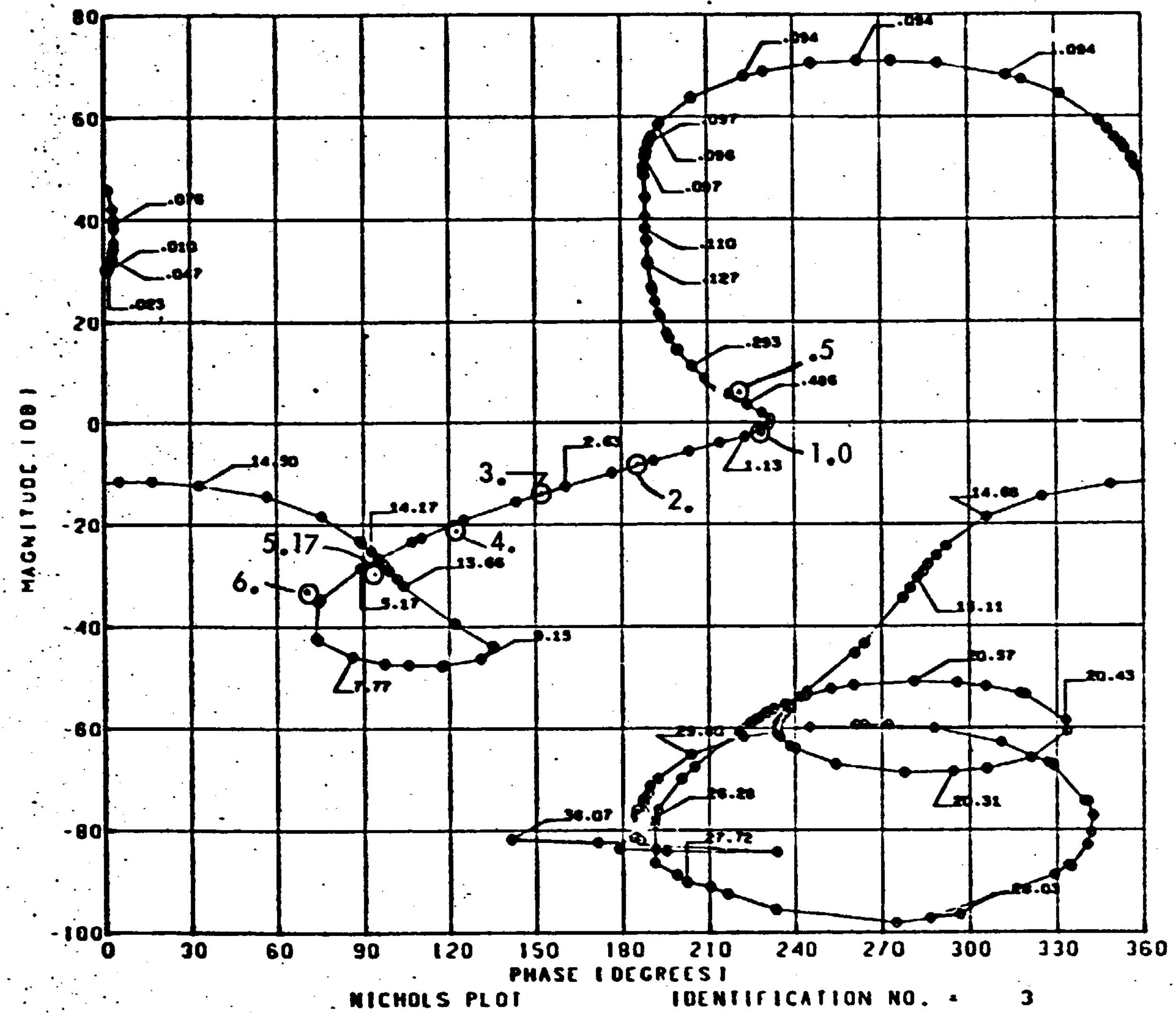

28 JUN 74

Figure 2.6.8: Nichol's Chart of Max Q Multirate System

O Simulation Derived Open Loop Frequency Response Points

Multirate Design for the Max Q System

The comparison between the analysis and simulation results for the max Q multirate design is shown in Figure 2.6.8. The results are seen to agree within the accuracy of the simulation for the frequencies considered.

2.7 Multirate Design Methodology

The following is a general outline to adhere to in designing multirate digital control systems. It follows closely the procedure used in designing the low Q multirate digital autopilot.

1. Root Locus of Continuous System - This allows the designer to see the effects of different sampling rates on the folding of system poles into the primary strip. No matter where the poles of a continuous stable system are located they will appear between ± $\omega_s/2$ for the sampled data system.

2. Z-Plane Root Locus and Frequency Response at Sampling Rates of Interest (Synchronous) - By the very nature of including a sample and hold element the root locus and frequency response of the system changes. A root locus and/or a frequency response of the basic system is necessary to design any type of system compensation.

3. Determination of High Update Rate and Low Update Rate Compensation Requirements - This involves determining the compensation that is necessary at the various sampling rates to meet the systems design requirements. This can include not only the various filters that meet the gain and phase requirements of the system but the machine requirements, such as coefficient word length, as well.

4. Multirate Frequency Response and Root Locus - From (3) a multirate sample data control system is put together. To get a total system description a frequency response and root locus plot are made.

5. Fine Tuning Multirate Design (Based upon (4)) - This can involve merely adjusting the system gain or moving the compensation poles and zeros to get the final design

3.0 MACHINE REQUIREMENT TRADES

The objective of this section is to point out the various effects software and hardware requirements impose on control system performance. Computer wordlength, A/D wordlength, sampling rate, synchronous versus multirate sampling, as well as how the arithmetic operations are performed and what state variable form is used, all affect control system performance. These considerations are treated in a general manner in Subsection 3.1. Subsection 3.2 presents a computer wordlength study which specifically answers a number of the questions raised by these considerations for the low Q multirate design. In Subsection 3.3 an assembly langJage program for the rigid and body bending mode compensated system for T = 0.08 seconds is presented. The purpose of this subsection is to give an indication of the storage and time requirements needed when a digital design is implemented.

3.1 Machine Requirements/Synthesis Approach Tradeoffs

A block diagram of a digital computer and the necessary peripherals to interface this system with both analog and digital devices is shown in Figure 3.1.1. In specifying the machine requirements it is necessary to study the resolution and noise characteristics of the various elements in this figure. For example the A/D element will have certain requirements and the computer will have memory, word length, and execution time requirements. The implication of these machine requirements will be discussed as they affect the synthesis approach tradeoffs and vice versa.

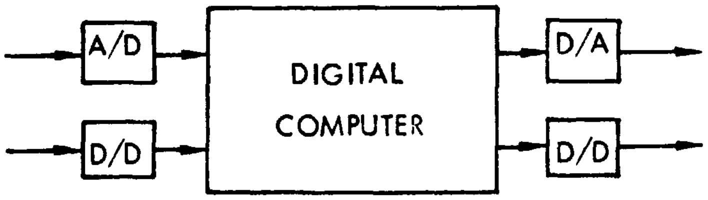

FIGURE 3.1.1: Hardware in a Digital Control System

Coefficient Quantization

The accuracy that a digital computer can store a coefficient is dependent upon the computer internal word length. The performance of recursive digital filters can be adversely affected due to coefficient quantization. This problem has received considerable attention in the past by Kaiser [1] and Rader and Gold [2]. The sensitivity of a filter to coefficient quantization has been shown to be greatest when the filter poles approach the plus one point in the z-plane. This situation arises when the sampling rate is large relative to the frequency of the digital filter poles. Due to the finite accuracy of a digital computer, the performance of a digital filter may become less like its corresponding analog counterpart rather than more, as the sampling rate is increased.

Some examples pointing out what is happening will now be reviewed. A simple first order example that graphically shows the problem is the following case considered by Rader and Gold [2]:

$$y\,(nT) = Ky\,(nT-T) + x(nT) \qquad (3.1)$$

The pole position for this filter is equal to K. When K is realized as K + ΔK the error in pole location is ΔK. The importance of this error becomes magnified when K is near unity. E.g., the maximum gain of this one pole filter is

$$\max \left| G(z) \right| = \frac{1}{1-K} \qquad (3.2)$$

Thus, as K approaches one the sensitivity of this filter to coefficient quantization effects becomes large. As things turn out this situation arises frequently in digitizing analog filters.

For example, the z-transform of a first order filter gives the following G(z):

$$G(z) = \frac{T\ \omega_A\ z}{z - e^{-\omega_A T}} \qquad (3.3)$$

The Tustin approximation to a first order lag filter gives

$$G(z) = \left(\frac{T\ \omega_A/2}{1 + T\ \omega_A/2}\right) \frac{(z+1)}{z - \left(\frac{1 - T\ \omega_A/2}{1 + T\ \omega_A/2}\right)} \qquad (3.4)$$

It can be shown that in the limit as T ⟶ 0 the denominators of both these equations reduce to the form

$$D(z) = z - 1 + \omega_A T + o(T) \qquad (3.5)$$

Therefore, as T ⟶ 0 the poles of these equations move toward the point $z = 1$ and the filters become very sensitive to parameter quantization effects.

The Tustin's approximation to a lead lag filter gives the following equation:

$$G(z) = \frac{\omega_B}{\omega_A} \left(\frac{1 + \frac{T}{2}\ \omega_A}{1 + \frac{T}{2}\ \omega_B}\right) \frac{\left[z - \left(\frac{1 - \frac{T\ \omega_A}{2}}{1 + \frac{T\ \omega_A}{2}}\right)\right]}{z - \left(\frac{1 - \frac{T}{2}\ \omega_B}{1 + \frac{T}{2}\ \omega_B}\right)} \qquad (3.6)$$

This equation is seen to have the same type of denominator as before but now the numerator has a zero that migrates as a function T approaching the plus one point as T ⟶ 0. In this type of filter both the gain and phase become very sensitive to coefficient quantization.

Similarly, for second order filters it has been shown by Rader and Gold [2] that the coefficient sensitivity problem is compounded. They use the following second order example to demonstrate their point:

$$y(nT) = Ky(nT-T) - Ly(nT-2T) + x(nT) \qquad (3.7)$$

This filter has complex poles in the z-plane given by

$$\rho = re^{\pm j\theta} \qquad (3.8)$$

where

$$r = \sqrt{L}$$

$$\theta = \cos^{-1} K/2 \sqrt{L}$$

Explicit expressions can be derived for the pole position errors caused by quantization of K and L. if it is assumed that the errors are small so that Newton's approximation can be applied, i.e.,

$$\Delta r = \frac{\partial r}{\partial L} \Delta L + \frac{\partial r}{\partial K} \Delta K$$

$$\Delta\theta = \frac{\partial\theta}{\partial L} \Delta L + \frac{\partial\theta}{\partial K} \Delta K \qquad (3.9)$$

Using the expressions for r and θ these equations become

$$\Delta r = \frac{1}{2r} \Delta L$$

$$\Delta\theta = {}^{\Delta L}/_{2r^2} \tan\theta - {}^{\Delta K}/_{2r} \sin\theta \qquad (3.10)$$

The error in the radius r is similar to the first order case while the error in the resonant angle θ is seen to be very sensitive at small angles. The resonant frequency error can also be seen to be inversely proportional to the sampling period T based upon the relationship

$$\Delta\theta = \Delta\omega_r T \qquad (3.11)$$

Research by Kaiser [1] has further pointed out that the bound on coefficient accuracy is dependent upon the order n of the filter as well as the sampling rate. Because of the multiplications involved between coefficients, it would take twice as many digits of accuracy to represent the coefficients of a 2 nth order filter versus an nth order filter. From the previous results, it has been demonstrated that increasing the sampling rate requires an increase in the accuracy of the digital approximation to the filter coefficients.

Thus, a potential benefit can be gained in terms of computer internal word length requirements by decreasi.,g the sampling rate. This is especially true for filters with poles in the vicinity of the plus one point in the z-plane. Root locus methods have been applied to study the migration of filter poles and zeros as a function of sampling period T to aid in the proper choice of T. Likewise, by realizing the filters as low order elements the computer internal word length requirements can again be reduced. In general, the transfer functions of a digital controller are realized in the cascade form:

$$D(z) = \prod_{i=1}^{m} K_i \left(\frac{z - z_i}{z - P_i} \right) \prod_{i=1}^{n} K_i \left(\frac{z^2 + b_i z + c_i}{z^2 + d_i z + e_i} \right) \qquad (3.12)$$

The real pole and zero filters are realized as first order elements and the filters with complex poles and zeros are realized as second order elements. It i- also possible to realize these filters in the analogous parallel form. The pros and cons of the parallel over cascade realization will be discussed in the section dealing with arithmetic noise.

A/D Requirements

The requirements on this element are primarily due to resolution and noise level. The resolution capability of the device is proportional to the number of binary bits used to represent the analog signal. The A/D quantization step is generally chosen so that it preserves the basic accuracy of the sampled signal . The effect of the A/D device on filter performance can be statistically analyzed by considering additive noise at the input to the filter computation. Assuming each noise sample is uncorrelated and has variance $E_0^2/12$, the steady state variance of the filte: output due to this noise is given by [2]:

$$\sigma_f^2 = \frac{E_0^2}{12} \frac{1}{2\pi j} \oint H(z)\ H\left(\frac{1}{z}\right) z^{-1}\, dz \qquad (3.13)$$

where E_0 = quantization level

$H(z)$ = filter transfer function.

In general the output noise variance is proportional to the gain of the filter and inversely proportional to E, the distance of the filter poles from the unit circle, e.g.

$$\sigma_f^2 \cong \frac{E_0^2 \; K_1}{12\,E} \tag{3.14}$$

The output noise for certain filters can also be shown to be dependent on the resonant angle of $\theta = \omega_r T$ of the filter [2] e.g.,

$$\sigma_f^2 = \frac{E_0^2 \; K_2}{12\,E \sin^2 \theta} \tag{3.15}$$

From this equation, it can be seen that a low frequency filter ($\omega_r \approx 0$) can have three or four more bits of noise standard deviation than a larger resonant angle implementation of the same filter. Thus, when trying to maintain a specified signal to noise ratio on the output, one might want to think about increasing T to increase the resonant angle $\omega_r T$. Root locus techniques can be applied to analyze the filter pole zero migration as a function of sampling period T.

Computer Arithmetic Requirements

The precision of arithmetic operations is related to the machine internal data word length and the method utilized by the computer to perform arithmetic calculations. The basic structure of a computer data word is shown in Figure 3.1.2. The first bit of the data word is the sign bit which is normally 0 for positive numbers and 1 for negative numbers. This leaves n-1 other bits to specify the number in binary form. When the decimal point for all calculations is assumed to be between the sign and the first bit and the remainder of the data word is considered as a single fractional number, this is a fixed point data word format. A fixed point data word has the following fixed dynamic range:

$$1/2^{n-1} \leq R \leq 1 - 1/2^{n-1} \tag{3.16}$$

Fixed point arithmetic utilizes the full wordlength but has the inherent problem of scaling quantities to remain within this fixed dynamic range. For example, in a high gain filter implementation using fixed point arithmetic, the input signal must be scaled down to prevent overflow. Therefore, the signal to noise performance of this filter is adversely affected. To get around this dynamic range problem, floating point arithmetic is typically used. In floating point, the data word is segmentized such that part or the word is the so-called normalized fraction of the number while the other part is the exponent. The normalization process involves shifting the contents of a register left until the contents of the registers sign bit and the contents of bit position one are not equal where vacated bit positions are filled with zeros. Normalizing causes the original fixed point number to be shifted into the most significant bit positions of the data word and also maintains a count on the number of left shifts. A floating point data word is shown in Figure 3.1.3 where the normalized fraction is stored in the fractional part of the word and the number of left shift is stored in the exponential section. A general floating point number is thus given by

$$N = \pm F \times 2^{\pm E} \qquad (3.17)$$

The arithmetic on most flight type computers is performed on hardware that is capable of performing only fixed point arithmetic. The reasons for using these types of machines are faster computational speed, increased reliability and cheaper cost. Therefore, it is necessary to perform some sort of scaling on the filter input, coefficients, and sometimes even internal state variables to not only prevent overflow but to also maintain maximum arithmetic precision. The type of scaling used to implement a given filter can effect filter performance in terms of signal to noise ratio. This error source for uncorrelated input signals can be considered similar to multiplication roundoff noise for analysis purposes. [21]

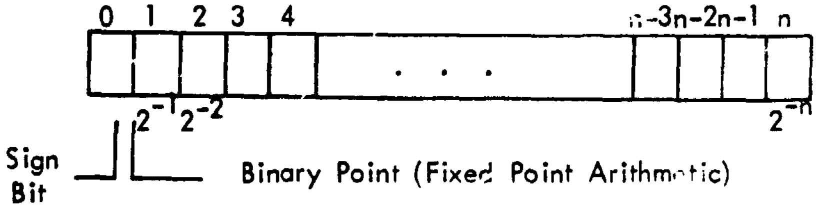

FIGURE 3.1.2: Computer Data Word Schematic

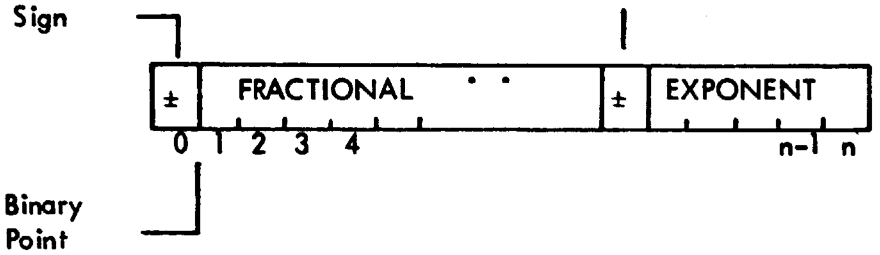

FIGURE 3.1.3: Floating Point Data Word Format

Arithmetic Noise (Uncorrelated Input)

The primary sources of computation noise in a digital filter are due to multiplication roundoff noise. Similar to the error model for A/D truncation, these error sources can be modelled by noise with the following variance:

$$\sigma_n^2 = \frac{E_o^2}{12} \qquad (3.18)$$

These noise sources are placed in the filter state variable diagram after scaling operations and multiplications. For example, consider the state variable diagram for the second order difference equation given below (see Figure 3.1.4):

$$D(z) = \frac{a_0 + a_1 z^{-1} + a_2 z^{-2}}{1 + b_1 z^{-1} + b_2 z^{-2}} \qquad (3.19)$$

This filter is seen to have 3 multiplications going into the first summer and three multiplications going into the second summer. The output noise variance for these multiplications is as follows:

$$N_o = \frac{E_o^2}{12} \left(3 + \frac{3}{2\pi j} \oint D(z)\, D(z^{-1})\, z^{-1}\, dz\right) \qquad (3.20)$$

This noise variance can be considered as additive to the noise variance of the A/D truncation giving a total noise variance for the combination of A/D truncation and arithmetic roundoff.

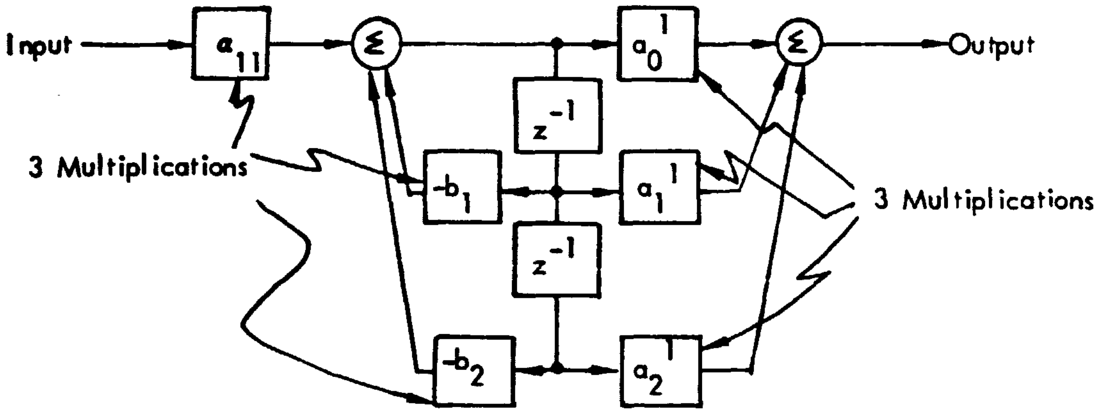

FIGURE 3.1.4: Scaled State Variable Diagram for $D_1(z)$

It is very difficult to give general ground rules for the best method of implementing digital filters in terms of state variable programming form and scaling technique. Most work to date has shown that the parallel state variable form gives good performance results for a wide class of filter implementations. But there are even variations in the performance of parallel filters depending upon the scaling method. Thus, the question arises as to why the cascade form is considered at all. The primary reason for considering it is that the various filter blocks can be changed without affecting all the coefficients for the total filter as happens when dealing with parallel filters. Also by choosing the proper state variable form, combining the proper poles and zeros in the respective blocks and then cascading the blocks correctly, performance comparable to and sometimes bettar than the parallel form can be derived. It might also be mentioned that although coefficient quantization problems dictate breaking filters into first order elements for real poles and zeros and second order elements for complex poles and zeros, the computer software can be simplified by utilizing a second order filter as the basic building block in either the parallel or cascade form.

The only general .esults in the literature are due to Jackson [21] whc considers the canonic second order form (See Figure 2.4) and its transpose and looks at the performance of this form for both parallel and cascade implementation. He finds that filter performance is dependent upon the type of scaling used (either max value or RMS) and state variable form. He also shows that the implementation scheme is dependent upon the measure of signal to noise performance. E.g., if one is trying to minimize the output noise variance (total average power) or the maximum value of the output noise, different implementation schemes would be required.

Summary of Machine Requirements/Synthesis Approach Trades

As pointed out in Section 2.1, the synthesis approach directly affects the machine requirements. For example, a high sampling rate synchronously sampled system will require much more computer capability than a slow sampling rate version of the same filter. In applications with wideband frequency response requirements, the computer requirements can often be reduced by going to a multirate realization. The multirate implementation could have a fast update rate front end to prevent folding and to meet the high frequency requirements, e.g. body bending filters. The low frequency filter requirements, e.g. rigid mode shaping filters, could be realized at a lower sampling rate which reduced the arithmetic and coefficient quantization problems. Besides giving better performance, a multirate filter can also free up computation time as not all the computations are performed every cycle.

How the filters are split in terms of computation rate is usually obvious from considering the respective filter bandwidth requirements. In wideband shaping filter applications, it is sometimes necessary to combine any free lag filters with the fast update rate filters as problems can arise meeting shaping requirements at frequencies greater than the break frequency of the lag filter due to the notching characteristics of digitized lag filters.

3.2 Computer Wordlength Study for Low Q Data

The computer wordlength study was run using the low Q multirate system design presented in Section 2.0. Four frequency responses were made using wordlengths of 39, 24, 16 and 8 bits. The scaled direct canonic state variable form was used in modeling the rigid and body bending mode filters as it was in the original multirate design. A block diagram of this state variable form was shown in Figure 2.6.4. In each run the scaled coefficients were calculated, then truncated. The results of each addition and subtraction were truncated as well as the results of each multiplication. Before storage, each state variable was truncated. In all four runs the A/D and D/A wordlengths were respectively 14 and 15 bits, including the sign bit.

In Table 3.1 the results of the computer wordlength study are shown for frequencies between 0.5 radians per second and 18 radians per second. The results show little phase and gain differences among the 39, 24 and 16 bit runs. This is not surprising. The poles for the rigid mode filter were shown, in Subsection 2.5, to be at $z = +.502$ and $z = +0.3153$ and the two zeros at $z = -1$. For the body bending mode filter the poles were placed at $z = 0.3 \pm j\, 0.519$ and the zeros at $z = 0.4 \pm j\, .85$. In each case the poles and zeros are well removed from the $z = +1$ region. This is the region of the rigid mode dynamics. The farther removed the compensation poles and zeros are from the unit circle encompassed by this region the less sensitive the rigid mode dynamics become to truncation error. Therefore a computer wordlength of 16 bits would accurately represent the low Q multirate design. A small computer wordlength could also be used to represent the low Q synchronous design. In the synchronous design for $T = 0.08$ seconds the rigid body compensation poles are the same as those for the multirate design. The complex poles and zeros for this design are respectively at $z = -0.4738 \pm j\, 0.6446$ and $z = -0.583 \pm j\, 0.750$. These complex poles and zeros are further removed from the $z = +1$ region than the corresponding poles and zeros in the multirate design. For the synchronous design at $T = 0.04$ seconds the complex poles are at $z = 0.35 \pm j\, 0.487$ and the rigid body compensation poles are at $z = +0.7221$ and $z = +0.60679$. These poles are well removed from the $z = +1$ region. Therefore a computer with small wordlength could also represent the low Q synchronous design without affecting filter sensitivity.

As stated in Subsection 2.5 the low Q multirate design has no distinct advantage over the single rate design. This is not surprising. One advantage that can be gained by going to a multirate system is when the design must meet wideband frequency response requirements. The fast update rate is used to prevent folding and to meet the high frequency requirements. The slow update rate is used for the low frequency requirements and the arithmetic and coefficient quantization problems. In the low Q system design there are no arithmetic and coefficient quantization problems with either sampling

TABLE 3.1: Effects of Computer Wordlength on the Low Q Multirate Frequency Response

	39 BITS		24 BITS		16 BITS		8 BITS	
	db	Phase	db	Phase	db	Phase	db	Phase
ω = 0.5	14.1	199°	14.1	199°	14.1	199°	11.03	204.9°
ω = 2.0	-3.8	209°	-3.8	209°	-3.86	209°	-4.82	210.2°
ω = 4.0	-9.49	188°	-9.47	190°	-9.49	189°		
ω = 6.0	-11.6	161°	-11.6	162°	-11.4	161.5°		
ω = 8.0	-11.5	137°	-11.54	140°	-11.54	140°		
ω = 10.0	-8.75	114°	-8.85	116°	-8.86	116°		
ω = 12.0	+14.82	318°	16.28	337°	13.97	329°		
ω = 14.0	-17	247°	-16.8	252°	-16.8	252°		
ω = 16.0	-27.7	223°	-27.21	224.2°	-27.23	218.4°		
ω = 18.0	-32.25	187.8°	-36.6	189.8°	-36.61	184.9°		

rate and all frequency response requirements can be met at T = 0.04 seconds or T = 0.08 seconds. There is folding for T = 0.08 seconds. The fourth body bending pole does fold into the primary strip but it folds near the second and third body bending poles. Here it becomes an advantage instead of a disadvantage in designing body bending compensation.

3.3 Machine Requirements

The machine requirements to implement the rigid and body bending mode filters for the synchronously sampled system are discussed in this section. Using the Teledyne TDY-214 minicomputer and accompanying instruction set, both filters can be realized with 47 core locations. A complete list of storage requirements, broken down into instruction total, temporary data storage, constants, variable data storage, multipliers, adds, loads, stores and transfers are shown in Figure 3.3.1.

26	Instructions
1	Temporary Storage Location
12	Constants
8	Variables
47	Total Storage Requirements

		Average Execution Time/Instruction
12	Additions	7 1/2 sec
12	Loads	6 2/3 sec
11	Store Accumulator	6 2/3 sec
2	Transfers	6 2/3 sec
15	Multiplications	31 sec

FIGURE 3.3.1: Machine Requirements for Filter Implementation

The filter realized with the 47 core locations is the digital autopilot for the rigid and body bending modes sampled at T = 0.08 seconds. The filter is shown below

$$\frac{0.34237\,(z+1)}{z-0.315261} \qquad \frac{0.248905\,(z+1)}{z-0.502190} \qquad \frac{0.57219z^2 + 0.66374z + 0.51434}{z^2 + 0.94758z + 0.64}$$

The state variables are defined as follows:

X1(k+1) = +0.315261 X1(k) + [0.342370 + 0.315261 (0.34237)] INPUT(k)
OUT1(k) = X1(k) + 0.34237 INPUT(k)
X2(k+1) = 0.502190 X2(k) + [0.248905 + 0.502190 (0.248905)] OUT1(k)
OUT2(k) = X2(k) + 0.248905 OUT1(k)
X3(k+1) = -0.94758 X3(k) + X4(k) + [0.66374 - 0.94758 (0.57219)] OUT2(k)
X4(k+1) = -0.64 X4(k) + [0.51434 - 0.64 (0.57219)] OUT2(k)
OUT3(k) = X3(k) + 0.57219 OUT2(k)

The instruction set for the TDY-214 is of the single address type and has the following format:

INSTRUCTION					TAG		ADDRESS												
0	1	2	3	4	5	6	7												19

The tag field is two bits in length and indicates which index register, if any, will modify the address portion of the instruction. For implementing the rigid and body bending mode filters only one of the three index registers is used as well as just one of the two accumulators available with the TDY-214. The assembly language program is shown below.

FILTER COMPUTATION PROGRAM

(X) means contents of address X

Location	Inst.	Tag.	Address	
01145	LDX	1	1200	Load index register 1 with (1200)
01146	LDU	1	1205	Load upper accumulator with (1205 +(index register 1))
01147	MPY	1	1202	Multiply (upper accumulator) by (1202 +(index register 1))
01150	ADD	1	1206	Add to (upper accumulator) (1206 + (index register 1))
01151	STU	1	1201	Store contents of upper accumulator in 1201 + (index register 1)
01152	LDU	1	1215	Load upper accumulator with (1215 + (index register 1))
01153	MPY	1	1205	Multiply (upper accumulator) by (1205 +(index register 1))
01154	ADD	1	1221	Add to (upper accumulator) (1221 + (index register 1))
01155	MPY	1	1202	Multiply (upper accumulator) by (1202 +(index register 1))
01156	STU		1177	Store contents of (upper accumulator) in 1177

FILTER COMPUTATION PROGRAM (Continued)

Location	Inst.	Tag	Address	
01157	LDU	1	1215	Load upper accumulator with (1215 + (index register 1))
01160	MPY	1	1211	Multiply (upper accumulator) by (1211 + (index register 1))
01161	ADD	1	1177	Add to (upper accumulator) (1177 + (index register 1))
01162	STU	1	1211	Store contents of upper accumulator in 1211 + (index register 1)
01163	TRX	1	1146	If (index register 1) ≠ 0, decrement contents of index register by one and transfer control to location 1146. If (index register 1) = 0 continue to next instruction
01164	LDU		1214	Load upper accumulator with (1214)
01165	MPY		1205	Multiply (upper accumulator) by (1205)
01166	ADD		1220	Add to (upper accumulator) the (1220)
01167	MPY		1201	Multiply (upper accumulator) by (1201)
01170	STU		1177	Store contents of upper accumulator in 1177
01171	LDU		121A	Load upper accumulator with (1214)
01172	MPY		1210	Multiply (upper accumulator) by (1210)
01173	ADD		1177	Add to (upper accumulator) the (1177)
01174	ADD		1211	Add to (upper accumulator) the (1211)
01175	STU		1210	Store (upper accumulator) in 1210
01176	TRI		XXXX	Transfer back to main program
01177	Temporary data location			
01200	2_{10} stored here			
01201	Storage location for OUT3			
01202	Storage location for OUT2			
01203	Storage location for OUT1			
01204	Storage location for the input			
01205	0.57219_{10} stored here			
01206	0.248905_{10} stored here			
01207	0.342370_{10} stored here			
01210	Storage location for X3(k)			
01211	Storage location for X4(k)			
01212	Storage location for X2(k)			
01213	Storage location for X1(k)			
01214	-0.94758_{10} stored here			
01215	-0.64_{10} stored here			
01216	0.502190_{10} stored here			
01217	0.315261_{10} stored here			
01220	0.66374_{10} stored here			
01221	0.51434_{10} stored here			
01222	0.248905_{10} stored here			
01223	0.342370_{10} stored here			

4.0 MULTIRATE SAMPLED DATA ANALYSIS METHODS

In the literature there are two major approaches to analyzing multiloop, multirate sampled data systems. The first approach was proposed by G. M. Kranc [11]. It involves replacing each sampler, T/N, by an equivalent configuration of advance and delay elements sampled at a single rate, T. This allows the already developed transform method of analysis for single rate systems to be applied to multirate systems. The second approach is the state transition method introduced by Kalman and Bertram [3]. Defining state variables for the continuous and digital elements as well as for the zero order hold elements allows the system to be described by a set of transition matrices. The multirate analysis is then carried out by manipulating the various transition matrices. The purpose of this section is to investigate these va ious approaches and to choose the most appropriate method for analyzing both synchronous and multirate sampled data control systems.

4.1 Kranc's Switch Decomposition Method

In Appendix A two approaches using Kranc's switch decomposition method for analyzing multiloop, multirate sampled data control systems are presented in detail. The first approach is Kranc's original method. The method is relatively straight forward but has the disadvantage of involving a substantial amount of work in separating each of the branch variables from the governing loop equations. For more complicated systems which utilize a digital computer for analysis, the amount of work required by the computer to separate the branch variables to form the characteristic equation is greater than the work required to do the actual system analysis. The second method discussed is the procedure outlined by Boykin and Frazier [12]. It extends Kranc's technique by introducing a vector notation for the advance and delay elements as well as a set of identities needed to convert the resulting vector/matrix equations to scalar equations. The procedure simplifies Kranc's original technique by allowing the governing loop equations to be easily written down by inspection of the signal flow graph. It offers little help, however, in separating the branch variables from the governing loop equations.

An extension to Kranc's switch decomposition method which partially reduces the problem of separating the branch variables from the loop equations is the method dsveloped by Thomas C. Coffey and Ivan J. Williams [13]. Their procedure is to approach the switch decomposition method in the frequency-domain. By incorporating appropriate shifts in the s-domain terms and by judiciously choosing the branch variables, Coffey and Williams develop an identity which can easily be implemented on a digital computer. The disadvantage of Coffey and Williams method is that, like Boykin and Frazier's method, considerable care is needed in applying the identity. Therefore the analyst needs extensive knowledge of the method or an intricate computer program for setting up the analysis.

Two relatively recent papers by E. I. Jury [14, 15] have extended Coffey and Williams switch decomposition method. Jury shows equivalence between the s domain approach and the z domain as well as the power of complex integration in formulating the z transform. Jury's contribution allows Coffey and Williams method to be worked in the z-domain but it too fails to reduce the computer implementation problem.

All three switch decomposition methods have one common advantage and one common disadvantage. From a block diagram or signal flow graph point of view the problem is straight forward and easy to understand. The disadvantage is in the degree of sophistication needed to implement the various techniques. For this reason, and for the relative simplicity in understanding and in implementing the state variable approach, Kranc's switch decomposition method was dropped as a tool for analyzing multirate sample data control systems. The remainder of this section is devoted to developing the state variable approach as an analytic technique for synchronous and multirate systems.

4.2 State Variable Approach to Multirate Sampled Data System Analysis

The application of state variable techniques to multirate systems was first proposed by Kalman and Bertram [3]. By using the concept of state and transition matrix, it is possible to analyze both synchronous and multirate systems within the same general framework. The state approach also overcomes a serious difficulty of transform methods by giving time response information at all times and not just at sampling instants. This approach is also easily implemented on a digital computer.

A typical linear sampled data control system block diagram is shown in Figure 4.2.1. From this diagram it can be seen that the sampled system contains the following types of dynamic elements: continuous dynamic elements, discrete dynamic elements and sample and hold dynamic elements. The dynamics of these various elements can be described by state variable relationships. The state of a dynamic element can loosely be defined as the minimum amount of information, e.g., an nx1 array of numbers, which is necessary to calculate the future behavior of the dynamic element when one knows the input/output relationship for the element and the input to the element.

4.3 States of Linear Sampled Data Systems

A linear sampled data system typically contains the following three types of state variables:

1. Continuous state variables - The continuous dynamic elements are described by ordinary linear differential equations with constant coefficients. The state variables are defined as the outputs of the integrators that appear in the state variable (first order) representation of the differential equation.

2. Discrete state variables - The discrete state variables are governed by linear difference equations. These equations are idealized representations of the computations that are performed in a digital computer. The computer actions necessary to implement these equations involve performing arithmetic operations on sampled input signals and stored data, storing the data necessary for the next round of computations and placing the output in a register or storage location where a D/A device has access to it. The state variables for the discrete dynamic elements are the numbers that must be stored in order to perform the next round of computations. These states get updated only during a computation and remain constant until the next computation involving these states. The state variables are defined as the outputs of the delay elements that appear in the state diagram representation of the difference equations.

3. Sample and Hold State Variables - The sample and hold element represents, in an idealized sense, the operation of sampling various types of information and

then applying this information through a smoothing filter to the input of a continuous dynamic element. So basically this element is a discrete-time element that gets updated at sampling instants and holds this value until the next sampling instant. The state of this element is equal to its output.

From the state variable descriptions, it can be seen that the continuous state variables transition in a continuous fashion while the discrete time and sample hold variables may be thought of as taking place at the sampling instants only.

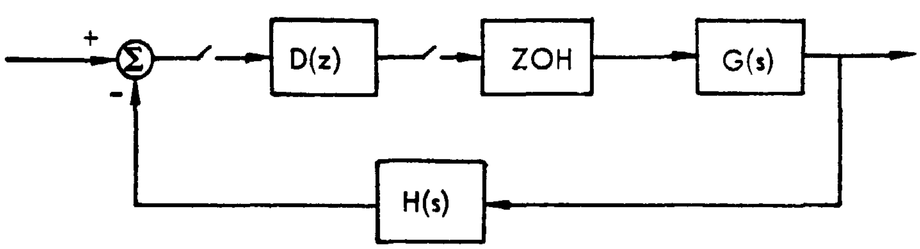

FIGURE 4.2.1: A Linear Sampled Data Control System

The state of the entire system can then be written as the nx1 column vector X defined as follows:

$$X = \begin{bmatrix} X^C \\ X^D \\ X^{SH} \end{bmatrix} \qquad (4.1)$$

where X^C is a $\gamma \times 1$ column vector of continuous states
X^D is a $\delta \times 1$ column vector of discrete states
X^{SH} is an $n - (\gamma + \delta)$ column vector of sample and hold states.

4.3 State Transition Equations

The state transitions for the various dynamic elements will now be described. Before discussing these relationships, it is interesting to look at the time sequence of events that transpire in a digital cont. l system in an idealized sense. First of all, it is assumed that the discrete dynamic elements and sample and hold dynamic elements that get updated at a sampling instant transition in the time instant $t_k \longrightarrow t_k^+$. Likewise the continuous dynamic elements remain unchanged over this instant but transition over the finite interval $t_k^+ \leq t \leq t_{k+1}$. This is shown graphically in Figure 4.3.1.

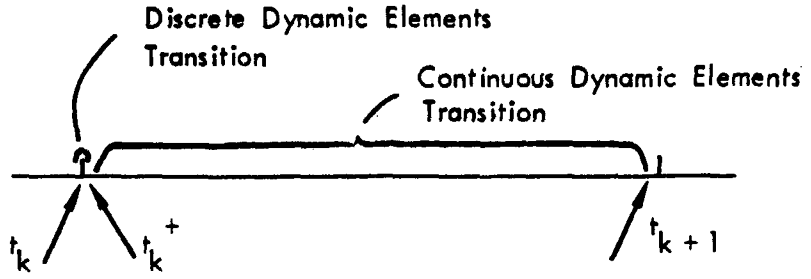
Discrete Dynamic Elements Transition
Continuous Dynamic Elements Transition
t_k
t_k^+
t_{k+1}

FIGURE 4.3.1: Idealized Time Sequence of Events

Under the assumption that the discrete and sample and hold variables transition instantaneously these two state variable forms can be combined and the state of the entire system simplifies to

$$X = \begin{bmatrix} X^C \\ X^D \end{bmatrix} \qquad (4.2)$$

Discrete State Transition

The discrete time states are transitioned by the following relationship:

$$x_i\,(t_k + \tau) = \sum_{j=1}^{n} d_{ij}\, x_k\,(t_k) + d_{i,\,n+1}\, r(t_k) \quad i = \gamma + 1, \ldots \gamma + \delta \qquad (4.3)$$

where τ is the time it takes the computer to complete the computations. As stated previously it is usually assumed that the computations are done instantaneously; therefore, the left side of this equation is written as t_k^+ giving

$$x_i\,(t_k^+) = \sum_{j=1}^{n} d_{ij}\, x_j\,(t_k) + d_{i,\,n+1}\, r\,(t_k) \qquad (4.4)$$

Sample and Hold State Transition

The sampling process is assumed to take place instantaneously. The state transition equation for the sample and hold element is thus given by

$$x_i(t_k^+) = \sum_{j=1}^{n} s_{ij}\, x_j(t_k) + s_{i,n+1}\, r(t_k) \qquad i = \gamma + \delta + 1, \ldots, n \tag{4.5}$$

System Transition at a Sampling Instant

Under the assumption that the discrete and sample and hold elements all transition instantaneously at a sampling instant, equations (4.4) and (4.5) can be combined into an overall system transition relationship at a sampling instant as follows:

$$x(t_k^+) = B\, x(t_k) + f\, r(t_k) \tag{4.6}$$

where

$$B = \begin{array}{c|c|c|c} & \gamma & \delta & n-(\delta+\gamma) \\ \hline \gamma & I & 0 & 0 \\ \hline \delta & \multicolumn{3}{c}{d_{ij}} \\ \hline n-(\delta+\gamma) & \multicolumn{3}{c}{s_{ij}} \end{array} \qquad f = \begin{array}{c|c} \gamma & 0 \\ \hline \delta & \begin{matrix} d_{\gamma+1} \\ \vdots \\ d_{\gamma+\delta} \end{matrix} \\ \hline n-(\delta+\gamma) & \begin{matrix} s_{\gamma+\delta+1} \\ \vdots \\ s_n \end{matrix} \end{array}$$

Continuous System Transition

The continuous dynamic elements are described by the following first order differential equation:

$$\dot{x}^c = A^c x^c + f^c m \tag{4.7}$$

The integral of this equation gives the state transition relationship for the continuous dynamic elements and is given below.

$$x^c (t_k + \tau) = \phi^c (\tau)\, x^c (t_k) + \int_{t_k}^{t} \phi (t - \sigma)\, f^c m (\sigma)\, d\sigma \tag{4.8}$$

where $t = t_k +$

In order to simplify the expressions that follow, it is convenient to assume the inputs to the continuous dynamic elements are from only sample and hold elements. Since these inputs are constant between sampling instants, the following closed form expression can be written for the integral:

$$\int_{t_k}^{t} x_j (t_k^+)\, \phi (t - \sigma)\, f^j\, d\sigma = x_j (t_k^+)\, h_i^j (\tau) \tag{4.9}$$

Therefore, the state transition equation (in component form) for the continuous dynamic elements is given by

$$x_i (t_k + \tau) = \sum_{j=1}^{\gamma} \phi^c{}_{ij} (\tau)\, x_j (t_k) + \sum_{j=\gamma+\delta+1}^{n} h_i^j (\tau)\, x_j (t_k^+) \quad i = 1, 2, \ldots \gamma \tag{4.10}$$

$$0 < \tau \le t_{k+1} - t_k$$

System Transition Between Sampling Instants

The total system transition relationship between sampling instants can be written as follows:

$$x (t_{k+1}) = \Phi (T_k)\, x (t_k^+) \tag{4.11}$$

where

$$\Phi(T_k) = \left[\begin{array}{c|c|c} \phi^c(T_k) & 0 & h_i^i(T_k) \\ \hline 0 & I & 0 \\ \hline 0 & 0 & I \end{array}\right] \begin{array}{l} \updownarrow \gamma \\ \updownarrow \delta \\ \updownarrow n-(\gamma+\delta) \end{array}$$

$$x(t_k^+) = \begin{bmatrix} x^c(t_k) \\ x^D(t_k^+) \end{bmatrix}$$

Stability of Synchronously Sampled Systems

The stability of synchronously sampled systems can be analyzed by using equations (4.6) and (4.11). The complete state transition from time n T to time (n+1) T is given by

$$x((n+1)T) = \Phi(T)\ (B\ x\ (nT)) + f\ r(nT)$$

$$= \psi(T)\ x\ (nT) + h\ (T)\ r\ (nT) \qquad (4.12)$$

where

$$\psi(T) = \Phi(T)\ B$$

$$h(T) = \Phi(T)\ f$$

Taking the z-transform of this expression and rearranging gives

$$x(z) = \left[z\,I - \psi(T)\right]^{-1} z\ x(0) + \left[z\,I - \psi(T)\right]^{-1} h(T)\ R(z) \qquad (4.13)$$

The characteristic equation for this system is therefore given by

$$\det \left| z\,I - \psi(T) \right| = 0 \qquad (4.14)$$

These results are summarized in the following theorem [3]:

Theorem !. A stationary linear system is stable if all n zeros, z_i, of the polynomial $\left| z \, I - \psi(T) \right|$ satisfy

$$\left| z_i \right| < 1$$

for i = 1, 2, ... , n.

These results are ε;υivalent to the results using z-transform theory. That this is the case will be demonstrn.ted by working an example problem by both z-transform and state variable methods.

Example 4.1

Consider the sampled data control system shown in Figure 4.3.2. Taking the z-transform of this system gives the following results:

$$G(z) = z \left\{ \frac{1 - e^{-sT}}{s^2 (s + 1)} \right\} = \frac{z(T - 1 + e^{-T}) + (1 - T e^{-T} - e^{-T})}{(z - 1)(z - e^{-T})} \qquad (4.15)$$

The open loop frequency response for this system can be evaluated by plotting the system poles and zeros in the z-plane and evaluating the magnitude and phase from these singularities to points on the unit circle. The root locus for this system can likewise be ascertained.

Example 4.2

Consider again the system shown in Figure 4.3.2. The state variable diagram for this system is shown in Figure 4.3.3. From this figure the state equations for the dynamic elements are given by

$$\begin{aligned} \dot{x}_1 &= -x_1 + x_2 \\ \dot{x}_2 &= x_3 \\ \dot{x}_3 &= 0 \end{aligned} \qquad (4.16)$$

and the state transition relationship at a sampling instant is

$$x_3 (nT^+) = r(nT) - kx_1 (nT) \qquad (4.17)$$

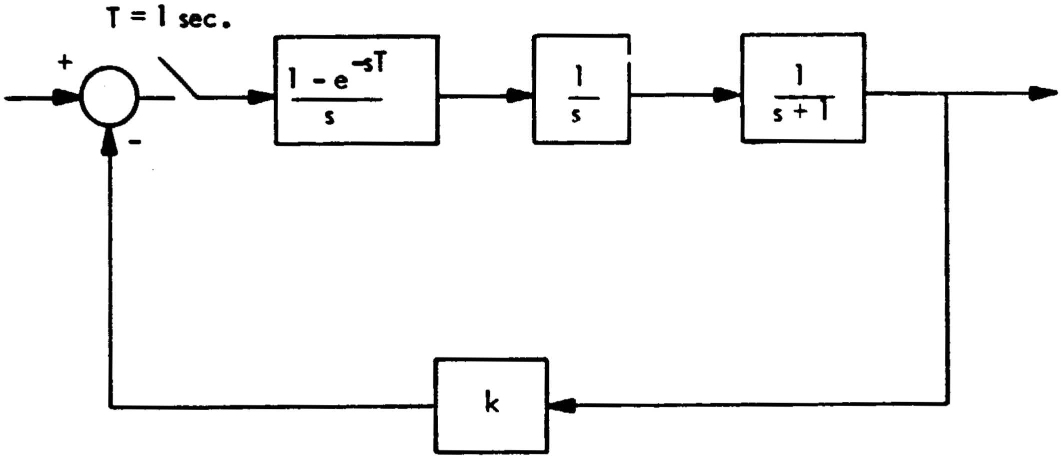

Figure 4.3.2: Sampled Data Control System

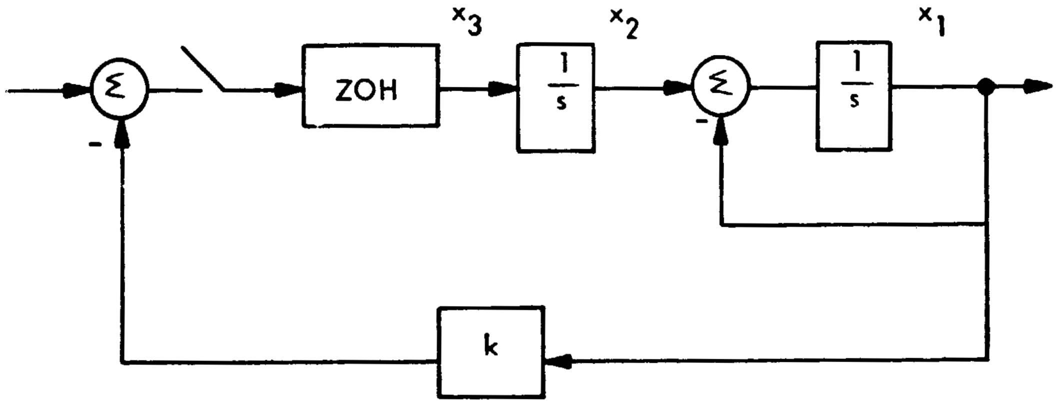

Figure 4.3.3: State Variable Diagram for Sampled System

The A and B matrices for this system are as follows:

$$A = \begin{pmatrix} -1 & 1 & 0 \\ 0 & 0 & 1 \\ 0 & 0 & 0 \end{pmatrix} ; \quad B = \begin{pmatrix} 1 & 0 & 0 \\ 0 & 1 & 0 \\ -k & 0 & 0 \end{pmatrix} \tag{4.18}$$

Evaluating the relationships

$$\emptyset(T) \overset{\Delta}{=} L^{-1} \left\{ (sI - A)^{-1} \right\}$$

or just numerically integrating the equation $\dot{X} = AX$ over a sampling period, the transition matrix $\emptyset(T)$ is

$$\emptyset(T) = \begin{pmatrix} e^{-T} & 1-e^{-T} & T - 1 + e^{-T} \\ 0 & 1 & T \\ 0 & 0 & 1 \end{pmatrix} \tag{4.19}$$

The system transition matrix $\psi(T)$ is therefore as follows:

$$\psi(T) = \Phi(T)\ B = \begin{pmatrix} e^{-T} - k(T-1+e^{-T}) & 1-e^{-T} & 0 \\ -Tk & 1 & 0 \\ -k & 0 & 0 \end{pmatrix} \tag{4.20}$$

The characteristic equation then becomes

$$\left| zI - \psi(T) \right| = z(z^2 + (k(T-1+e^{-T}) - 1 - e^{-T})z + e^{-T}(1-k(1+T)) + K) \tag{4.21}$$

The open loop poles* for this system can be found by evaluating the characteristic equation at $k = 0$ giving

$$z(z-1)(z-e^{-T}) \tag{4.22}$$

The open loop zeros for the system can be determined by subtracting the characteristic equation with $k = 0$ from the characteristic equation with $k = 1$ giving

$$z(z(T-1+e^{-T}) + (1 - T e^{-T} - e^{-T})) \tag{4.23}$$

Thus, the system transfer function is given as shown below:

$$G(z) = \frac{z(z(T-1+e^{-T}) + (1 - T e^{-T} - e^{-T}))}{z(z-1)(z-e^{-T})} \tag{4.24}$$

- - - - - - - - - - - - - -

* These results are based upon the assumption that the system transfer function is of the form:

$$\frac{C}{R} = \frac{k\,G(z)}{1 + k\,G(z)} = \frac{k\,N(z)}{D(z) + kN(z)}$$

This transfer function is seen to be equal to the results as derived from z-transform theory. The root locus for this system can be found by solving the characteristic equation (4.21) at difference values of k. Likewise, the frequency response can also be evaluated for this system.

The presented simple example gives the impression that the state space approach leads to a more complicated solution than analysis by the classical methods. This might be the case for this simple example except that a computer implementation of the classical approach would require partial fraction expanding the function G(s) and then possibly doing a table look up of stored z-transforms. It is then necessary to recombine the z-transforms to get the transfer function. The state space approach is seen to involve matrix manilupations which can be readily carried out on digital computers. More will be said in the next section concerning the general applicability of state transition approach techniques to the analysis of more complex systems. It might also be mentioned that the state transition approach also leads quite readily to optimal synthesis and to the concepts of controllability and observability for discrete and continuous time systems.

4.4 Extending the State Transition Technique to More Complex Systems

Theorem 1 has been shown to be identical to z-transform results that require the system closed loop poles to lie within the unit circle in the z-plane for stability. The use of z-transform techniques has been limited to studying synchronously sampled systems. Modifications and extensions have been proposed to the z-transform but these results have been shown to be cumbersome to apply and not applicable to a wide class of problems. The state space approach of Kalman and Bertram can be applied to a much broader spectrum of sampled data problems. Also, for problems where a staiionary transition matrix can be defined, Theorem 1 is applicable with the appropriately defined ψ . It has been pointed out in Reference [3] that a stationary transition matrix can be obtained whenever the sampling operations repeat in a periodic fashion. Some sample cases where stationary transition matrices arise will now be reviewed.

Cyclic Variable Rate Sampling

The sampling operation in a cyclic variable rate system could be assumed to follow a pattern as shown in Figure 4.4.1. The samples are synchronous but the rate is seen to vary in a fixed cyclic manner.

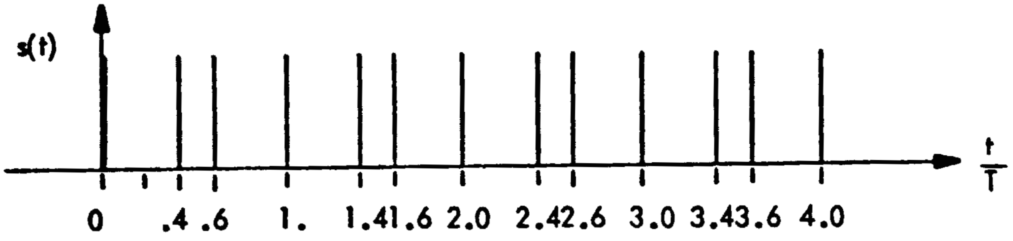

Figure 4.4.1: The Sampling Process for a Cyclic Variable Rate Sampler

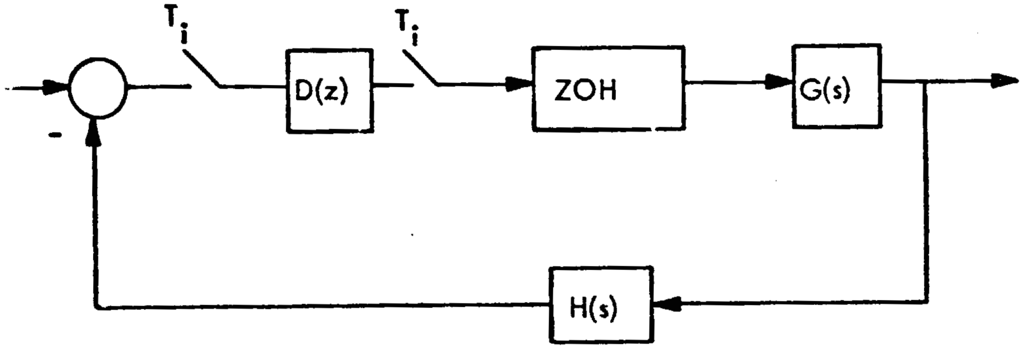

Figure 4.4.2: Cyclic Sampling Rate System

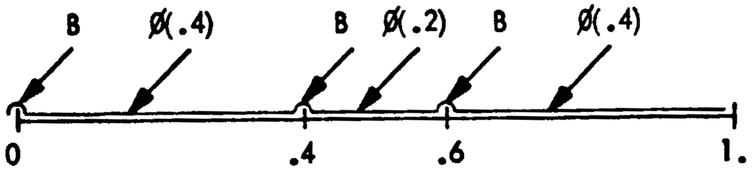

Figure 4.4.3: Time Sequence of Transitions

The transition matrix for this system will be stationary if a basic sampling period of one second is considered. For the simple system shown schematically in Figure 4.4.2 the stationary transition matrix would be computed as follows·

First, define the relationships

$$\dot{x} = AX \qquad (4.25)$$

$$x(t_k^+) = B\,x(t_k) \qquad (4.26)$$

Second, solve equation (4.25) for $\phi(T_i)$ and then use the B matrix to define the following stationary transition matrix (see Figure 4.4.3).

$$\psi(1) = \phi(.4)\,B\ \ \phi(.2)\,B\ \ \phi(.4)\,B \qquad (4.27)$$

The characteristic equation for this system is given by

$$\det \left| z\,I - \psi(1) \right| = 0 \qquad (4.28)$$

and it is thus possible to conduct both frequency response, root locus and time response analysis of this type system.

Multirate Sampled Data System Design

A multirate sampled data system is assumed to have more than one sampler where the sampling process could be as shown in Figure 4.4.4. Multirate systems will exhibit a stationary transition matrix whenever the samplers act synchronously in a cyclic manner. This will be the case whenever the ratio of the various sampling periods is rational. For example, for the samplers in Figure 4.4.5 the period T for which all the samples act synchronously is T = 1 second. In general, the shortest period for a stationary transition matrix is given by

$T_i/T_j = p/q$ where p and q are relatively prime integers.

The sampling patterns have a least common period given by

$$T = T_i q = T_j p$$

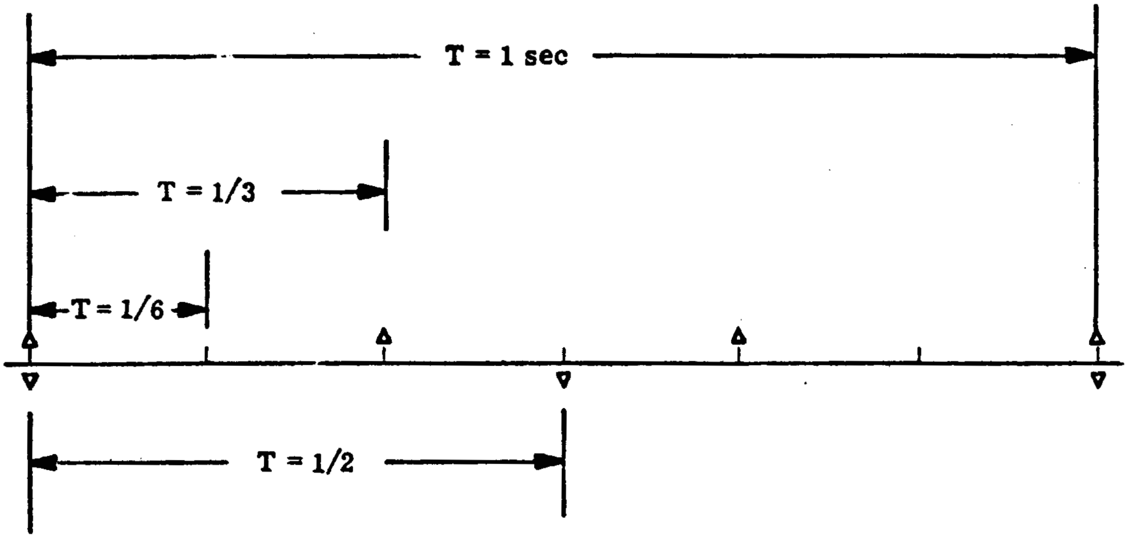

FIGURE4.4.4:SAMPLING PATTFRNS FO? MULTIRATE SYSTEM

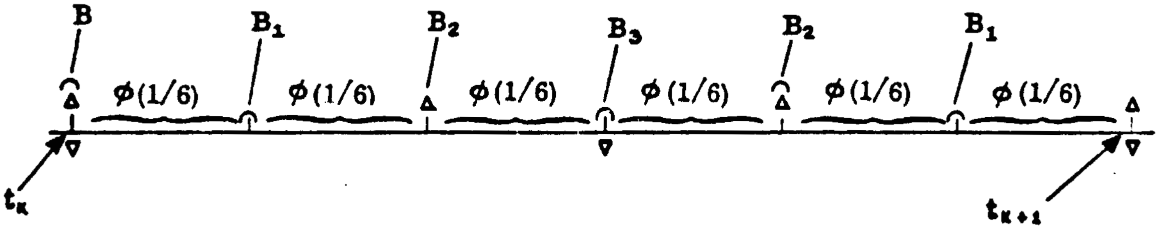

FIGURE4.4.5:TRANSITIONS FOR MULTIRATE SYSTEM

When T_i/T_j is irrational, it is impossible to write a stationary transition matrix. If p and q are large integers then almost the same situation arises as it takes a very large number of intervals to define the overall stationary transition matrix.

For multirate systems where it is possible to define a stationary transition matrix, the analysis proceeds as for the other types of systems analyzed. For the system considered in Figure 4.4.4, the operations that must be performed to definc the matrix (T) are as follows (see Figure 4.4.5):

$$\psi(1) = \emptyset(1/6)\ B_1\ \emptyset(1/6)\ B_2\ \emptyset(1/6)\ B_3\ \emptyset(1/6)\ B_2\ \emptyset(1/6)\ B_1\ \emptyset(1/6)\ B \qquad (4.28a)$$

where the B matrices are given by

B = discrete transition matrix when all samplers are acting synchronously

B_1 = discrete transition matrix when sampler with T = 1/6 is acting

B_2 = discrete transition matrix when samplers with T = 1/6 and T = 1/3 are acting

B_3 = discrete transition matrix when samplers with T = 1/6 and T = 1/2 are acting

and $\emptyset(1/6)$ is the continuous transition relationship evaluated for t = 1/6 sec.

Using the ψ (T) defined by equation (4.28a), system stabilit, can be analyzed by applying Theorem 1. Thus, the characteristic equation for this system would be given by

$$\left| zI - \psi(T) \right| = 0$$

Some example solutions using the state transition approach developed in this section will now be compared with the solution technique of Kranc for the system shown in Figure 4.4.6.

State Transition Solution

The state relationship for this system between sampling instants is as follows from inspecting Figure 4.4.6.

$$\begin{aligned} \dot{x}_1 &= x_3 \\ \dot{x}_2 &= x_4 \\ \dot{x}_3 &= 0 \\ \dot{x}_4 &= 0 \end{aligned} \qquad (4.29)$$

or in matrix form

$$\dot{x} = Ax \tag{4.30}$$

where

$$A = \begin{bmatrix} 0 & 0 & 1 & 0 \\ 0 & 0 & 0 & 1 \\ 0 & 0 & 0 & 0 \\ 0 & 0 & 0 & 0 \end{bmatrix} \tag{4.31}$$

The state transition relationship when both samplers act synchronously is given by

$$x\,(nT_i^{+}) = B\,x\,(n\,T_i) \tag{4.32}$$

where

$$B = \begin{bmatrix} 1 & 0 & 0 & 0 \\ 0 & 1 & 0 & 0 \\ 0 & -1 & 0 & 0 \\ 1 & 0 & 0 & 0 \end{bmatrix} \tag{4.33}$$

Likewise, the state transition relationship when only the fast sampler is acting is described by

$$x\,(nT_i^{+}) = B_1\,x\,(nT_i) \tag{4.34}$$

where

$$B_1 = \begin{bmatrix} 1 & 0 & 0 & 0 \\ 0 & 1 & 0 & 0 \\ 0 & 0 & 1 & 0 \\ 1 & 0 & 0 & 0 \end{bmatrix} \tag{4.35}$$

The two B matrices are seen to differ only in the third row.

Using the relationship

$$\emptyset\,(1/N) = L^{-1}\left[s\ \ I\ -A\right]^{-1}\Big|\ T/N. \tag{4.36}$$

or just numerically integrating equation (4.30) over a period T/N, $\emptyset$ (T/N) is found to be as follows:

$$\text{Ø}\,(T/N) = \begin{bmatrix} 1 & 0 & T/N & 0 \\ 0 & 1 & 0 & T/N \\ 0 & 0 & 1 & 0 \\ 0 & 0 & 0 & 1 \end{bmatrix} \qquad (4.37)$$

For this example, assume that N = 2. The stationary transition matrix for this situation involves the transition shown in Figure 4.4.7 which is as follows:

$$\psi\,(T) = \text{Ø}\left(\frac{T}{2}\right) \quad B_1\, \text{Ø} \; \left(\frac{T}{2}\right) \quad B \qquad (4.38)$$

Performing these matrix multiplications, gives the following $\psi(T)$:

$$\psi\,(T) = \begin{bmatrix} 1 & -T_2 & 0 & 0 \\ T & 1 - \frac{T}{4} & 0 & 0 \\ 0 & -1 & 0 & 0 \\ 1 & -T/2 & 0 & 0 \end{bmatrix} \qquad (4.39)$$

The characteristic equation is given by $\det \left| z \ \ I - \psi \right| = 0$ and using (4.39) this relationship is as follows:

$$z^2 \ \left[z^2 + \left(\frac{T^2}{4} - 2\right) z + 1 + \frac{3}{4} \ T^2 \right] = 0 \qquad (4.40)$$

Kranc's Time Domain Sampler Decomposition Solution

It is instructive to rework the example of Figure 4.4.6 using Kranc's technique. For N = 2, the fast sampler must be replaced with two parallel samplers acting at the slower rate but with appropriate time shifts in their channels so that the sum of the two is equivalent to the single fast sampler. The equivalent system is shown in Figure 4.4.8.

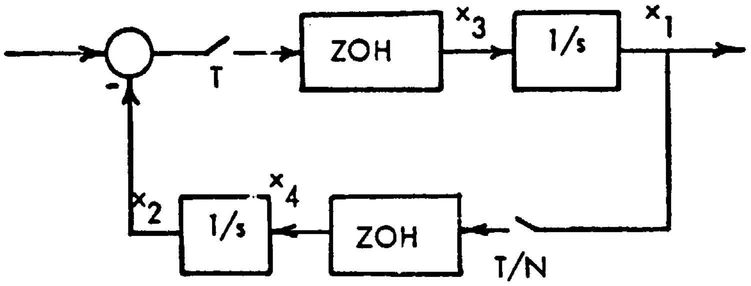

FIGURE 4.4.6: EXAMPLE SYSTEM

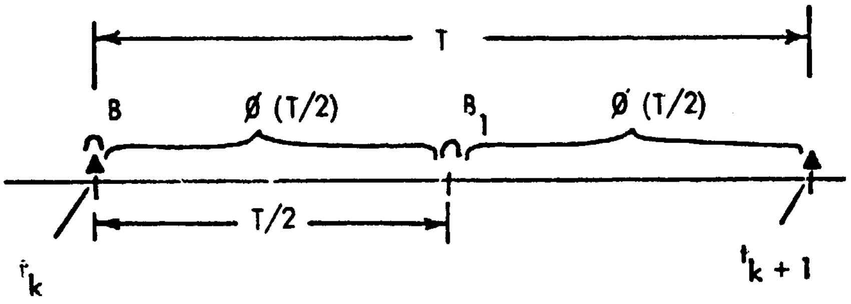

FIGURE 4.4.7: TIME SEQUENCE OF TRANSITIONS FOR N = 2

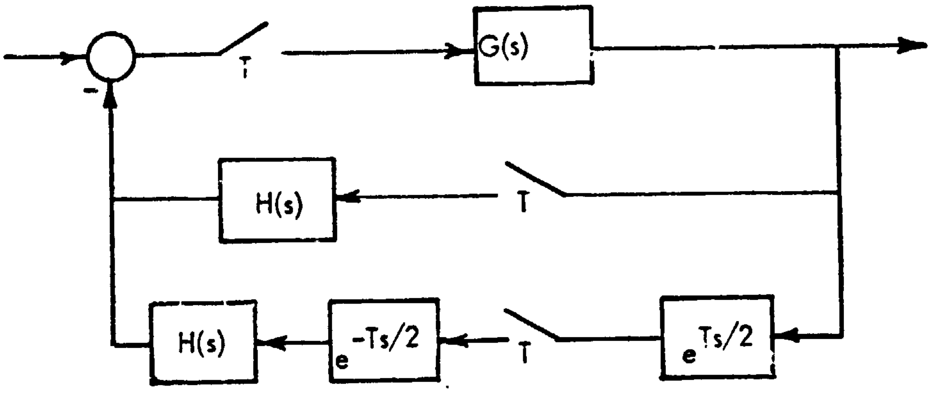

FIGURE 4.4.8: EQUIVALENT SINGLE RATE SYSTEM

The blocks labelled G(s) and H(s) represent the combination of the zero order holds and the original transfer functions and are defined as follows:

$$G(s) = \frac{1 - e^{-sT}}{s^2} \qquad (4.41)$$

$$H(s) = \frac{1 - e^{-sT}}{s^2} \qquad (4.42)$$

From Figure 4.4.8 the system transfer function in the z-domain can be written as

$$\frac{C(z)}{R(z)} = \frac{G(z)}{1 + G(z)\ H(z) + Z\left[e^{sT/2}\ G(s)\right]\ Z\left[e^{-sT/2}\ H(s)\right]} \qquad (4.43)$$

where the characteristic equation is found by equating the denominator of this expression to zero.

The z-transforms of the various terms in equation (4.43) are given below:

$$G(z) = \frac{T}{z-1}$$

$$H(z) = \frac{T}{2(z-1)}$$

$$Z\left[e^{sT/2}\ G(s)\right] = \frac{T(z+1)}{2(z-1)}$$

$$Z\left[e^{-sT/2}\ H(s)\right] = \frac{T}{2(z-1)}$$

Plugging these expressions into the denominator of (4.43), the characteristic equation for this system becomes:

$$z^2 + \left(\frac{T^2}{4} - 2\right) z + 1 + \frac{3}{4} T^2 = 0 \qquad (4.44)$$

This equation is seen to equal equation (4.40) (the state transition derived characteristic equation) except for the two extra zeros in (4.40). These extra zeros result from the discrete states x_3 and x_4 and correspond to the two zero columns in the matrix $\psi(T)$. Based upon the fact that $\psi(T)$ is being used to define the stationary transition relationship

$$x((k+1)T) = \psi(T)\ x(kT) + h(T)\ r(kT) \qquad (4.45)$$

The zero columns of $\psi(T)$ imply that the states x_3 and x_4 need not be known at the k^{th} sampling instant in order to find the state vector at the $(k + 1)^{st}$ sampling instant [3]. Thus, x_3 and x_4 can be dropped from (4.45) and the evaluation of the determinant for the characteristic equation can be greatly simplified by reducing the order of the matrix $|z\ I - \psi|$. It must be pointed out that $\psi(T)$ could not have expressed as a simple product of matrices if x_3 and x_4 had bee:i dropped before obtaining the final result. Therefore, only after $\psi(T)$ has been computed can simplifications be made.

4.5 Multirate Sampled Data Analysis Methods

The following technique- were considered for analyzing multirate sampled data control systems:

1) Time-domain switch decomposition method of Kranc [11].
2) Vector operator signal flow graph technique of Boykin, Frazier, et al [12].
3) Frequency domain approach of Coffey and Williams [13].
4) Z-plane technique of Jury [15].
5) State variable approach of Kalman and Bertram [3].

The state transition approach of Kalman and Bertram was found to be the method with the most general applicability and was also found to be amenable to digital computer solution.

It was demonstrated for systems described by stationary difference equations that the characteristic equation is given by the following expression:

$$\left| z\,I - \psi(T_k) \right| = 0$$

where $\psi(T_k) = \prod_{i=1}^{\ell} \phi(T_i)\, B_i$

$\phi(T_i)$ = Transition relationship between sampling instants

B_i = Transition relationship at a sampling instant

$T_k = \sum_{i=1}^{\ell} T_i$ the shortest period for a stationary transition equation.

A stationary multirate system is stable if the n zeros of the characteristic equation are less than one i.e., $|z_i| < 1$.

If a system is nonstationary, the previous expression no longer holds and one is forced to return to the basic definition of stability to analyze these systems. That is, a stable system will have bounded outputs for all bounded inputs. Applying this definition of stability to nonstationary sampled data control systems implies that the product of the transition matrices approaches zero as the number of products gets large. This can be formalized as follows:

$$\psi(T_1) \quad \psi(T_2) \; . \; . \; . \quad \psi(T_N) \longrightarrow 0 \text{ as } N \longrightarrow \infty$$

From a control system designer's standpoint, this approach to stability is not very enlightening as it says nothing of relative stability.

5.0 MULTIRATE ADAPTIVE CONTROL SYSTEM TECHNIQUES

This section discusses the results of a literature search, and study of adaptive control schemes that appear applicable to space shuttle. Gibson [31] has shown the classical adaptive control problem to be separable into (a) parameter identification, (b) state estimation, (c) control. The parameter identification task is by far the most difficult problem to solve; therefore, it will be emphasized in the work that follows.

5.1 Online Technique of Lobbia and Saridis

The first technique to be discussed is due to Lobbia and Saridis [7]. The, consider the problem of online identification and control of a stochastic process that can be expressed as a linear model with unknown parameter coefficients. This adaptive control system minimizes a quadratic performance criteria in an asymptotic sense. Figure 5.1.1 shows a block diagram of this controller. The system is required to be: (a) linear, (b) time invariant, and (c) closed loop stable, and is assumed to be completely controllable and observable. The disturbances are assumed to be independent and Gaussian with zero mean. A known Gaussian sequence with zero mean is added to the control sequence to act as a system probe to facilitate identification.

For the n-dimensional system, and r-dimensional observation, the input-output information is used to define "auxiliary" vectors. These (gr)-dimensional ($g \leq 2n$) vectors contain information necessary for a new system parameter estimate:

$\hat{\theta}$ = $(\hat{\theta}_i)$ contain information on current parameter estimates (gr x gr)

$$\hat{\theta}_i^T = \left[h_i^T B_o,\ h_i^{o\,T} A_o B_o,\ \ldots,\ h_i^o A_o^{g-1} B_o\right]$$

$$Y_{(k)}^{-(k+g-1)} = \left[y^T(k+g-1),\ y^T(k+g-2),\ \ldots\ y^T(k)\right] \quad (gr \times 1)$$

vector of gr known input noise samples.

$$U_{(k)}^{(k+g-1)} = \left[u^T(k+g-1,\ u^T(k+g-2),\ \ldots,\ u^T(k)\right] \quad (gr \times 1)$$

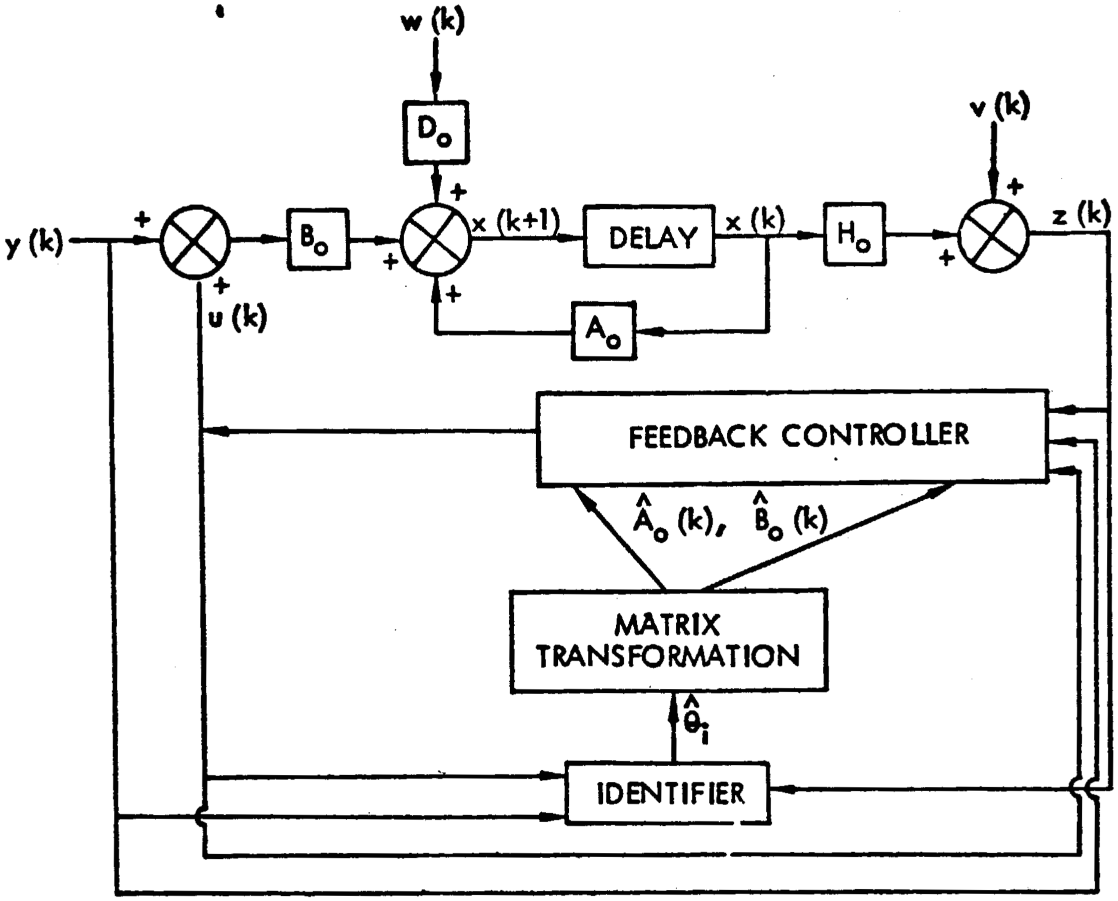

SYSTEM DESCRIPTION:

$S (k+1) = As (k) + B \quad u (k) + y (k) \quad + Dw(k)$ (mx1)

$z (k) = Hs (k) + v (k)$ (mx1)

$u (k)$ = CONTROLLER (rx1)

$A_o = PAP^{-1}, \quad B_o = PB, \quad H_o = HP^{-1}$

FIGURE 5.1.1: SELF-ORGANIZING CONTROLLER IN CANONICAL FORM

Assuming that the system is controlled in a stable manner, then the above vectors provide a new estimate of the system parameters as indicated in Figure 5.1.2. This figure also illustrates the computational sequence of the identification algorithm.

The heart of the algorithm is the iteration sequence indicated in Figure 5.1.3.

Possible Problems

This identification algorithm presents the following questions:

(1) Would parameter estimation algorithm converge for a non-stationary system, i.e. the formulation only provides for the "asymptotic" convergence of a quadratic cost function based on a linear, stationary system.

(2) Would the identification algorithm converge if the true system is nonlinear i.e. would the estimation algorithm converge to a finite dimensional linear-model equivalent to the nonlinear system.

(3) If the estimation algorithm is constrained to some n-dimensional linear system, and if the actual linear system is of dimention $n^1 > n$ would in this case (a) the algorithm attempt to estimate the "dominant" system dynamics (b) would the algorithm be stable.

(4) The impact of practical computer storage and computation time limitations is unknown.

Any real-world problem is to some extent non-stationary and nonlinear. Computer limitations dictate limiting system models (and associated calculations) to significantly smaller dimensions than the best estimate of the actual system (i.e. space shuttle equations).

Due to the above potential problems, a high technical risk is assigned to the implementation of the identification algorithm as given.

5.2 Maximum Likelihood Method of Stepner and Mehra

Before a practical autopilot can be designed much preliminary data on aircraft stability and control derivatives must be derived. This suggests some sort of off-line identification algorithm [16]. A satisfactory solution of the off-line identification problem can significantly simplify the adaptive autopilot problem, by:

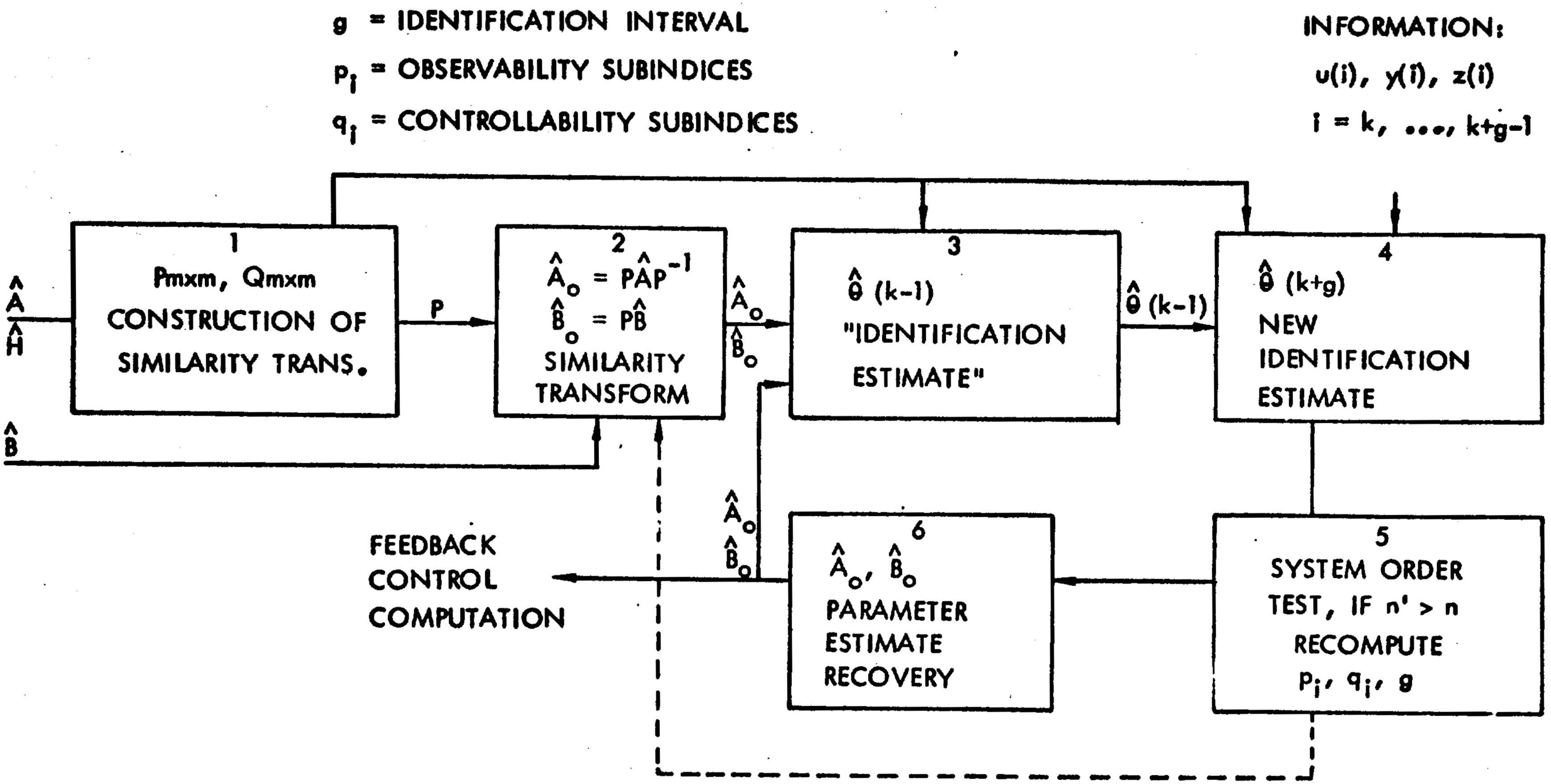

FIGURE 5.1.2: IDENTIFICATION ALGORITHM

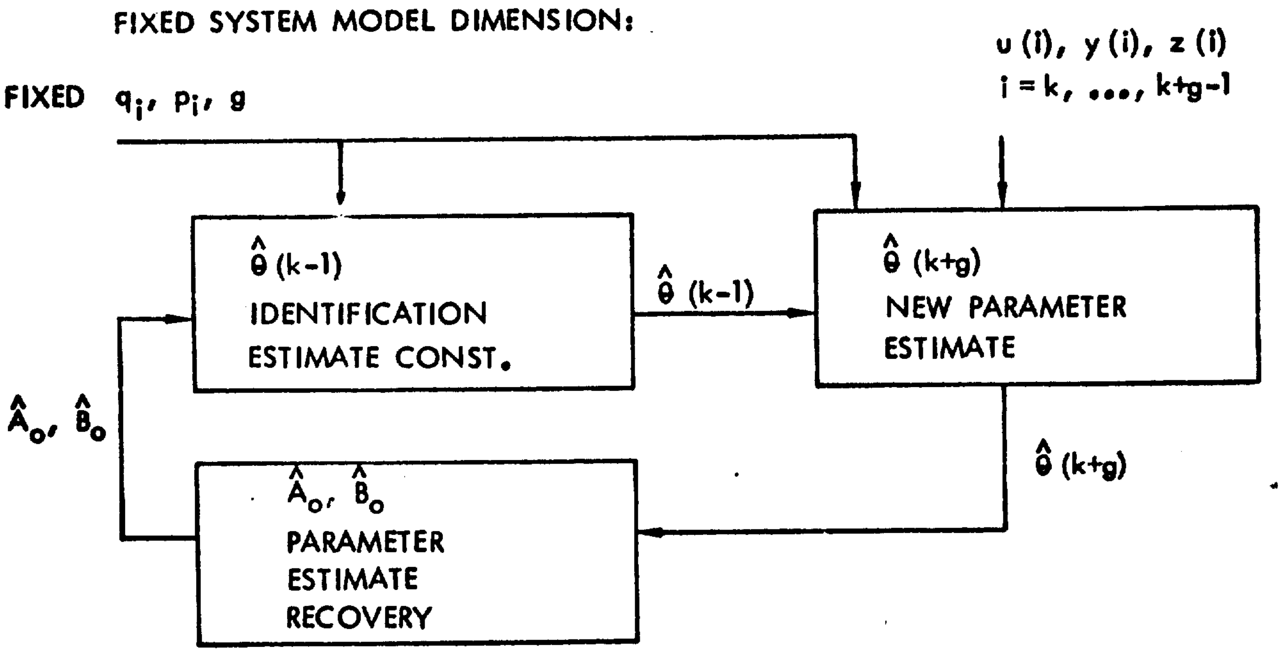

FIGURE 5.1.3: PARTIAL IDENTIFICATION ALGORITHM

(a) establishing relationships between sensed data and key stability parameters,

(b) simplifying the general model by indicating the dominant dynamics.

For example, off-line analysis [16] may indicate that explicit on-line parameter identification is not necessary for a successful autopilot implementation. Hence, we are led to a review of the off-line parameter identification algorithms of Stepner and Mehra [16].

Reference [16] discusses the application of a generalized identification method for Flight Test Data Analysis. The method is based on the Maximum Likelihood (ML) criterion and includes output error and equation error methods as special cases.

The development of the Generalized Maximum Likelihood (ML) Method for Aircraft Parameter Identification has been motivated by several considerations. First, the Maximum Likelihood methods are known to provide better estimates than other methods [20]. Second, ML methods are more general and can handle both measurement and process noise. In cases where no process noise is present, and the covariance of the measurement noise is known, ML methods reduce to the Output Error Method [17, 18]. Similarly, in cases where no measurement noise is present, the ML Method reduces to the Equation Error Method [18, 19]. Third, ML Methods yield realistic values of the variances of the parameters. Fourth, ML Methods can be used to estimate the covariances of the noises. This eliminates the problem of specifying the weighting matrix or the covariance of the measurement errors.

Outline of Algorithm

The maximum likelihood identification method, as implemented by SCI, is indicated schematically in Figure 5.2.1.

It is assumed that the structure of the system is known. The unknown parameters are expressed as a vector θ. A maximum likelihood (ML) estimate of θ is desired. A maximum likelihood function is constructed assuming that the constrained model is near optimal, so that the error between the model output and actual system output is a gaussian zero mean white noise innovation sequence ν.

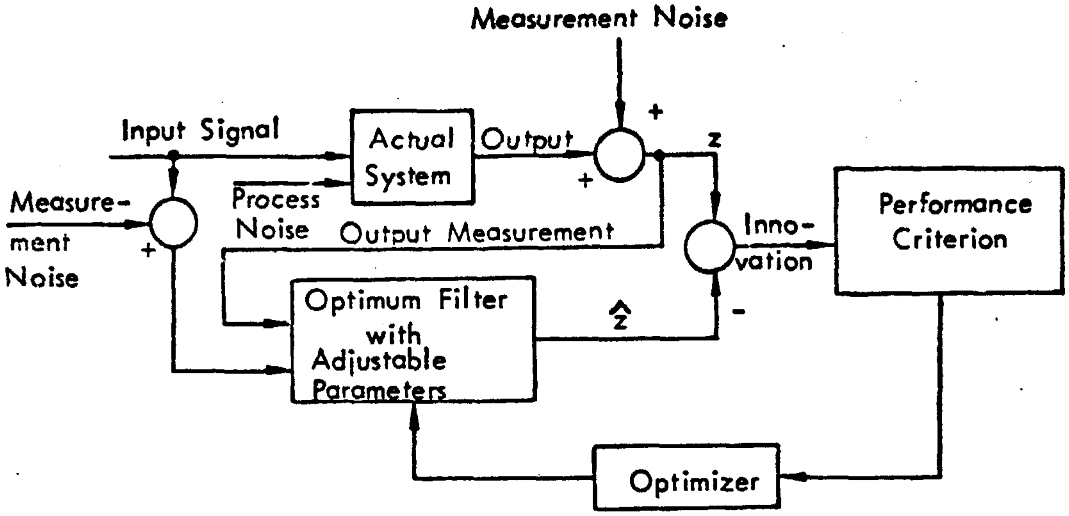

FIGURE 5.2.1: IMPLEMENTATION OF MAXIMUM LIKELIHOOD ESTIMATOR

The ML estimate θ is obtained by maximizing a conditional probability density function, or minimizing

$$J = \frac{1}{2} \sum_{i=1}^{N} \left[\nu^{T}(i)\, B^{-1}(i)\, \nu(i) + \log \left| B(i) \right| \right] \qquad (5.1)$$

where $B(i) = H_i P_i H^T + R_i$

H = model measurement matrix

P = state error covariance matrix

R = measurement error covariance matrix.

Minimizing Equation 5.1 subject to the covariance model constraints is simplifie' by a steady state B and Kalman Filter assumption [16]. The problem is consequently reduced to finding the roots for

$$\sum_{i=1}^{N} \nu(i) + B^{-1} \frac{\partial \nu(i)}{\partial \hat{\theta}^{o}} = 0 \qquad (5.2)$$

The roots of Equation 5.2 are found by a modified Newton-Raphson algorithm. This modified Newton-Raphson algorithm is considered the main advance over previous identification algorithms. The key feature is the use of the "information matrix" based on the innovation sequence sensitivity to parameters:

$$M = \sum_{i=1}^{N} \left(\frac{\partial \nu}{\partial \theta}\right)^T B^{-1} \frac{\partial \nu}{\partial \theta} \tag{5.3}$$

The parameter update is calculated as follows

$$\Delta\theta = -M^{-1} \left(\frac{\partial J}{\partial \theta}\right)^T \tag{5.4}$$

In conclusion, the Maximum Likelihood method developed by Systems Control, Inc. is a combination of three steps: [16] Kalman filtering to estimate the states and generate a residual or "innovation" sequence; [10] a modified Newton-Raphson algorithm for the parameter estimates and [17] an algorithm to estimate the noise statistics (mean and variances of the measurement and process noise).

Results of Identifying Aircraft Stability and Control Derivatives

Data in three aircraft were analyzed using this algorithm. The three aircraft data were from:

(a) X-22 VTOL computer simulation

(b) HL-10 lifting body flight data

(c) M2/F3 lifting body flight data

In all 23, 20, and 22 parameters, respectively, were identified. Each identification task had its unique problems, requiring non-standard fix up.

Problems in Identification

Most of the problems encountered could be related to attempting to identify parameters associated with unexcited modes. These problems are called "identifiability" problems. For example an inadequate "reference model structure" may force the parameters of the model to account for some major unmodeled effect.

Errors in instrumentation may result in non-physical parameter values. When control input is expressible as a linear combination of the A/C response variables, the information matrix (M) should be computer leaving out one or more of the smallest eigenvalues. Each eigenvalue which is left out relates to a singular direction in parameter space and therefore indicates a combination of parameters which can not be uniquely identified.

Comments

The Maximum Likelihood identification program described in [16] is considered as the "state of the art." The reported performance is considered exceptional. Neither the program nor algorithms are available for inspection and verification, i.e., they are not government property. Reference [16] reports on the parameter identification results and merely describes in general the actual identification program.

5.3 System Identification Technique of Lion

Introduction

The system parameter identification method of Lion [22] summarized here appears suitable for use in adaptive autopilots [26]. The problem considered is the identification of the dynamics of a plant where only the input and output can be observed. Lion's identification algorithm does this by continuously adjusting the parameters of a model of the plant so as to null some measure of error (ϵ) between the model and the plant. The two most widely analyzed error measures are (a) the response error, and (b) the equation error [25]. The response error system has the advantage that only the input and output of the system need be measured. The equation error, on the other hand, is an algebraic function of the parameters, and therefore has the advantage of giving a parameter adjustment method according to a "steepest descent" law. However, in equation error systems, all state variables must be measured or generated (estimated). Lion's "generalized equation error" method possesses the advantage of both types; that is (a) only input and output need be measured, and (b) it is an algebraic function of the parameters, therefore allowing a true steepest descent path in parameter space. Global asymptotic stability for a large class of inputs is proven.

The development is for a single input, single output stationary linear system. The system input signal is required to excite all modes associated with the parameters to be identified. The method [22] is applicable to nonlinear sysiems as long as the parameters to be identified enter linearly; ie: parameter "c" in Equation (5.5).

$$\ddot{y} + a_1\dot{y} = A_0 y + cy^3 = u \tag{5.5}$$

It is necessary that the form of the nonlinearity be known.

The usefulness of the identification method [22] in adap ive autopilot design is its rapid convergence rate. If the parameter variation with time is much slower than the system time constants, satisfactory parameter identification is obtainable [22, 24, 26].

Summary of Lion's [22] Parameter Identification Algorithm

Consider the system to be identified represented by the transfer function

$$G(s) = \frac{N\ (s,b)}{D\ (s,a)} = \frac{\sum_{1}^{n-1} b_i s^{i-1}}{s^n + \sum_{1}^{n-1} a_i s^{i-1}} = \frac{y(s)}{u(s)} \tag{5.6}$$

Let "u" and "y" be the plant input and output, respectively. We want a real tir parameter estimator such that $(\hat{a}, \hat{b})$ converges rapidly to (a, b), ie: $\hat{a}_i \rightarrow a_i$, $\hat{b}_i \dashrightarrow$

The parameter estimate error requiring only the system input and output is derived as follows:

$$N(s,b)\ U(s) - D(s,a)\ Y(s) = 0 \tag{5.7}$$

$$\left(\sum_{i=1}^{n-1} b_i s^{i-1} \right) U(s) - \left[s^n + \sum_{1}^{n-1} a_i s^{i-1} \right] Y(s) = 0 \tag{5.8}$$

If we replace b_i and a_i by some estimators $\hat{b}_i$, $\hat{a}_i$ we have a measure of the error in the estimates as follows:

$$N(s,\hat{b})\,Y(s) - D(s,\hat{a})\,U(s) \quad \text{Error} \tag{5.9}$$

The above $N(s,\hat{b})$ and $D(s,\hat{a})$ are not realistic "state variable filters" since they represent differentiation of y and u. Therefore a low-pass filter, $H(s)$, is introduced as follows:

$$H(s)\left[N(s,\hat{b})\;\;Y(s) - D(s,\hat{a})\;U(s)\right] = \text{Error} \tag{5.10}$$

Next the polynomials $N(s, b)$ and $D(s, b)$ are generalized by replacing "s^i" by "independent" polynomials in s.

$$\hat{N}(s) \triangleq N(p_i(s),\hat{b}) \triangleq \sum_{i=1}^{n-1} p_i(s)\,\hat{b}_i \tag{5.11}$$

and

$$\hat{D}(s) \triangleq D(p_i(\cdot),\hat{a}) \triangleq \sum_{i=1}^{n-1} p_i(s)\,\hat{a}_i \tag{5.12}$$

The polynomials $p_i(s)$ are constrained as follows:

(a) $p_i(s)$ are "independent", that is there exists no constants c_{ij} such that $p_i(s) = c_{ij}\,(p_j(s)$ for all $i \neq j$.

(b) $H(s)\,p_i(s)$ are "low-pass"

With the introduction of the polynomials, $p_i(s)$, the correspondence between (a_i, b_i) and $(\hat{a}_i, \hat{b}_i)$ may no longer be one-to-one. The relationship between (a_i, b_i) and $(\hat{a}_i, \hat{b}_i)$ can be derived by comparing coefficients of like powers of "s" in

$$\hat{D}(s) = D(s) \text{ and } \hat{N}(s) = N(s) \tag{5.13}$$

Finally using Equation (5.11) and (5.12) we have the generalized parameter estimation error, ε .

$$H(s) \left[\hat{N}(s) \quad U(s) \quad - \hat{D}(s) \quad Y(s)\right] = \varepsilon \tag{5.14}$$

where $H(s)\ p_i(s) \overset{\Delta}{=} M_i$ are the "state variable filters." Next define the following "state variables."

$$y_i \overset{\Delta}{=} H(s)\ p_i(s)\ Y(s) \overset{\Delta}{=} M_i\ Y(s) \tag{5.15}$$

$$u_i \overset{\Delta}{=} M_i\ U(s) \tag{5.16}$$

Using these definitions Equation (5.14) becomes

$$-y_n - \sum_{i=1}^{n-1} y_i \hat{a}_i + \sum_{i=1}^{n-1} u_i \hat{b}_i = \varepsilon \tag{5.17}$$

Having defined the error ε a performance criterion $P(\varepsilon) = \varepsilon^2/2$ is selected. The method of "steepest descent" or gradient to the P(0) surface leads to the parameter estimate adjustment law:

$$\dot{\hat{a}}_i = -k \frac{\partial P}{\partial \hat{a}_i} = -k\ \varepsilon \frac{\partial \varepsilon}{\partial \hat{a}_i} = +k\ \varepsilon\ y_i \tag{5.18}$$

and

$$\dot{\hat{b}}_i = -k\ \varepsilon\ u_i \tag{5.19}$$

The $\varepsilon = 0$ surface describes a hyperplane in the space spanned by the parameter estimates $(\hat{a}_i, \hat{b}_i)$. The desired estimates of (a_i, b_i) correspond to a unique "match point" in the hyperplane. Parameter estimation convergence to this unique point in the (ε = 0) -hyperplane is guaranteed by excitation of all variables (y_i, u_i). Or in other words, the system input must excite all system modes in order to guarantee convergent estimation of parameters.

Extensions:

Preliminary investigations on the "state variable filters" for Lion's algorithm, indicate a relationship to the "observer," state estimation filters [27]. This state variable observer relationship allows for the extension of Lion's algorithm to systems containing process and measurement noise. Lion's approach to non-linear systems may provide an extension to the "observer identifier" approach of Reference [28].

Conclusion

Lion's [22, 23] parameter identification algorithm appears applicable to real time autopilot applications [26]. State estimation filters ("observers") Ref. [27] provide guidance in the selection of the "state variable filters" for the identification algorithm.

The system input must have the necessary harmonic content to excite all system modes for the algorithm to converge. This appears not to be a practical problem since random disturbances can provide this excitation.

5.4 Extensions of Lion's Technique (Luder's Technique)

Introduction

Lion's [22] parameter identification technique was recently rediscovered in the literature [29]. The re-interpretation of Lion's results [29] in the light of observer theory [27] provides a minimal state and parameter estimator. The development is for a single-input single output case; extension to the more general is straight forward [30].

Summary of State and Parameter Estimator

Given the system transfer function (5.20) with unknown parameters (α, β)

$$G(s) = \frac{\sum_{1}^{n} \beta_i s^{i-1}}{s^n - \sum_{1}^{n} \alpha_i s^{i-1}} \tag{5.20}$$

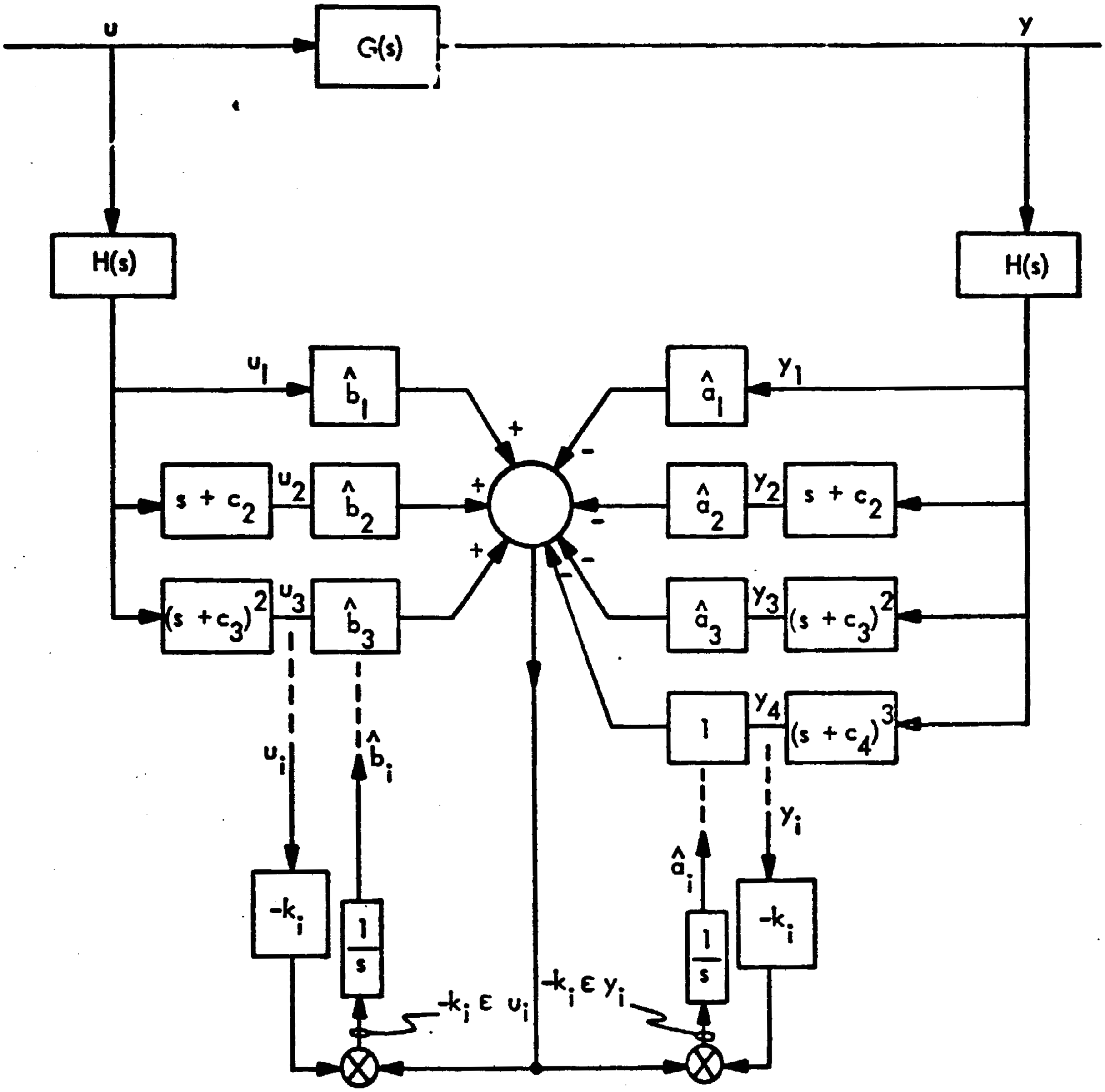

$$\hat{b}_3 = b_3, \; b_2 = \hat{b}_2 - 2c_3, \; b_1 = \hat{b}_1 + \hat{b}_2 c_2$$

$$a_3 = \hat{a}_3 + 3c_4, \; a_2 = \hat{a}_2 + 2c_3 \hat{a}_3 + 3c_4^2$$

$$a_1 = \hat{a}_1 + \hat{a}_2 c_2 + \hat{a}_3 c_3 + c_4^3$$

FIGURE 5.3.1: PARAMETER IDENTIFICATION EXAMPLE

This transfer function is expressed in terms of known design pgrameters (λ) gives Equation (5.21)

$$G(s) = \frac{b_1 + \sum_{2}^{n} \frac{b_i}{s + \lambda_i}}{(s - a_1) - \sum_{2}^{n} \frac{a_i}{s + \lambda_i}} \qquad (5.21)$$

The relationship between (α , β) and (a, b) in terms of (λ) can be derived by equating (5.19) and (5.20).

The state vector equations (5.21) are motivated by the desire to associate the output of Lion's [1] state variable filter with actual system states. See Figure 5.4.1 for the block diagram representation of Equation (5.21).

$$\dot{w} = \begin{pmatrix} 0 & \cdots & 0 \\ \cdots & \cdots & \cdots \\ r & \vdots & F \end{pmatrix} w \qquad (5.21a)$$

$$\dot{v} = \begin{pmatrix} & a^T & \\ \cdots & \cdots & \cdots \\ r & \vdots & F \end{pmatrix} v + \begin{pmatrix} 1 \\ 0 \\ \vdots \\ 0 \end{pmatrix} b^T w \qquad (5.21b)$$

where $a^T = (a_1, \ldots, a_n)$

$b^T = (b_1, \ldots, b_n)$

$r^T = (1, \ldots, 1)$

$F = \text{diag}\,(-\lambda_2, \ldots, -\lambda_n)$

$w_1 = u, \; v_1 = y$

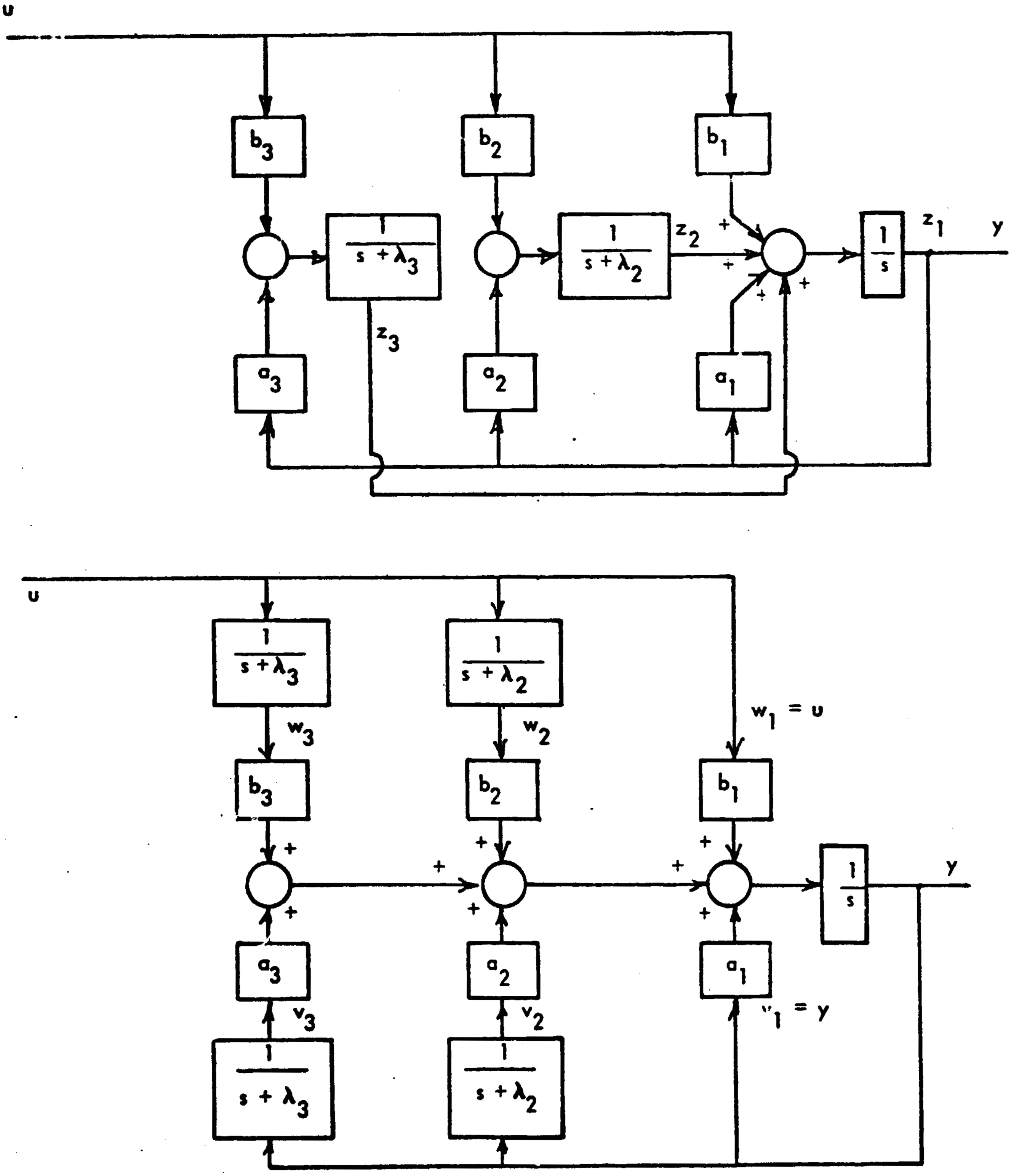

FIGURE 5.4.1: STATE VARIABLE BLOCK DIAGRAM EQUIVALENCE

The "observer" [27] equation based on Equation 5.21b with w as input is given by

$$\dot{\hat{v}} = \left(\begin{array}{c|c} & a^T \\ \hline r & F \\ & \end{array}\right) \hat{v} + \begin{pmatrix} 1 \\ 0 \\ \vdots \\ 0 \end{pmatrix} b^T w + K (y - \hat{y})$$

if the observer gain is as follows:

$$K^+ = \Big((a_1 - \lambda_1) , 0, \ldots, 0 \Big) \qquad (5.23)$$

Thus we have the adaptive observer of Reference [29]. Finally using the "steepest descent" [22] parameter adjustment law,

$$\begin{aligned} \dot{\hat{a}}_i &= \gamma_i v_i \epsilon \\ \dot{\hat{b}}_i &= \delta_i w_i \epsilon \qquad (5.24) \\ \epsilon &= y - \hat{y} = y - \hat{v}_1 \end{aligned}$$

We have the parameter and state estimation algorithm [29]. This algorithm is summarized in Figure 5.4.2 .

Lion's [22] development is more general than [29]. Specifically non-stationary, noisy, and nonlinear problems can be treated by Lion's [22] method but not by the method of [29]. Analytic extension of [29] and computer simulations are considered to be potentially fruitful areas of effort [29].

Example:

Given: A third order system with unknown parameters (a_i, b_i)

$$G(s) = \frac{b_1 + \dfrac{b_2}{s + \lambda_2} + \dfrac{b_3}{s + \lambda_3}}{(s - a_1) - \dfrac{a_2}{s + \lambda_2} - \dfrac{a_3}{s + \lambda_3}} \qquad (5.25)$$

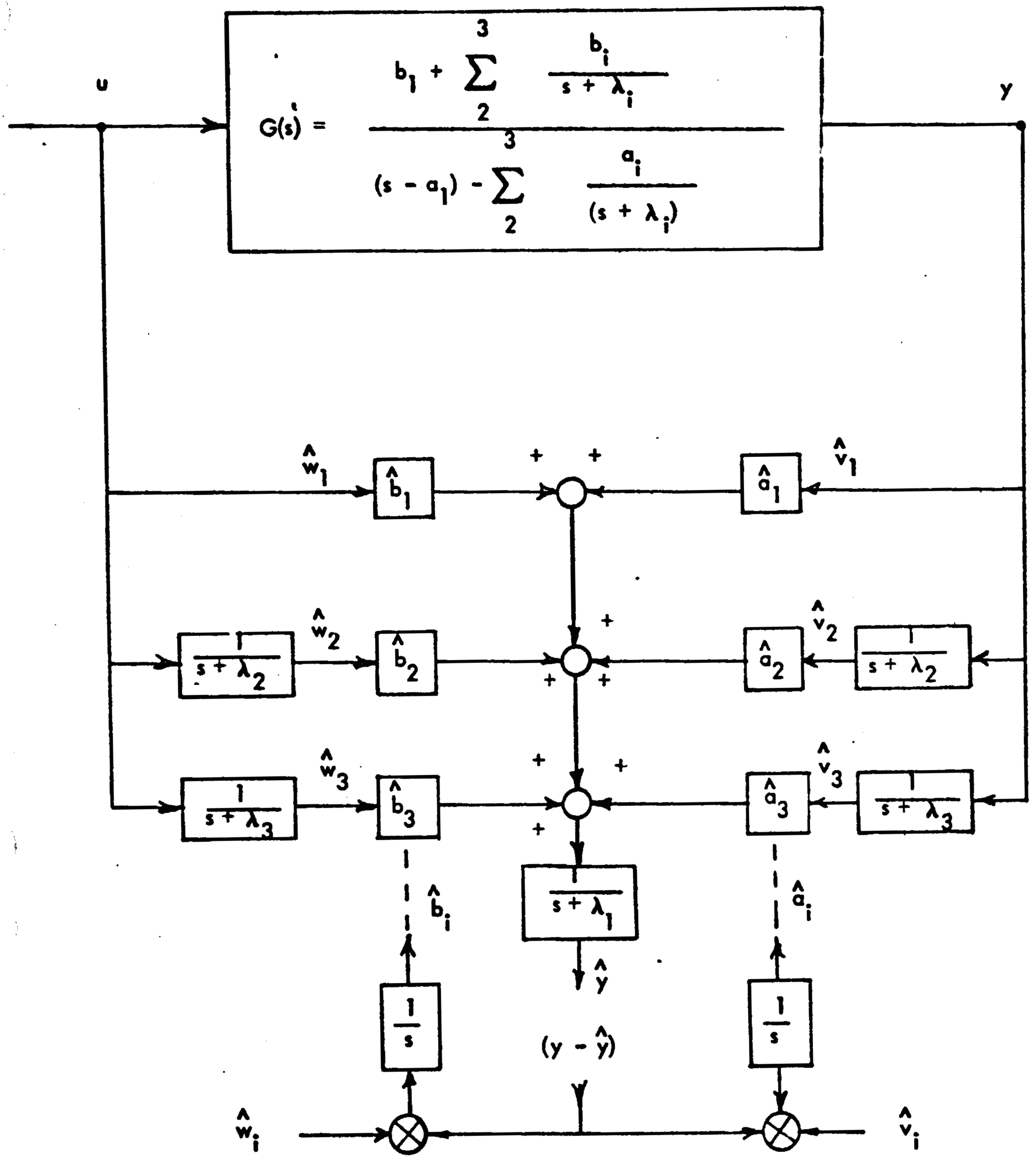

FIGURE 5.4.2: STATE AND PARAMETER ESTIMATOR

Find: The adaptive ccntrol law that fixes the closed-loop characteristics, e.g. suppose it is desired to set the closed loop poles at

$$(-r_1, -r_2, -r_3) \tag{5.26}$$

Solution: Since the system eigenvalues are invariant under similarity transformation any convenient coordinate system can be used (see Figure 5.4.1).

$$\begin{aligned} z_1 &= v_1 = y \\ z_2 &= a_2 v_2 + b_2 w_2 \\ z_3 &= a_3 v_3 + b_3 w_3 \end{aligned} \tag{5.27}$$

The dynamics matrix in terms of (z) becomes

$$\begin{pmatrix} \dot{z}_1 \\ \dot{z}_2 \\ \dot{z}_3 \end{pmatrix} = \overbrace{\begin{pmatrix} a_1 & 1 & 1 \\ a_2 & -\lambda_2 & 0 \\ a_3 & 0 & -\lambda_3 \end{pmatrix}}^{A} z + \begin{pmatrix} b_1 \\ b_2 \\ b_3 \end{pmatrix} u \tag{5.28}$$

The adaptive control law is derived by assuming:

$$u = (c_1 \; c_2 \; c_3) \begin{pmatrix} z_1 \\ z_2 \\ z_3 \end{pmatrix} \tag{5.29}$$

Then Equation (5.28) becomes

$$\dot{z} = Az + bu = (A + b\, c^T)\, z \tag{5.30}$$

The adaptive gains (c_1, c_2, c_3) are determined from Equation 5.30 by equating coefficients of like powers of s in Equation (5.31).

$$\det \left[- I\, s + A + b\, c^T \right] = -(s + r_1)(s + r_2)(s + r_3) \tag{5.31}$$

replacing (a, b) by $(\hat{a}, \hat{b})$ we have the adaptive gain elements (c_1, c_2, c_3) as a function of $(\hat{a}, \hat{b}, \lambda, r)$.

The above algorithm is considered as the "state-of-the-art" in on-line adaptive control system techniques.

5.5 Extensions to Luder's Technique

An extension to Luder's [28] parameter-state estimation algorithm is presented in this section. This extension is considered superior to the formulation given in [28] because of the greater "state variable filter" output separation [22]. This greater filter separation results in better parameter observability, and hence better algorithm performance.

Brief Development

It is assumed that the completely observable system can be described by an n-th order time-invariant differential equation. For the sake of simplicity, the new canonical form is derived only for the single-input single-output case. Nevertheless the extension of this canonical form to the multi-input case is straight forward.

Given: A stable stationary observable system transfer function with unknown parameters (α, β)

$$G(s) = \frac{\sum_{1}^{n} \beta_i \; s^{i-1}}{s^n + \sum_{1}^{n} \alpha_i \; s^{i-1}} \tag{5.32}$$

Find: Convergent parameter and state estimator

Solution:

Restriction of Lion's [22] "state variable filter" to a simple form leads to a state estimate (observer) relationship. The transfer function (5.32) can be expressed more conveniently in terms of known parameters (λ_i) as follows:

$$G(s) = \frac{b_n + \sum_{1}^{n-1} M_i \, b_i}{s + a_n + \lambda_n + \sum_{1}^{n-1} M_i \, a_i} \tag{5.33}$$

where

$$M_i \triangleq \prod_{j=i}^{n-1} \frac{1}{(s + \lambda_j)}$$

In expression (5.33) the (a, b) are now the parameters to be identified. The transformation relating (a, b) to (α ,β) involving (λ_i) can be derived easily by equating coefficients of like powers of s (see appendix B). The form of Equation (5.33) is motivated by convergence requirement, and results from the replacement of the integrators in Figure 5.5.1b by "lossy integrators" Figure 5.5.2.

The new canonic form is as follows:

$$\dot{w} = \left(\begin{array}{c|c} & 0 \\ & \vdots \\ \bigwedge & 0 \\ & 1 \\ \hline 0 \; . \; . \; . \; . \; . & 0 \end{array} \right) w \tag{5.34}$$

$$\dot{v} = \left(\begin{array}{c|c} & 0 \\ & \vdots \\ \bigwedge & 0 \\ & 1 \\ \hline -a_1 \cdots -a_{n-1} & -\lambda_n - a_n \end{array} \right) v + \begin{pmatrix} 0 \\ \vdots \\ 0 \\ 1 \end{pmatrix} b^T w \tag{5.35}$$

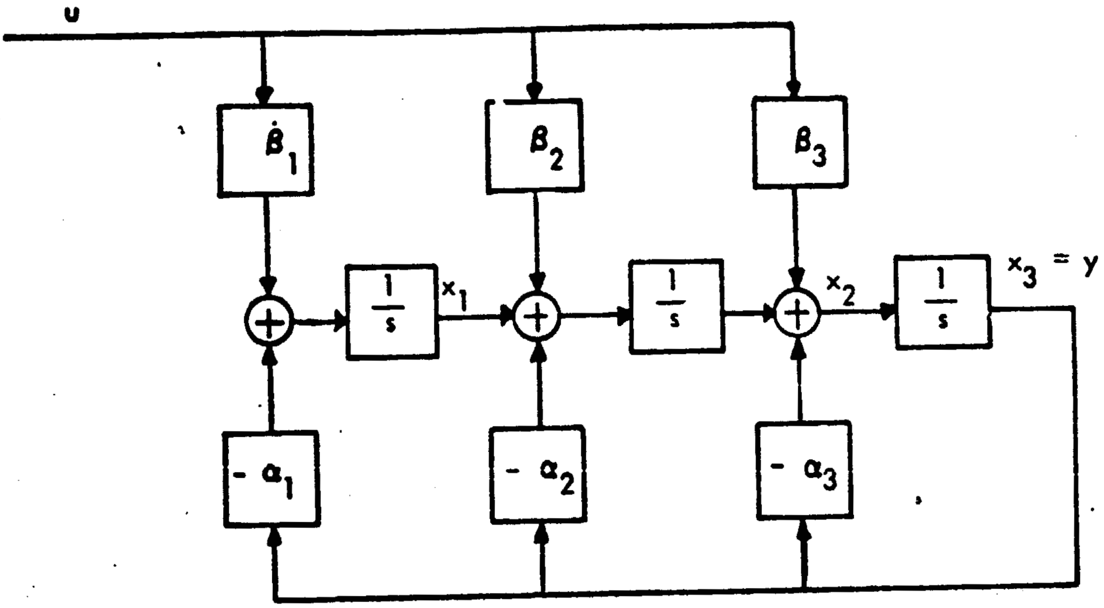

FIGURE 5.5.1a: OBSERVABLE CANONIC FORM

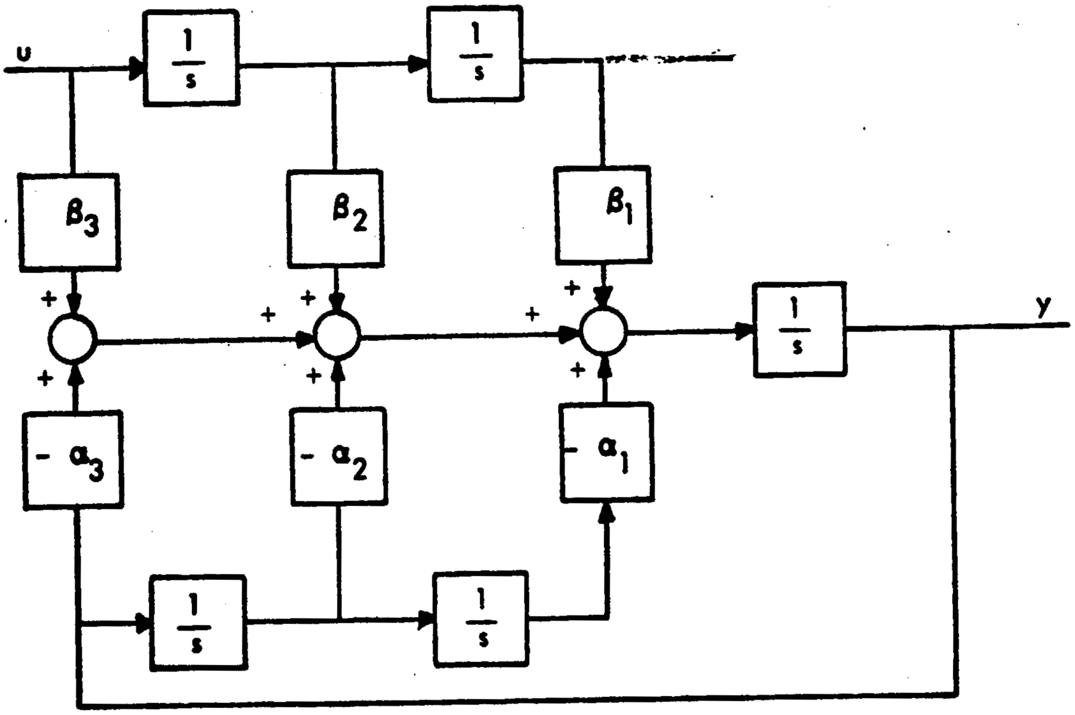

FIGURE 5.5.1b: EXPANDED FORM

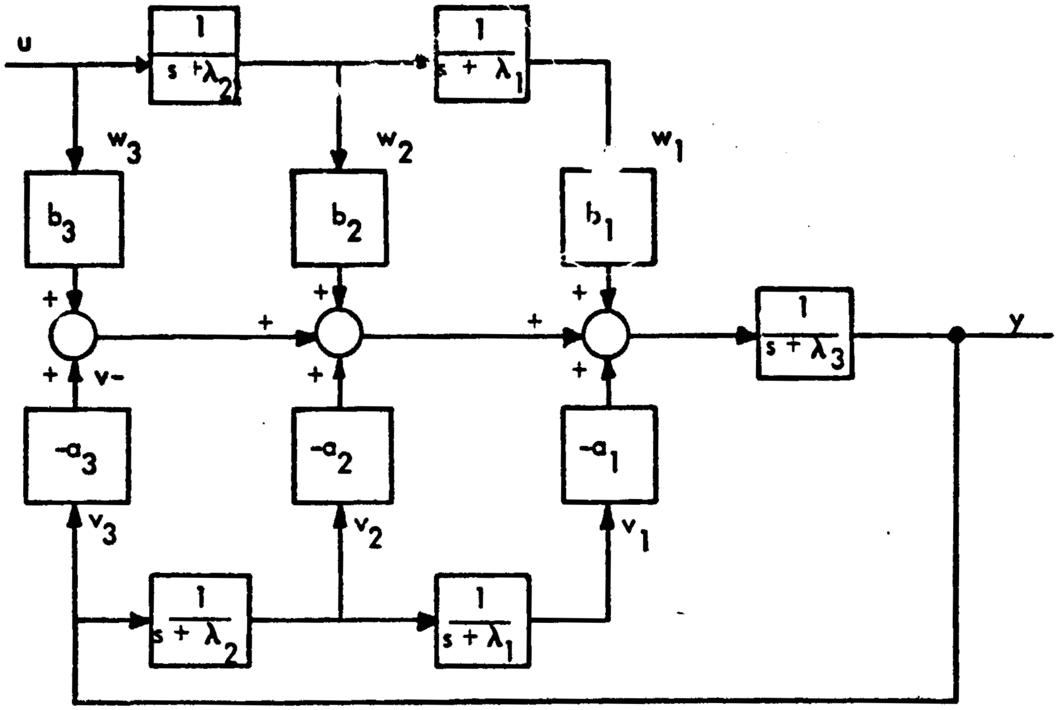

FIGURE 5.5.2a THE SYSTEM

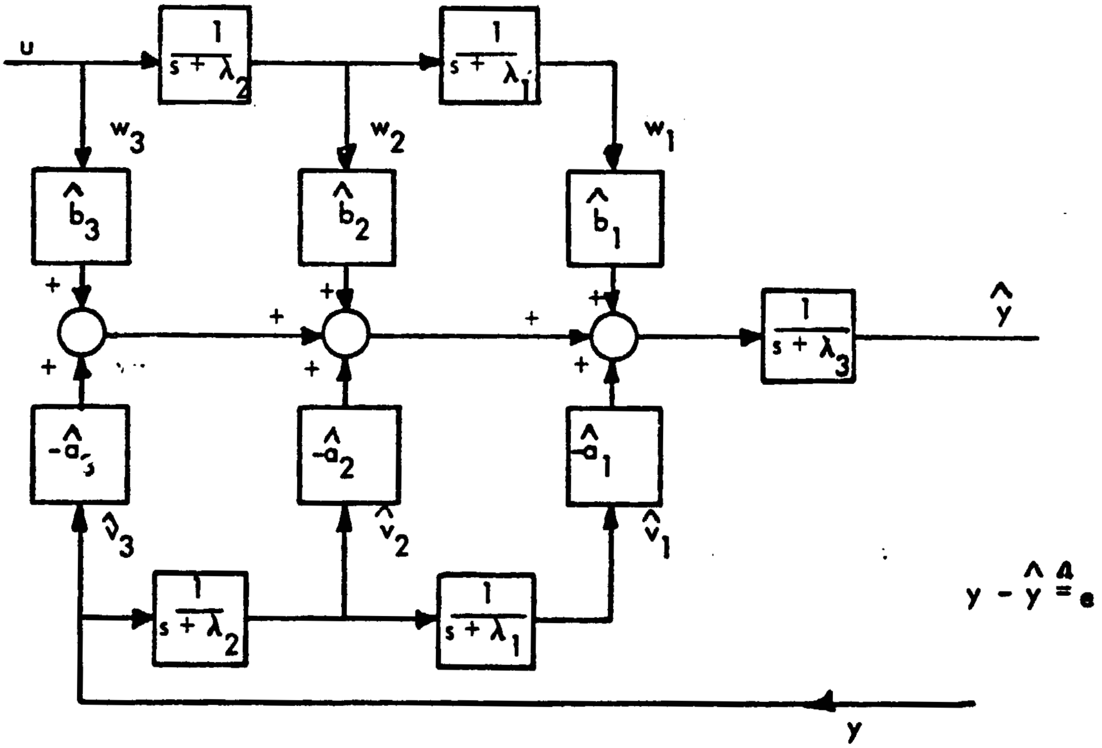

FIGURE 5.5.2b THE NEW CANONIC IDENTIFIER

where

$$\Lambda = \begin{pmatrix} -\lambda_1 & 1 & & 0 \\ & \ddots & \ddots & \\ & & \ddots & 1 \\ 0 & & & -\lambda_n \end{pmatrix}$$

and where

$b^T = (b_1, \ldots b_n)$; $v_n = y$ = system output

$w_n = u$ = system input

Figure 5.5.2 summarizes the above state variable form, note that if all $\lambda_i = 0$ then $(\alpha, \beta) = (a, b)$ and we have the "expanded controllable canonic form" indicated in Figure 5.5.1b.

Consider Equation (5.35), treat w as a system input, then the state "observer" [27] equation is given by Equation (5.36):

$$\dot{\hat{v}} = \left(\begin{array}{c|c} \Lambda & \begin{matrix} 0 \\ \vdots \\ 0 \\ 1 \end{matrix} \\ \hline -a_1 \ldots -a_{n-1} & -a_n - \lambda_n \end{array}\right) \hat{v} + \begin{pmatrix} 0 \\ \vdots \\ 0 \\ 1 \end{pmatrix} b^T w + k(y - \hat{y}) \qquad (5.36)$$

Next select the "adaptive observer" gain

$$\boxed{k^T = (0, \ldots 0, 1, -a_n)} \qquad (5.37)^{**}$$

and substitute (a, b, w) for (a, b, w) in (5.36) yields the identifier (5.38), which is summarized in Figure 5.5.2b.

$$\begin{pmatrix} \dot{\hat v}_1 \\ \cdot \\ \cdot \\ \cdot \\ \dot{\hat v}_{n-1} \\ \dot{\hat y} \end{pmatrix} = \left(\begin{array}{ccc:c} & & & 0 \\ & & & \cdot \\ & & & \cdot \\ & & & \cdot \\ & & & 0 \\ & \underline{\Lambda} & & 1 \\ \hdashline -\hat a_1 & \ldots & -\hat a_{n-1} & -\hat a_n \end{array}\right) \begin{pmatrix} \hat v_1 \\ \cdot \\ \cdot \\ \cdot \\ \hat v_{n-1} \\ y \end{pmatrix} + \begin{pmatrix} 0 \\ \cdot \\ \cdot \\ \cdot \\ 0 \\ 1 \end{pmatrix} \left[b^T \hat w - \lambda_n \hat y \right] \qquad (5.38)$$

The "steepest descent" parameter adjustment law [22] adjusts the parameters towards the $e = (\dot y - \hat y) = 0$ surface. From Equations (5.35) and (5.38) we have:

$$\dot e = \sum_1^{n-1} -a_i v_i + \sum_1^{n-1} \hat a_i \hat v_i - (a_n + \lambda_n) y + \lambda_n \hat y + \hat a_n y + b^T w - \hat b^T \hat w \qquad (5.39)$$

The normal to the $\dot e = 0$ hyperplane in the space spanned by the parameter estimates $(\hat a, \hat b)$ is in the direction of "steepest descent." Define $F \triangleq 1/2\, (\dot e)^2$ as a metric to the $e = 0$ surface, then

$$\dot{\hat a}_i = -\gamma_i \frac{\partial F}{\partial \hat a_i} = -\gamma_i\, e\, \hat v_i \qquad (5.40)$$

$$\dot{\hat b}_i = -\delta_i \frac{\partial F}{\partial \hat b_i} = -\delta_i (-e\, \hat w_i) = +\delta_i\, e\, \hat w_i \qquad (5.41)$$

** A minimal stationary (non-adaptive) observer results if we select $k^T = (0, \ldots, 0, 1, -\lambda_n)$

This parameter adjustment law completes the adaptive observer identification algorithm, as summarized in Figure 5.5.3. The above parameter adjustment laws can also be developed as a convenient selection satisfying the estimate convergence proof given in the next section.

Proof of Estimate Convergence

The Lyapunov proof developed here is based on [28]. This is considered more elegant than the convergence proof given in [22] , since no hueristic argument on hyperplane motions is required. Before proceeding with the proof it is convenient to recall the superposition theorem; that is the solution to (5.34) in terms of the solution to (5.32) is given by (5.43).

$$\begin{pmatrix} \dot{\hat{w}}_1 \\ \cdot \\ \cdot \\ \cdot \\ \dot{\hat{w}}_{n-1} \\ \dot{u} \end{pmatrix} = \left(\begin{array}{c|c} & 0 \\ & \cdot \\ & \cdot \\ & \cdot \\ & 0 \\ \Lambda & 1 \\ \hline 0 \; . \; . \; . \; . & 0 \end{array}\right) \begin{pmatrix} \hat{w}_1 \\ \cdot \\ \cdot \\ \cdot \\ \hat{w}_{n-1} \\ u \end{pmatrix} \qquad \hat{w}\,(0) \neq w(0) \qquad (5.42)$$

$$w(t) = \hat{w}(t) + \exp\left(\underset{\sim}{\Lambda}\, t\right) \; \Delta\, w(0) \qquad (5.43)$$

where $w_n = \hat{w}_n = u$,

$$\underset{\sim}{\Lambda} = \left(\begin{array}{c|c} & 0 \\ & \cdot \\ & \cdot \\ & \cdot \\ & 0 \\ \Lambda & 1 \\ \hline 0 \; . \; . & 0 \end{array}\right)$$

$$\Delta w(0) \triangleq w(0) - \hat{w}(0)$$

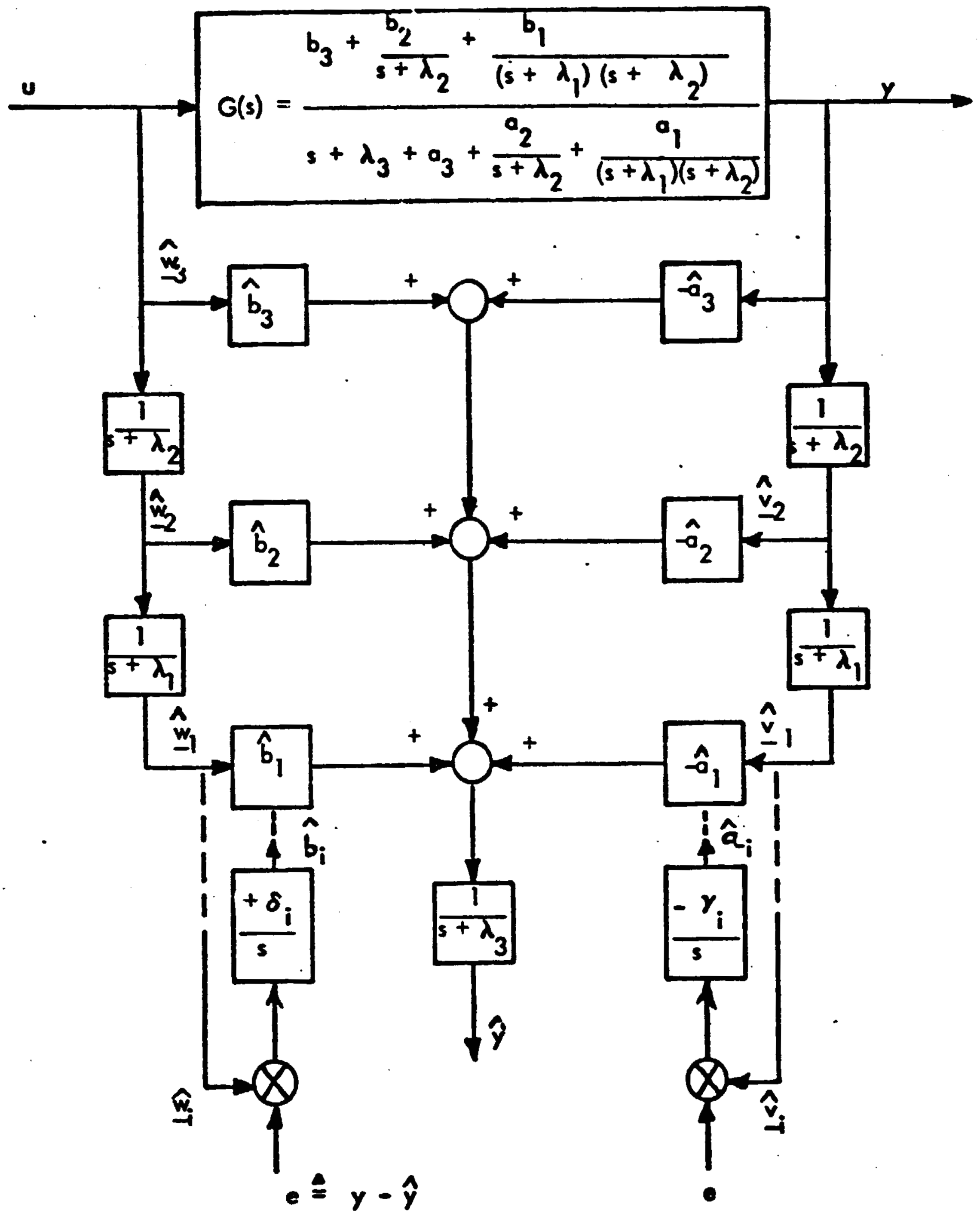

The (â, b̂) are estimates of (a, b). The (δ, γ, λ) are design parameters.

FIGURE 5.5.3: THE PARAMETER AND STATE ESTIMATOR

Clearly if $\lambda_1 > 0$, then the influence of any initial estimate error ($\Delta w(0) \neq 0$) will decay to zero as $t \longrightarrow \infty$.

Similarly the solution to (5.35) in terms of the vector $\hat{\underline{v}}^T \triangleq (\hat{v}_i, \ldots \hat{v}_{n-1}, y)$ is:

$$\underline{v}(t) = \hat{\underline{v}}(t) + \exp\left[-\underset{\sim}{\Lambda}(t)\right] \Delta v(0) \qquad (5.44)$$

where $v_n = y$, $\Delta v(0) \triangleq v(0) - \hat{v}(0)$

Using equations (5.43) and (5.44) in (5.39) results in

$$\dot{e} = -(a^T - \hat{a}^T)\hat{\underline{v}} - a^T \exp(-\underset{\sim}{\Lambda} t)\ \Delta v(0)$$

$$-\lambda_n e + (b^T - \hat{b}^T)\hat{\underline{w}} + b^T \exp(-\underset{\sim}{\Lambda} t)\ \Delta w(0) \qquad (5.45)$$

where $a^T \triangleq (a_1, \ldots, a_n)$;

$b^T \triangleq (\cdot_1, \ldots, b_n)$.

Now select a Lypunav function

$$V = 1/2\, e^2 + 1/2\ \|\Lambda a\|_\gamma^{\ 2} + 1/2\ \|\Delta b\|_\delta^{\ 2}$$

$$= 1/2\, e^2 + 1/2 \sum_1^n \frac{(a_i - \hat{a}_i)^2}{\gamma_i} + 1/2 \sum_1^n \frac{(b_i - \hat{b}_i)^2}{\delta_i} \qquad (5.46)$$

Using the stationary system assumption ($\dot{a} = \dot{b} = 0$) we have:

$$\dot{V} = e\dot{e} + \sum_{1}^{n} \frac{\left(a_i - \hat{a}_i\right)}{\gamma_i} (-\dot{\hat{a}}_i) + \sum_{1}^{n} \frac{\left(b_i - \hat{b}_i\right)}{\delta_i} (-\dot{\hat{b}}_i) \qquad (5.47)$$

inserting the "steepest descent" parameter adjustment law, Eq. 5.40 and 5.41, we have:

$$\dot{V} = e\dot{e} + e \sum_{1}^{n} (a_i - \hat{a}_i)\ \hat{v}_i - e \sum_{1}^{n} (b_i - \hat{b}_i)\ \hat{w}_i$$

$$(5.48)$$

$$= e\dot{e} + e\,(a^T - \hat{a}^T)\ \underline{\hat{v}} - e\,(b - \hat{b})\ \underline{\hat{w}}$$

Substitute Eq. (5.45) into (5.48) results in

$$\boxed{\dot{V} = -\lambda_n e^2 + e\left[-a^T \exp\,(\underset{\sim}{\Lambda}\,t)\ \ \Delta v(0) + b^T \exp\,(\underset{\sim}{\Lambda}\,t)\ \ \Delta w(0)\right]} \quad (5.49)$$

Recall that the autonomous or "unforced solution to (5.34) and (5.35) is:

$$(\dot{y}_A + \lambda_n y_A) = -a^T \exp\,(\underset{\sim}{\Lambda}\,t)\ v(0) + b^T \exp\,(\underset{\sim}{\Lambda}\,t)\ w(0) \qquad (5.50)$$

Clearly $(\dot{y}_A + \lambda_n y_A) \longrightarrow 0$ as $t \longrightarrow \infty$ if the system to be identified is stable; i.e. strictly LHP poles. Hence for a stable system (5.49) becomes negative definite, therefore parameter and state estimate convergence is guaranteed.

Implicit in the above is ,he requirement that the input u contain at least n-distinct frequencies (real or complex) [22].

Convergence Proof for Non-Stationary Systems

It is instructive to consider the non-stationary state and parameter estimation convergence. These considerations yield guidelines in initial design parameter selection.

Consider the time derivative of Equation 5.46 with $\dot{a} \neq 0$ and $\dot{b} \neq 0$. Carrying out steps analogous to those resulting in Equation 5.49 results in Equation 5.51.

$$\dot{V} = -\lambda_n e^2 + \sum_1^n \left(\frac{a_i - \hat{a}_i}{\gamma_i}\right) \dot{a}_i + \sum_1^n \left(\frac{b_i - \hat{b}_i}{\delta_i}\right) \dot{b}_i$$

$$+ e \left[-a^T \exp(-\tilde{\Lambda} t) \; \Delta v(0) + b^T \exp(-\tilde{\Lambda} t) \; \Delta w(0)\right] \tag{5.51}$$

Equation 5.51 indicates that maximum $(\lambda, \delta, \gamma)$ are desirable for maximum state and parameter estimate convergence rate. A set of large $\lambda_i > 0$ provides for rapid state estimation convergence. A set of large (δ, γ) accelerates tme "steepest descent" parameter adjustment law.

A limitation on parameter estimate rate is presented by the frequencies of the system to be identified. To see how this comes abour, consider the highest natural frequency associated with parameter a_i. This natural mode determines the rate of change of $v_i a_i$, which in turn governs the "observability" of any error in estimate and hence removal of the error.

In conclusion the practical upper bound on $(\delta, \gamma) > 0$ is dictated by the unknown system natural frequencies. The maximum (λ) is dictated by various numerical conditioning considerations.

Conclusion

It has been shown that for any general input u, the adaptive observer described by Equations 5.38, 5.40, 5.41, 5.42 will asymptotically yield the states and parameters of an nth order linear time-invariant system [27]. This adaptive observer does not require auxiliary signals to be fed back into it [27], and hence its implementation is very simple (see Figure 5.5.3).

5.6 Quasi-Adaptive Control Systems

Most of the adaptive control techniques discussed to date are still in the research stage and present a high technical risk. Therefore, it is necessary to consider proven quasi-adaptive systems for a space shuttle type application. The quasi-adaptive scheme to be discussed has been applied successfully by Boeing on the U.S. Air Force SRAM missile. This is an aerodynamically controlled missile that operates over a dynamic pressure range of 240 to 1 inch. The static stability of this missile expressed in terms of fins unlocked natural frequency ranges from 14 rad/sec unstable to 10 rad/sec stable. The structural modes also limited the design of the stabilization compensation for the missile.

The basic autopilot was an attitude type similar to the system on shuttle. The missile is guided by an onboard inertial measurement unit so that knowledge of the current flight condition is available. The guidance system provides an attitude error signal to the flight control system.

The flight control system design made use of the aforementioned attitude error signals, along with rate gyros in all three axes, forming an essentially conventional attitude control system configuration. Control fins were operated by proportional hydraulic position servos. The system was unconventional in that dynamic compensation networks were designed with four selectable sets of characteristics to accommodate the wide range of flight conditions. Network selection was determined on the basis of on-board computed dynamic pressure, obtained from inertially sensed total velocity and altitude. The compensation network design required careful optimization to minimize the number of networks required, within the constraints of missile static stability and structural bending coupling. This network optimization was accomplished through trade studies of gain and phase margins vs. compensation network parameters.

This design approach is amenable to well established analysis and simulation techniques, permitting a thorough understanding and evaluation of the system prior to commitment to actual flight test. The basic stabilization design was accomplished using root locus and Nichols chart linearized stability analysis techniques. Simulations, digital, analog, and hybrid, were used to evaluate nonlinear system characteristics, such as aerodynamics and fin actuator behavior. The control system has demonstrated unqualified success, performing its intended mission without significant modification since the start of flight testing in 1969.

System Description

The flight control system block diagram for this missile is shown in Figure 5.6.1. The missile digital computer is seen to be the brains of this system selecting the rigid mode and body bending mode filters. The four rigid mode filters are chosen based upon dynamic pressure while the two body bending filters are selected based upon moment of inertia data.

Flight control gains were computed onboard based on inertially measured information, along with programmed representations of control fin effectiveness and missile moment of inertia. The control gain computation and network selection logic are shown in Figure 5.6.2.

The onboard determination of flight control gains and selection of compensation networks as functions of missile-measured flight condition constituted a quasi-adaptive mode of operation. The system adjusted itself according to measured flight condition, but not through a dynamic mode of closed-loop sensing in the usual sense associated with adaptive control. This is a significant advantage when there is a severaly constraining closeness between the frequency regime of rigid body control and that of structural body bending, as was the case with SRAM.

The high degree of success of the design approach used on SRAM merits consideration of this concept on other applications. It is especially amenable to any system that requires an onboard digital computer to perform the guidance and navigation tasks. The computer's functions can then be expanded to provide computational services for the flight control stabilization task, using the basic information that is generated as part of the inertial guidance function. The use of variable compensation characteristics and flight control gains based on inertially sensed flight condition is not restricted to an attitude controller; it is conceptually applicable to normal acceleration control systems, or to any technique used to augment stability or derive stability for a statically unstable or marginally stable vehicle.

FIGURE 5.6.1: FLIGHT CONTROL SYSTEM BLOCK DIAGRAM

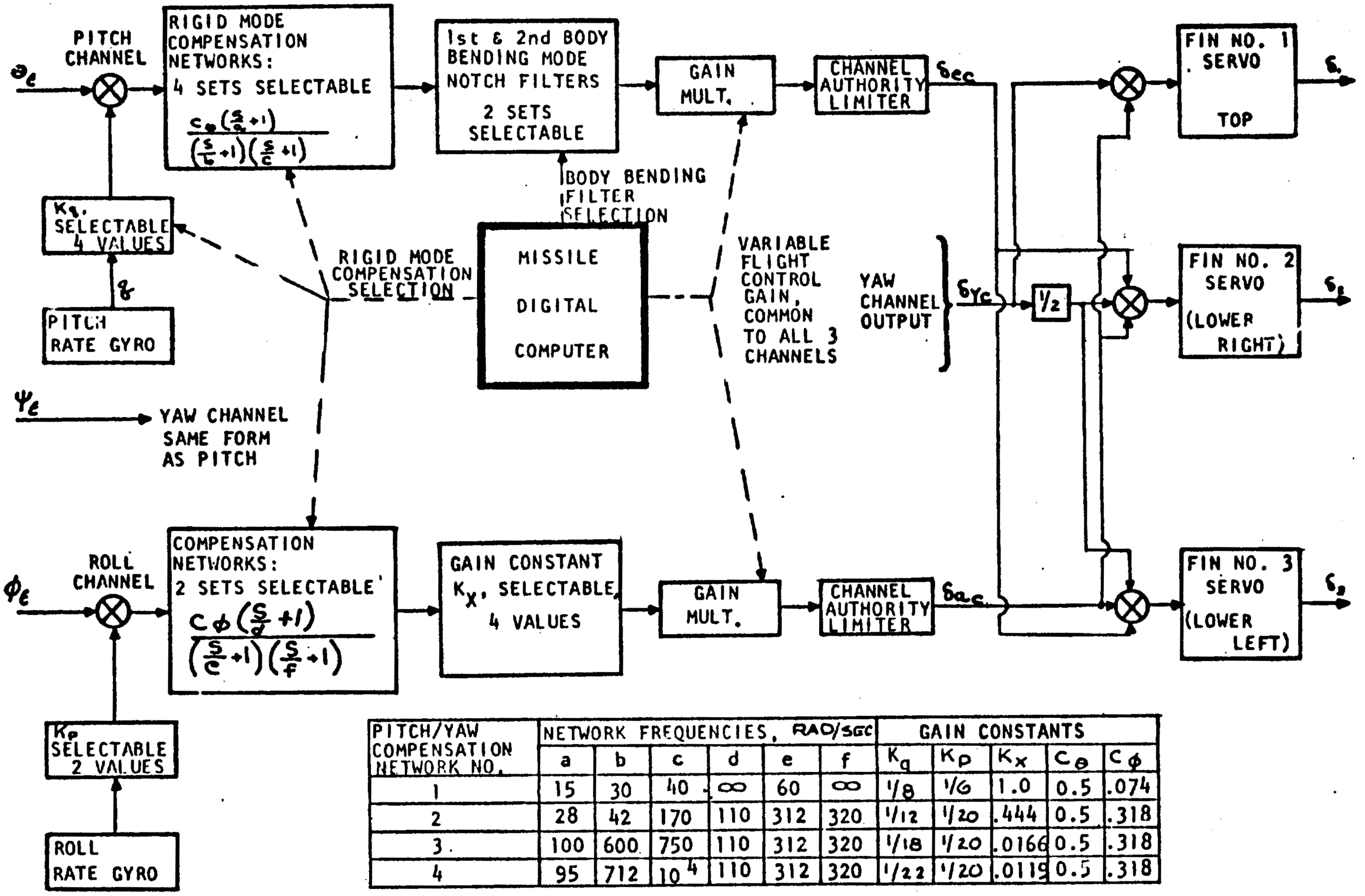
PITCH CHANNEL
θ_ϵ
RIGID MODE COMPENSATION NETWORKS: 4 SETS SELECTABLE
$\frac{C_\theta(\frac{s}{a}+1)}{(\frac{s}{b}+1)(\frac{s}{c}+1)}$
1st & 2nd BODY BENDING MODE NOTCH FILTERS 2 SETS SELECTABLE
GAIN MULT.
CHANNEL AUTHORITY LIMITER
δ_{ec}
FIN NO. 1 SERVO TOP
δ_1
K_q, SELECTABLE 4 VALUES
q
PITCH RATE GYRO
BODY BENDING FILTER SELECTION
RIGID MODE COMPENSATION SELECTION
MISSILE DIGITAL COMPUTER
VARIABLE FLIGHT CONTROL GAIN, COMMON TO ALL 3 CHANNELS
YAW CHANNEL OUTPUT
δ_{Yc}
1/2
FIN NO. 2 SERVO (LOWER RIGHT)
δ_2
ψ_ϵ
YAW CHANNEL SAME FORM AS PITCH
ROLL CHANNEL
ϕ_ϵ
COMPENSATION NETWORKS: 2 SETS SELECTABLE
$\frac{C\phi(\frac{S}{d}+1)}{(\frac{S}{e}+1)(\frac{S}{f}+1)}$
GAIN CONSTANT K_X, SELECTABLE, 4 VALUES
GAIN MULT.
CHANNEL AUTHORITY LIMITER
δ_{ac}
FIN NO. 3 SERVO (LOWER LEFT)
δ_3
K_p SELECTABLE 2 VALUES
ROLL RATE GYRO

PITCH/YAW COMPENSATION NETWORK NO.	NETWORK FREQUENCIES, RAD/SEC						GAIN CONSTANTS				
	a	b	c	d	e	f	K_q	K_p	K_x	C_θ	C_ϕ
1	15	30	40	∞	60	∞	1/8	1/6	1.0	0.5	.074
2	28	42	170	110	312	320	1/12	1/20	.444	0.5	.318
3	100	600	750	110	312	320	1/18	1/20	.0166	0.5	.318
4	95	712	10^4	110	312	320	1/22	1/20	.0119	0.5	.318

FIGURE 5.6.2: FLIGHT CONTROL GAIN COMPUTATION & NETWORK SLECTION

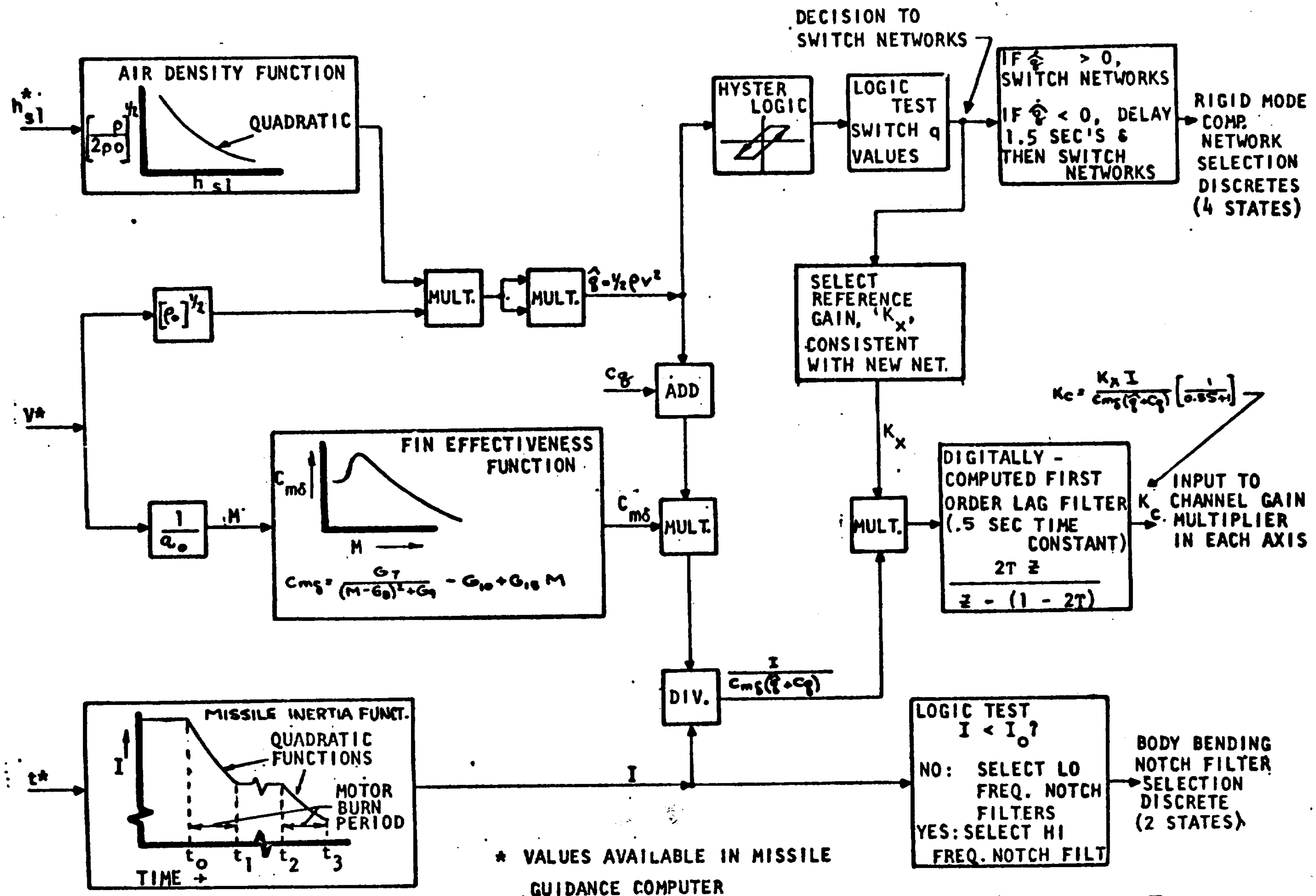
DECISION TO SWITCH NETWORKS
AIR DENSITY FUNCTION
h_{sl}^{*}
$\left[\frac{\rho}{2\rho o}\right]^{1/2}$
QUADRATIC
h_{sl}
HYSTER LOGIC
LOGIC TEST SWITCH q VALUES
IF $\hat{\dot{q}}$ > 0, SWITCH NETWORKS
IF $\hat{\dot{q}}$ < 0, DELAY 1.5 SEC'S & THEN SWITCH NETWORKS
RIGID MODE COMP. NETWORK SELECTION DISCRETES (4 STATES)
MULT.
MULT.
$\hat{q} = \frac{1}{2}\rho v^2$
$[\rho_o]^{1/2}$
SELECT REFERENCE GAIN, 'K$_x$' CONSISTENT WITH NEW NET.
V*
C_q
ADD
K_x
$K_c = \frac{K_x I}{C_{m\delta}(\hat{q}+C_q)}\left[\frac{1}{0.5S+1}\right]$
FIN EFFECTIVENESS FUNCTION
$C_{m\delta}$
M
$\frac{1}{a_o}$
$C_{m\delta} = \frac{G_7}{(M-G_8)^2+G_9} - G_{10} + G_{11} M$
$C_{m\delta}'$
MULT.
MULT.
DIGITALLY - COMPUTED FIRST ORDER LAG FILTER (.5 SEC TIME CONSTANT)
$\frac{2T\,z}{z-(1-2T)}$
K_c
INPUT TO CHANNEL GAIN MULTIPLIER IN EACH AXIS
DIV.
$\frac{I}{C_{m\delta}(\hat{q}+C_q)}$
MISSILE INERTIA FUNCT.
I
QUADRATIC FUNCTIONS
MOTOR BURN PERIOD
t_o t_1 t_2 t_3
TIME →
t*
I
LOGIC TEST $I < I_o$?
NO: SELECT LO FREQ. NOTCH FILTERS
YES: SELECT HI FREQ. NOTCH FILT
BODY BENDING NOTCH FILTER SELECTION DISCRETE (2 STATES)
* VALUES AVAILABLE IN MISSILE GUIDANCE COMPUTER

THE BOEING COMPANY
SEATTLE, WASHINGTON

This quasi-adaptive design approach is applicable to any vehicle with widely varying flight regimes. Therefore, a design similar to this could be applied to the shuttle vehicle.

While in the mixed reaction-jet/aerodynamic and totally aerodynamic modes the filters could be switched as a function of dynamic pressure, the loop gains could be changed as a function of fin effectiveness and the mixing of control modes could be performed as a function of dynamic pressure.

5.7 Digitizing Adaptive Control Systems

The previous discussions have not considered methods of choosing sampling rates for the adaptive control system. Two methods of converting parameter adaptive control systems into multirate designs will now be discussed. The first involves using the identified parameters to determine the dominant response modes of the system. It is precisely these modes which dictate the sampling rate requirements from a frequency folding effects standpoint. Since the folding effects usually place a higher requirement on sampling rate than stability considerations, this technique could be used if analysis verified that this was in fact the case. The second involves adapting the sampling rate to meet the time varying control system requirements. Assuming that the control system was functionally dependent on time varying parameters, a digital implementation could require different time varying sampling rates on the various control loops. From strictly a digital realization standpoint the sampling rate could become a function of the time varying filter break frequencies e.g. $\omega_s \geq N\,\omega_{max}$ where ω_{max} is the highest filter break frequency. Care would have to be exercised in blindly applying this technique especially if the high frequency behavior of signals being sampled was unknown. This situation could be alleviated by analog prefilters on specific signals. A possible implementation might involve using both of these methods.

APPENDIX A

THE SWITCH DECOMPOSITION METHOD OF ANALYZING MULTIRATE SAMPLED DATA CONTROL SYSTEMS

It is illustrative to work a sample problem using both the original switch decomposition method of Kranc [11] and the updated version using the vector operation signal flow graph technique. First let us find the system transfer function shown in Figure A-1 using Kranc's original method.

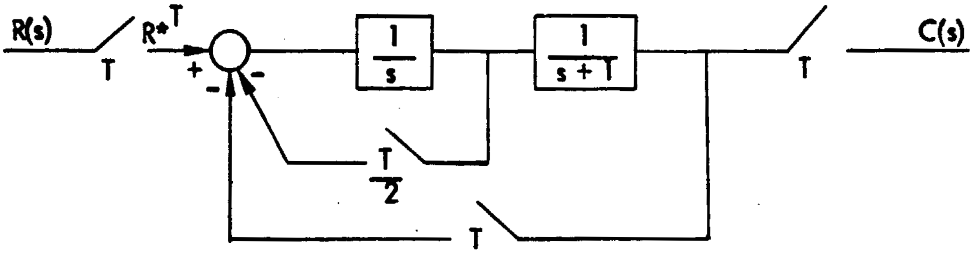

FIGURE A-1

KRANC'S ORIGINAL SWITCH DECOMPOSITION METHOD

The system in Figure A-1 is redrawn replacing the T/2 sampler by the equivalent parallel combination of samplers sampling at rate T. The equivalent system is shown in Figure A-2.

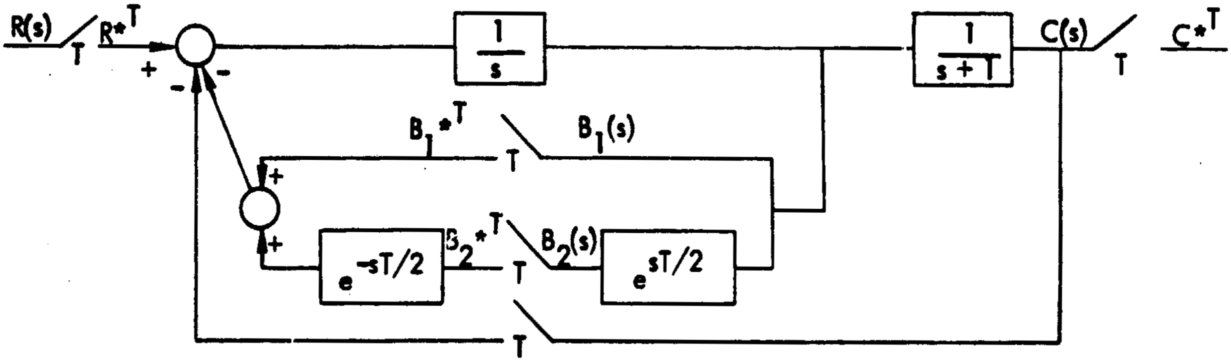

FIGURE A-2

EQUIVALENT SYSTEM IN BLOCK DIAGRAM FORM

The loop equations necessary to find th. ransfer function are written in terms of the unknowns $B_1(s)$ and $B_2(s)$ and the output quantity $C(s)$. They are

$$B_1(s) = \left(\frac{1}{s}\right) R^{*T} - \left(\frac{1}{s}\right) B_1(s) - \left(\frac{e^{-sT/2}}{s}\right) B_2(s) - \left(\frac{1}{s}\right) C^{*T} \qquad \text{(A-1)}$$

$$B_2(s) = \left(\frac{e^{sT/2}}{s}\right) R^{*T} - \left(\frac{e^{sT/2}}{s}\right) B_1(s) - \left(\frac{1}{s}\right) B_2(s) - \left(\frac{e^{sT/2}}{s}\right) C^{*T} \qquad \text{(A-2)}$$

$$C(s) = \left(\frac{1}{s(s+1)}\right) R^{*T} - \left(\frac{1}{s(s+1)}\right) C^{*T} - \left(\frac{1}{s(s+1)}\right) B_1(s) - \left(\frac{e^{-sT/2}}{s(s+1)}\right) B_2(s) \text{(A-3)}$$

The Laplace transform of each sampler output is obtained from (A-1), (A-2) and (A-3). They are

$$B_1{}^{*T} = \left(\frac{1}{s}\right)^{*T} R^{*T} - \left(\frac{1}{s}\right)^{*T} B_1{}^{*T} - \left(\frac{e^{-sT/2}}{s}\right)^{*T} B_2{}^{*T} - \left(\frac{1}{s}\right)^{*T} C^{*T} \qquad \text{(A-4)}$$

$$B_2{}^{*T} = \left(\frac{e^{s1/2}}{s}\right)^{*T} R^{*T} \left(\frac{e^{sT/2}}{s}\right)^{*T} B_1{}^{*T} - \left(\frac{1}{s}\right)^{*T} B_2{}^{*T} - \left(\frac{e^{sT/2}}{2}\right)^{*T} C^{*T} \qquad \text{(A-5)}$$

$$C^{*T} = \left(\frac{1}{s(s+1)}\right)^{*T} R^{*T} - \left(\frac{1}{s(s+1)}\right)^{*T} C^{*T} - \left(\frac{1}{s(s+1)}\right)^{*T} B_1{}^{*T} - \left(\frac{e^{-sT/2}}{S(s+1)}\right)^{*T} B_2{}^{*T} \qquad \text{(A-6)}$$

Rearranging and taking the z-transform yields

$$Z(1 + 1/s)\ B_1\ (z) + Z_{1/2}\ (1/s)\ B_2\ (z) + Z\ (1/s)\ C(z) = Z(1/s)\ R(z) \qquad \text{(A-7)}$$

$$z\ Z_{1/2}\ (1/s)\ B_1(z) + Z\ (1 + 1/s)\ B_2(z) + z\ Z_{1/2}\ (1/s)\ C(z) = z\ Z_{1/2}\ (1/s)\ R(z) \qquad \text{(A-8)}$$

$$Z\left(\frac{1}{s(s+1)}\right) B_1(z) + Z_{1/2}\left(\frac{1}{s(s+1)}\right) B_2(z) + Z\left(1 + \frac{1}{s(s+1)}\right) C(z)$$
$$= Z\left(\frac{1}{s(s+1)}\right) R(z) \qquad \text{(A-9)}$$

where

$$z = e^{sT},\ Z\,(f(s)) = F(z) \text{ and } Z_{1/2}\,(f(s)) = F(z,\ 1/2) \qquad \text{(A-10)}$$

Applying Cramer's rule to Equations (7), (8), and (9) yields the transfer function $\frac{C(z)}{R(z)}$ as a ratio of two determinants.

$$\frac{C(z)}{R(z)} = \frac{\begin{vmatrix} Z(1 + 1/s) & Z_{1/2}(1/s) & Z(1/s) \\ z\,Z_{1/2}(1/s) & Z(1 + 1/s) & z\,Z_{1/2}(1/s) \\ Z\left(\frac{1}{s(s+1)}\right) & Z_{1/2}\left(\frac{1}{s(s+1)}\right) & Z\left(\frac{1}{s(s+1)}\right) \end{vmatrix}}{\begin{vmatrix} Z(1 + 1/s) & Z_{1/2}(1/s) & Z(1/s) \\ z\,Z_{1/2}(1/s) & Z(1 + 1/s) & Z_{1/2}(1/s) \\ Z\left(\frac{1}{s(s+1)}\right) & Z_{1/2}\left(\frac{1}{s(s+1)}\right) & Z\left(1 + \frac{1}{s(s+1)}\right) \end{vmatrix}} \tag{A-11}$$

Expanding each determinate along the first column allows C(z)/R(z) to be written as a ratio of two polynomials.

$$\frac{C(z)}{R(z)} = \frac{Z\left(\frac{1}{s(s+1)}\right) + Z(1/s)\,Z\left(\frac{1}{s(s+1)}\right) - z\,Z_{1/2}(1/s)\,Z_{1/2}\left(\frac{1}{s(s+1)}\right)}{1 + 2Z(1/s) + Z(1/s)\,Z(1/s) - z\,Z_{1/2}(1/s)\,Z_{1/2}(1/s) + Z\left(\frac{1}{s(s+1)}\right) + Z(1/s)\,Z\left(\frac{1}{s(s+1)}\right) - z\,Z_{1/2}(1/s)\,Z_{1/2}\left(\frac{1}{s(s+1)}\right)} \tag{A-12}$$

Each of the terms in the numerator and denominator of C(z)/R(z) can be converted to functions of z by consulting a table of z and modified z transform pairs.

Vector Operation Signal Flow Graph Technique

Using the vector operation signal flow graph technique the flow graph for the system shown in Figure A-1 can be drawn. The flow graph is presented in Figure A-3.

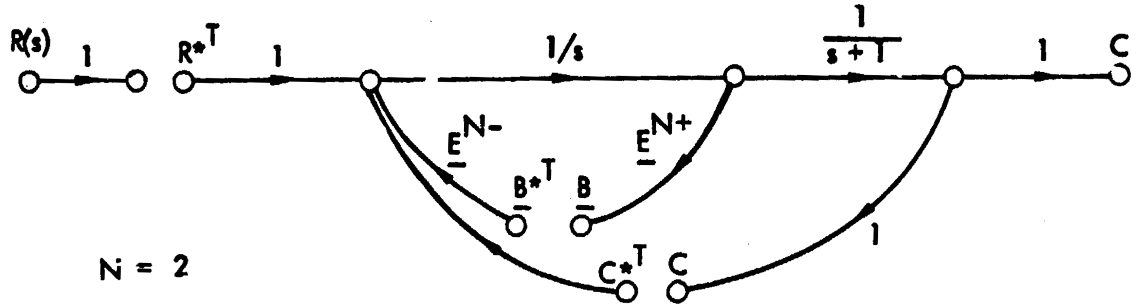

FIGURE A-3
EQUIVALENT SYSTEM IN SIGNAL FLOW FORM

The equations for each output node immediately follow from Figure A-3.

$$\underline{B} = \underline{E}^{N+} (1/s) (R^{*T} - \underline{E}^{N-} \underline{B}^{*T} - C^{*T}) \qquad \text{(A-13)}$$

$$C = (1/s) \left(\frac{1}{s+1}\right) (R^{*T} - \underline{E}^{N-} \underline{B}^{*T} C^{*T} \qquad \text{(A-14)}$$

where $\underline{E}^{N+}$ is the column vector of advances with components $E_i^{N+} = e^{sT (i-1)/N}$, $i = 1, 2, \ldots, N$ and $\underline{E}^{N-}$ is the row vector of delays with components $E_i^{N-} = e^{-sT (i-1)/N}$, $i = 1, 2, \ldots, N$.

The Laplace transform of each output node, after sampling, is given by Equations (A-15) and (A-16).

$$\underline{B}^{*T} = \left\{\underline{E}^{N+} (1/s)\right\}^{*T} (R^{*T} - \underline{E}^{N-} \underline{B}^{*T} - C^{*T}) \qquad \text{(A-15)}$$

$$C^{*T} = \left\{(1/s) (1/s+1)\right\}^{*T} (R^{*T} - \underline{E}^{N-} \underline{B}^{*T} - C^{*T}) \qquad \text{(A-16)}$$

If we shorten our notation by defining

$$\underline{D}^{*T} \triangleq \underline{I}\left\{N \times N + \underline{E}^{N+} (1/s) \underline{E}^{N-}\right\}^{*T}, \quad \underline{a}^{*T} \triangleq \left\{\underline{E}^{N+} (1/s)\right\}^{*T}, \qquad \text{(A-17)}$$

$$\underline{b}^{*T1} \triangleq \left\{(1/s) (1/s + 1) \underline{E}^{N-}\right\}^{*T} \text{ and } F^{*T} \triangleq \left\{(1/s) (1/s + 1)\right\}^{*T} \qquad \text{(A-18)}$$

where the prime (A-1) indicates the transpose, (A-15) and (A-16) combine to form the following matrix input-output transfer function.

$$\frac{C(z)}{R(z)} = \frac{F(z) - \underline{b}^1(z)\,\underline{D}^{-1}(z)\,\underline{a}(z)}{1 + F(z) - \underline{b}^1(z)\,\underline{D}^{-1}(z)\,\underline{a}(z)} \tag{A-19}$$

Using the identities developed by Boykin and Frazier [12] C(z)/R(z) can easily be converted to a ratio of polynomials. The identities, which are used to break down vector/matrix relationships of the form $\underline{E}^{N+}\,G$, $G\,\underline{E}^{N-}$, and $\underline{E}^{N+}\,G\,\underline{E}^{N-}$ into scalar equations are listed in Equations (A-20) through (A-23).

$$\left(\underline{E}^{N+}\,Y\,\underline{E}^{N-}\right)(z) = \sum_{P=0}^{N-1} (\underline{e}_p\,\underline{v}'_p)\,Y^{T/N}(z_p\,w_p) \tag{A-20}$$

$$\left(\underline{E}^{N+}\,Y\right)(z) = \frac{1}{N}\sum_{P=0}^{N-1} Y^{T/N}(z_p\,w_p)\,\underline{e}_p \tag{A-21}$$

$$\left(Y\,\underline{E}^{N-}\right)(z) = \sum_{P=0}^{N-1} Y^{T/N}(z_p\,w_p)\,\underline{v}'_p \tag{A-22}$$

$$\left(X\,\underline{E}^{N-}\right)\left(\underline{E}^{N+}\,Y\,\underline{E}^{N-}\right)^{-1}\left(\underline{E}^{N+}\,R\right) = 1/N \sum_{P=0}^{N-1} \frac{X^{T/N}(z_p\,w_p)\,R^{T/N}(z_p\,w_p)}{Y^{T/N}(z_p\,w_p)}. \tag{A-23}$$

where $w_p = e^{i2\pi p/N}$, $z = e^{sT}$, $z_N = e^{sT/N}$

X, Y and R are scalar functions in $z_p\,w_p$

$$\left\{\begin{array}{ll} \underline{e}_p = \begin{bmatrix} 1 \\ \lambda_{1P} \\ \vdots \\ \lambda_{1P}^{N-1} \end{bmatrix} & \underline{v}_p = \begin{bmatrix} 1 \\ \lambda_{1P}^{-1} \\ \vdots \\ \lambda_{1P}^{N-1} \end{bmatrix} \\ \lambda_{1P} = z^{1/N}\,e^{i2\pi P/N} & P = 0, 1, \ldots, N-1 \end{array}\right.$$

$$\text{and}\quad\left\{\begin{array}{ll} X^{T/N}(z_N w_k) = \displaystyle\sum_{P=0}^{N-1} (z_N w_k)^P X^T(z, {}^{1-P/N}) & \text{(A-24a)} \\[2ex] X^T(z_N{}^N, P/N) = 1/N \displaystyle\sum_{k=0}^{N-1} X^{T/N}(z_N w_k)(z_N{}^{-1} w_k)^{N-P} & \text{(A-24b)} \end{array}\right.$$

To expand (A-19) into a ratio of polynomials let G = 1/s and H = 1/s+1 and note that

$$\sum_{P=0}^{N-1} \underline{e}_p \underline{v}'_p = \underline{I}_{N\times N} \tag{A-25}$$

Expanding $D^{-1}(z)$

$$\begin{aligned} D^{-1}(z) &= \left[\underline{I} + \left(\underline{E}^{N+} G \underline{E}^{N-}\right) \cdot \left(z_N{}^N\right)\right]^{-1} \\ &= \left[\sum_{P=0}^{N-1} (\underline{e}_p \underline{v}'_p)^{-1}(1 + G^{T/N}(z_p w_p)^{-1}\right] \\ &= \left[\sum_{P=0}^{N-1} (\underline{e}_p \underline{v}'_p) \left(\frac{1}{1 + G^{T/N}(z_p w_p)}\right)\right] \end{aligned} \tag{A-26}$$

Using Equations (A-21), (A-22) and (A-23)

$$\begin{aligned} \underline{b}' D^{-1} \underline{a} &= \left(\sum_{k=0}^{N-1} G H^{T/N}(z_N w_k) \underline{v}'_k\right)\left(\sum_{\ell=0}^{N-1} \underline{e}_\ell \underline{v}'_\ell \left[\frac{1}{1 + G^{T/N}(z_N w_\ell)}\right]\right) \\ &\quad \left(1/N \sum_{m=0}^{N-1} G^{T/N}(z_N w_m) \underline{e}_m\right) \\ &= 1/N \sum_{P=0}^{N-1} \frac{G H^{T/N}(z_p w_p) G^{T/N}(z_p w_p)}{1 + G^{T/N}(z_N w_p)} \end{aligned} \tag{A-27}$$

Finding $F^T (z_N{}^N) \triangleq G H^T (z_N)'$ letting N = P in Equation (A-24b)

$$F^T (z_N{}^N) = 1/N \sum_{P=0}^{N-1} \frac{G H^{T/N}(z_p w_p) + G^{T/N}(z_p w_p) G H^{T/N}(z_N w_p)}{1 + G^{T/N} (z_N w_p)} \quad \text{(A-28)}$$

Subtracting expression (A-27) from (A-28) yields the numerator of the input-output transfer function

$$F^T (z_N N) - \underline{b}^1 \underline{D}^{-1} \underline{a} (z_N{}^N) = 1/N \sum_{P=0}^{N-1} \frac{G H^{T/N}(z_p w_p)}{1 + G^{T/N} (z_N w_p)} \quad \text{(A-29)}$$

Therefore

$$\frac{C(z)}{R(z)} = \frac{\frac{1}{N} \sum_{P=0}^{N-1} \frac{G H^{T/N}(z_p w_p)}{1 + G^{T/N} (z_p w_p)}}{1 + \frac{1}{N} \sum_{P=0}^{N-1} \frac{G H^{T/N} (z_p w_p)}{1 + G^{T/N} (z_p w_p)}} \quad \text{(A-30)}$$

The expression is valid for any positive integer N. For our example N = 2 and Equation (A-30) reduces to

$$\frac{C(z)}{R(z)} = \frac{Z (GH) + Z(G)\ Z(GH) - z\, Z_{1/2} (G)\ Z_{1/2} (GH)}{1 + 2Z(G) + Z(G)\ Z(G) - z\, Z_{1/2} (G)\ Z_{1/2} (G) + Z\ (GH) + Z(G)\ Z(GH)}$$

$$\frac{}{- z\, Z_{1/2} (G)\ Z_{1/2} (GH)} \quad \text{(A-31)}$$

If 1/s is substituted for G and 1/s + 1 for H Equation (A-31) is equal to Equation (A-12), the answer which was obtained using Kranc's original switch decomposition method.

Both Kranc's switch decomposition method and the vector operation signal flow graph technique have inherent advantagcs and disadvantages. Kranc's original method is straight forward but becomes cumbersome as the complexity of the system increases. The vector operation signal flow graph technique has the advantage of all.·wing the governing loop equations to be easily written down by inspection of the flow graph. The resulting vector/matrix equations however can become hard to deal with even though the identities and relationships introduced by Boykin and Frazier [12] makes this task somewhat easier.

APPENDIX B

RELATING (α, β) TO (a, b)

Example of the relationship between (α, β) and (a, b) of Equations (5.32) and (5.33)

$$G(s) = \frac{b_4 + \dfrac{b_3}{s+\lambda_3} + \dfrac{b_2}{(s+\lambda_3)(s+\lambda_2)} + \dfrac{b_1}{(s+\lambda_3)(s+\lambda_2)(s+\lambda_1)}}{(s+\lambda_4+a_4) + \dfrac{a_3}{s+\lambda_3} + \dfrac{a_2}{(s+\lambda_3)(s+\lambda_2)} + \dfrac{a_1}{(s+\lambda_3)(s+\lambda_2)(s+\lambda_1)}} \qquad \text{(B-1)}$$

$$G(s) = \frac{\beta_4 s^3 + \beta_3 s^2 + \beta_2 s + \beta_1}{s^4 + \alpha_4 s^3 + \alpha_3 s^2 + \alpha_2 s + \alpha_1} \qquad \text{(B-2)}$$

Multiplying both numerator and denominator of Equation (B-1) by $(s+\lambda_3)(s+\lambda_2)(s+\lambda_1)$ results in a ratio of polynomials of the form of Equation (B-2). Comparing coefficients of like powers of "s" results in the following transformations.

$$\begin{pmatrix} 1 \\ 2 \\ 3 \\ 4 \end{pmatrix} = \underbrace{\left(\begin{array}{c|c|c|c} 1 & \lambda_1 & \lambda_1\lambda_2 & \lambda_1\lambda_2\lambda_3 \\ \hline 0 & 1 & \lambda_1+\lambda_2 & \lambda_1\lambda_2+\lambda_2\lambda_3+\lambda_1\lambda_3 \\ \hline 0 & 0 & 1 & \lambda_1+\lambda_2+\lambda_3 \\ \hline 0 & 0 & 0 & 1 \end{array}\right)}_{T} \begin{pmatrix} b_1 \\ b_2 \\ b_3 \\ b_4 \end{pmatrix}$$

$$\begin{pmatrix} \alpha_1 \\ \alpha_2 \\ \alpha_3 \\ \alpha_4 \end{pmatrix} = T \begin{pmatrix} a_1 \\ a_2 \\ a_3 \\ a_4 \end{pmatrix} + \left(\begin{array}{c} \lambda_1\lambda_2\lambda_3\lambda_4 \\ \hline \lambda_1\lambda_2\lambda_4+\lambda_1\lambda_2\lambda_3+\lambda_2\lambda_3\lambda_4+\lambda_1\lambda_3\lambda_4 \\ \hline \lambda_1\lambda_2+\lambda_3\lambda_4+\lambda_4\lambda_1+\lambda_3\lambda_2+\lambda_1\lambda_3+\lambda_2\lambda_4 \\ \hline \lambda_1+\lambda_2+\lambda_3+\lambda_4 \end{array}\right)$$

Note that the triangular form simplifies inversion.

REFERENCES

1. J. F. Kaiser, "Digital Filters," Chapter 7 in System Analysis by Digital Computer, F.F. Kuo and J. F. Kaiser (eds), John Wiley & Sons, Inc., New York, 1966.

2. Charles M. Rader and Bernard Gold, Digital Processing of Signals, McGraw-Hill Book Co., 1969.

3. R. E. Kalman and J. Bertram, "A Unified Approach to the Theory of Sampling Systems," J. Franklin Inst., Vol. 267, pp. 405-436, May 1959.

4. J. T. Tou, Modern Control Theory, McGraw-Hill Book Co., New York 1964.

5. B. C. Kuo, Analysis and Synthesis of Sampled Data Control Systems, Prentice-Hall, Englewood Cliffs, N.J., 1963

6. B. C. Kuo, Discrete Data Control Systems, Prentice-Hall, Englewood Cliffs, N.J., 1970

7. G. N. Saridis and R. N. Lobbia, "Parameter-Adaptive Self-Organizing Control of Stochastic Linear Discrete-Time Systems," TR-EE 71-40, December 1971.

8. J. E. Gibson, Nonlinear Control Systems, Chapter 11, McGraw-Hill 1962.

9. R. A. Nash, et al, "Error Analysis of Hybrid Aircraft Inertial Navigation Systems," 1972 AIAA Conference on Navigation Guidance and Control, paper #72-848.

10. R. K. Mehra, "Identification of Stochastic Linear Dynamic Systems with Kalman Filter Representation," AIAA Journal, Vol. 9,#1, January 1971.

11. G. M. Kranc, "Input-Ouput Analysis of Multirate Feedback Systems," IRE Trans. on Automatic Control, Vol. PG AC-3, pp. 21-28, November 1957

12. Boykin, Frazier, et al, "Analysis and Design of Sampled Data Systems," University of Florida Tech. Report E637-4, NASA Contract NAS8-26832 MSFC, Chapter 5, 1973.

13. T. C. Coffey and I. J. Williams, "Stability Analysis of Multiloop Multirate Sampled Systems," AIAA Journal, Vol. 4, No. 12, pp. 2178-2190, December 1966.

14. E. I. Jury, "A Note on Multirate Sampled Data Systems," IEEE Trans. on Automatic Control, Vol. AC-12, pp. 319-320, June 1967.

15. E. I. Jury, "A General Z-Transform Formula for Sampled-Data Systems," IEEE Transactions on Automatic Control, Vol. AC-12, pp. 606-608, October 1967.

16. Stepner, D. E. and R. K. Mehra, "Maximum Likelihood Identification and Optimal Input Design for Identifying Aircraft Stability and Control Derivatives" Contract Report by SCI, Contract #NAS1-10700, NASA CR-2200, March 1973.

17. Larry Taylor, et al, "A Comparison of Newton-Raphson and Other Methods for Determining Stability Derivatives from Flight Data," Third Technical Workshop on Dynamic Stability Problems, Ames Research Center, 1968.

18. Marvin Shinbrot, "On the Analysis of Linear and Nonlinear Dynamical Systems from Transient Response Data," NACA TN 3288, December 1954.

19. Dante DiFranco, "In-Flight Parameter Identification by the Equation-of-Motion Technique -- Application to the Variable Stability T-33 Airplane, "Cornell Aero Lab Report No. TC-1921-F-3, December 15, 1965.

20. D. C. Denery, "An Identification Algorithm Which is Insensitive to Initial Parameter Estimates," AIAA Eighth Aerospace Science Conference, January 1970.

21. L. B. Jackson, "Round-Noise Analysis for Fixed Point Digital Filters Realized in Cascade or Parallel Form," IEEE TAU, Vol. AU-18, No. 2, June 1970

22. Lion, P. M., "Rapid Identification of Linear and Non-Linear Systems," AIAA Journal, Vol. 5, No. 10, October 1967, pp. 1835-42.

23. Kushner, H. J., "On the Convergence of Lion's Identification Method with Random Inputs, "IEEE Transactions on Automatic Control, Vol. AC-15, No. 6, December 1970, pp. 652-4.

24. Marsik, J., "Quick-Response Adaptive Identification," Identification in Automatic Control Systems, IFAC, Part 2, Section 5.5, Institute of Information Theory and Automation, Czechoslovak Academy of Sciences, Academia, Prague, 1968.

25. Price, C. F. and Koenigsberg, W.D., Adaptive Control and Guidance for Tactical Missiles, TR-170-1, The Analytical Sciences Corporation, Reading, Massachusetts, 1970.

26. Mullen, M. D., "An On-Line Identification Technique for Adaptive Autopilot Applications," TN404-155, Naval Weapons Center, China Lake, California January 1973.

27. Bryson, A. E. and Luenberger, D.G., "The Synthesis of Regulator Logic Using State-Variable Concepts," Proceedings of IEEE, November 1970.

28. Luders, G. and Narendra, K.S., "An Adaptive Observer and Identifier for a Linear Sysrem," IEEE Transaction on Automatic Control, October 1973.

29. Luders, G. and Norendra, "A New Canonical Form for an Adaptive Observer," IEEE AC-19, April 1974 (pp. 117-119)

30. Chen, C. T., Introduction to Linear System Theory, New York, Holt, Rinehart, and Winston, 1970.

31. Gibson, J. E., Nonlinear Automatic Control, New York, McGraw-Hill, 1963.